

Techno-Economic Analysis of An Integrated Direct Air Capture and Mineralization System

A Feasibility Study

SET3901: Graduation Project
Imran bin Khairrul Saleh

Techno-Economic Analysis of An Integrated Direct Air Capture and Mineralization System

A Feasibility Study

by

Imran bin Khairrul Saleh

Student Name	Student Number
Imran bin Khairrul Saleh	5479878

TU Delft Supervisor: Prof. dr. ir. Earl Goetheer
Company Supervisors: Dr. Ann-Sophie Farle
Piotr Kasper
Eleni Lymeropoulou
Project Duration: December, 2022 - August, 2023
Faculty: Faculty of Electrical Engineering, Mathematics and Computer Science, Delft



Preface

Completing this thesis has been a transformative journey, encompassing valuable experiences that have not only equipped me with essential engineering skills but also taught me the importance of embracing the process and maintaining optimism in the face of adversity. Over the past 7-8 months, I have grown significantly as an individual, a friend, a colleague, and an employee. It all began when I discovered the world of carbon capture during a lecture at TU Delft, which set the course for my professional career and fueled my passion to contribute and advance this field of science. My experiences at TNO and Skytree further solidified my decision.

Throughout the process of completing this thesis, I have had the privilege of learning from some of the industry's finest. I am deeply grateful to the following individuals, without whom this thesis would not have been possible:

First and foremost, I would like to express my gratitude to my supervisor, Earl Goetheer, for his outstanding guidance and expertise in process and energy related to the mineralization system. His input has always been invaluable, and his feedback has consistently enriched my understanding of carbon capture technologies and process engineering. Despite his numerous responsibilities, he has consistently provided precious insights, enabling me to learn something new every step of the way.

I would also like to extend my personal thanks to Eleni, Piotr, and Ann-Sophie for their supervision at Skytree. Their support has ensured that I stay focused on the task at hand, and their daily oversight has provided me with valuable advice and knowledge. I am especially grateful to my fellow colleague Tarun Ravi, who, despite not officially being my thesis supervisor, has always found time to assist me with the challenges I faced with constructing my mineralization system as well as enriching me with knowledge regarding process modelling. His expertise in Aspen and process engineering has ignited a spark within me to pursue this path further.

Lastly, I am immensely thankful to my friends and family, whose unwavering support has been a pillar of strength throughout my journey of completing this thesis. Their presence has provided me with stability, and their encouragement has propelled me forward in overcoming everyday challenges.

With a sense of pride and fulfillment, I now conclude my chapter as a student at TU Delft, eagerly looking forward to what lies ahead. This work represents my personal contribution to the scientific world, and I hope that it will be of value to students exploring the realm of carbon mineralization, inspiring them to build upon and improve the existing body of knowledge.

*Imran bin Khairrul Saleh
Delft, July 2023*

Abstract

Carbon sequestration involves the conversion of carbon dioxide gas into carbonates through reactions with magnesium or calcium bearing minerals, presenting a potential method to mitigate CO₂ emissions and reduce their release into the atmosphere. This process can be classified into two categories: in-situ (subsurface) and ex-situ (surface). CO₂ mineralization has demonstrated the ability to permanently store substantial quantities of CO₂ without the need for extensive post-monitoring efforts, while also offering potential business model benefits for the generated end products. However, the field of mineralization still faces substantial technical and economic challenges, including high cost projections and slow carbonation kinetics, impeding further technological advancements in the field. Additionally, logistical challenges related to plant design and associated emissions contribute to the complexity of finding solutions to these problems.

In this particular study, the investigation focused on ex-situ carbon dioxide sequestration primarily through direct aqueous mineral carbonation, incorporating a direct air capture element. This approach was chosen due to the flexibility provided by direct air capture in terms of CO₂ supply and the desirable characteristics of direct aqueous carbonation. Various models were developed using Aspen Plus software and compared, leading to the selection of the direct aqueous carbonation system as the optimal choice for CO₂ carbonation. Further enhancements were implemented in the system, including recycled streams and heat integration, to reduce overall energy consumption. Optimization steps were also undertaken to determine the appropriate sizing of key equipment that make up the majority of the system's overall costs and to improve system efficiency.

An economic analysis was then performed, revealing that plant scales of 50 ktons/year yielded a positive Net Present Value (NPV), indicating profitability. Conversely, smaller-scale plants of 0.5 ktons/year and 5 ktons/year did not generate positive revenue, even with a high carbon credit price. This was followed by a sensitivity analysis that showcased the relevant parameters that holds significant effects on the economic performance of the system.

Moreover, business model cases were also explored, and it was concluded that utilizing the end products in building materials and road construction could potentially generate additional revenue for the mineralization system beyond storage options.

Overall, this investigation highlights the potential of ex-situ carbon sequestration through direct aqueous mineral carbonation, considering direct air capture, and emphasizes the importance of economic viability and revenue diversification in the successful implementation of mineralization systems to mitigate the effects of global warming.

Contents

Preface	i
Summary	ii
Nomenclature	v
1 Introduction	1
1.1 Background	1
1.2 Research Question	2
1.3 Research Approach	3
2 Direct Air Capture & Mineralization Framework	4
2.1 Direct Air Capture	4
2.1.1 Adsorption	5
2.1.2 Absorption	6
2.1.3 Cost	7
2.2 Carbon Capture and Storage (CCS)	7
2.3 Mineral Carbonation	8
2.4 Feedstocks	10
2.4.1 Natural Minerals	10
2.4.2 Industrial By-products	12
2.5 Carbonation Routes	12
2.5.1 Direct Carbonation	13
2.5.2 Indirect Carbonation	14
2.6 Factors Affecting Mineralization	16
2.6.1 Feed Material	17
2.6.2 Particle Size	17
2.6.3 Temperature and Pressure	18
2.6.4 Water or Steam	19
2.6.5 pH	20
2.7 Cost of Mineralization	21
3 Design Selection	22
3.1 Feed Mineral Selection	22
3.2 Direct Carbonation vs Indirect Carbonation	22
3.3 Design Methods	23
3.3.1 Boundary Conditions	23
3.3.2 Partial Pressures	23
3.3.3 Grinding Energy	24
3.3.4 Equation of State	24
3.3.5 Reaction Kinetics	25
3.4 Gas-Solid Carbonation Comparison	26
3.5 Direct Aqueous Carbonation Comparison	30
4 Process Design	34
4.1 Non-Integrated and Integrated System	34
4.1.1 DAC Unit	34
4.1.2 Final Model	34
4.2 Comparison	37
5 Equipment Selection & Economic Analysis	39
5.1 Scaling	39

5.2 Pressure Drop	40
5.3 Grinding	42
5.4 Heat Exchanger	43
5.5 Reactor	46
5.6 Pump, Compressor, Filter, & Flash Drum	49
5.7 Economic Analysis	51
5.7.1 Carbon Footprint	51
5.7.2 CapEx and OpEx	53
5.7.3 Sensitivity Analysis	57
5.8 Business Case Opportunities	57
5.8.1 Building Materials	58
5.8.2 Asphalt Mixtures	59
6 Conclusion & Recommendations	61
6.1 Conclusion	61
6.2 Recommendation	61
References	63
A Appendix	72

Nomenclature

Abbreviations

Abbreviation	Definition
BECCS	Bio-Energy with Carbon Capture and Storage
BET	Brunauer-Emmett-Teller
CAPEX	Capital Expenses
CCS	Carbon Capture and Storage
CF	Cash Flow
CDR	Carbon Dioxide Removal
CSTR	Continuous Stir Tank Reactor
DAC	Direct Air Capture
DAQC	Direct Aqueous Carbonation
DACCS	Direct Air Capture with Carbon Storage
FC	Fixed Costs
FCI	Fixed Capital Investment
GGR	Greenhouse Gas Removal
GSC	Gas Solid Carbonation
LG-MC	Low-Grade Magnesium Carbonate
LMTD	Logarithmic Mean Temperature Difference
NET	Negative Emission Technologies
NPV	Net Present Value
OPEX	Operational Expenses
PEC	Purchased Equipment Cost
PSA	Pressure Swing Adsorption
SCM	Supplementary Cementitious Material
SSA	Supercapacitive Swing Adsorption
STOIC	Stoichiometry Reactor
TCI	Total Capital Investment
TSA	Temperature Swing Adsorption
UCL	Universal de Caracterizacion de Ligantes
VC	Variable Costs

Symbols

Symbol	Definition	Unit
P	Pressure	[bar]
P_t	Pressure Drop	[bar]
F	Original Particle Size of Feedstock	[m]
P	Imaginary Sieve Size Passing 80% of Grounded Feedstock	[m]
W_i	Bond's Working Index	[kWh/ton]
k	Reaction Constant	[s ⁻¹]
r	Reaction Rate	[·]
E_a	Activation Energy	[kJ/mol]
R	Universal Gas Constant	[J/(K mol)]
A	Pre-Exponential Factor	[·]

Symbol	Definition	Unit
T	Temperature	[K]
v	Velocity	[m/s]
L	Length of Pipe	[m]
d_{ti}	Diameter of Pipe	[m]
f	Fanning Factor	[·]
a, b	Fanning Equation Constants	[·]
$v_{settling}$	Settling Velocity	[m/s]
g	Gravity	[m/s ²]
Re	Reynolds Number	[·]
K	Consistency Index	[Pa·s]
n	Flow Behaviour Index	[·]
T_A	Temperature Difference on Hot Stream	[K]
T_B	Temperature Difference on Cold Stream	[K]
Nu	Nusselt's Number	[·]
Pr	Prandtl's Number	[·]
k	Thermal Conductivity of Fluid	[W/(K·m)]
U, h	Heat Transfer Coefficient	[W/(K·m ²)]
A	Heat Exchanger Area	[m ²]
Q	Heat Duty	[W]
c_p	Specific Heat Capacity	[J/(kg·K)]
C_1	Cost of Facility 1	[€]
C_2	Cost of Facility 2	[€]
D	Annual Depreciation Cost	[€]
S	Annual Sales	[€]
Q_1	Capacity of Facility 1	[€]
Q_2	Capacity of Facility 2	[€]
X	Scale Factor	[·]
t	Taxation Rate	[·]
N	Period of Years (Lifetime)	[·]
ρ	Density	[kg/m ³]
α	CO ₂ Concentration	[·]
μ	Dynamic Viscosity of Medium	[Pa·s]

1

Introduction

1.1. Background

The primary challenge of climate change, being human emissions of carbon dioxide and other greenhouse gases presents one of the most critical problems the world faces [31]. In 2022, global carbon dioxide emissions from the use of fossil fuels and the production of cement reached a new record high of 36.6 billion tonnes (GtCO₂), marking a 1.0% increase [45]. In response to this challenge, the Paris Agreement was approved in 2016, with over 197 countries committing to carbon neutrality to limit the temperature increase to below 1.5°C compared to pre-industrial levels [44]. Addressing the persistent rise in atmospheric carbon dioxide levels has since become a central focus of global initiatives.

Figure 1.1 illustrates global greenhouse gas emissions and global warming projections under various scenarios. Despite the implementation of current climate and energy policies, the trajectory is still far from aligning with the 1.5°C target. Therefore, there is an urgent need for continuous development and research efforts to get CO₂ out of the air and steer the trend towards net zero emissions achieve the desired target set forth in the Paris Agreement.

However, to achieve net zero emissions global efforts have to go beyond simply reducing CO₂ emissions. It also involves offsetting emissions from challenging sectors like the steel and cement industries, which account for 7.0% and 6.5% of global CO₂ emissions, respectively [33]. This is where greenhouse gas removal becomes crucial, ensuring a balance at 'net' zero. Greenhouse Gas Removal (GGR) technologies, also known as Negative Emission Technologies (NET), play a significant role in this area by actively extracting CO₂ from the atmosphere [93]. Once captured, the CO₂ gas can either be sequestered or utilized. NETs can contribute to the overall objective of mitigating climate change and are essential for preventing its worst effects.

One of the methods of storing CO₂ is through geological storage, which is a technology that is readily available and being applied to various projects [77]. However, there exist an uncertainty surrounding CO₂ gas being stored underground where post-monitoring efforts are required to prevent leakage aside from the availability of storage facilities worldwide.

In addition, CO₂ can be utilized as a feedstock for a particular process like carbonized beverages or cleaning products that utilizes the usage of CO₂. Consideration of using CO₂ as feedstock in this case often involves knowing about the circularity of the product as the CO₂ will be released again to the atmosphere at the end of the product's life cycle. Therefore, the permanency aspect of CO₂ storage via this method is limited.

Another option for CO₂ storage is through CO₂ mineralization. The concept of carbon mineralization is based on the natural process of mineral weathering, where rocks and minerals undergo chemical reactions to form new compounds. In the case of CO₂ in the atmosphere, rain combines with the CO₂ to create a weak bicarbonate acid. This acid can then interact with certain minerals on the Earth's surface, eventually leading to the formation of carbonate minerals. However, this natural process occurs over long timescales, spanning thousands of years [132], which is not sufficient to address the current rates of CO₂ emissions. Therefore, further research and advancements are necessary to accelerate the reaction rates and make carbon mineralization a more effective climate mitigation strategy.

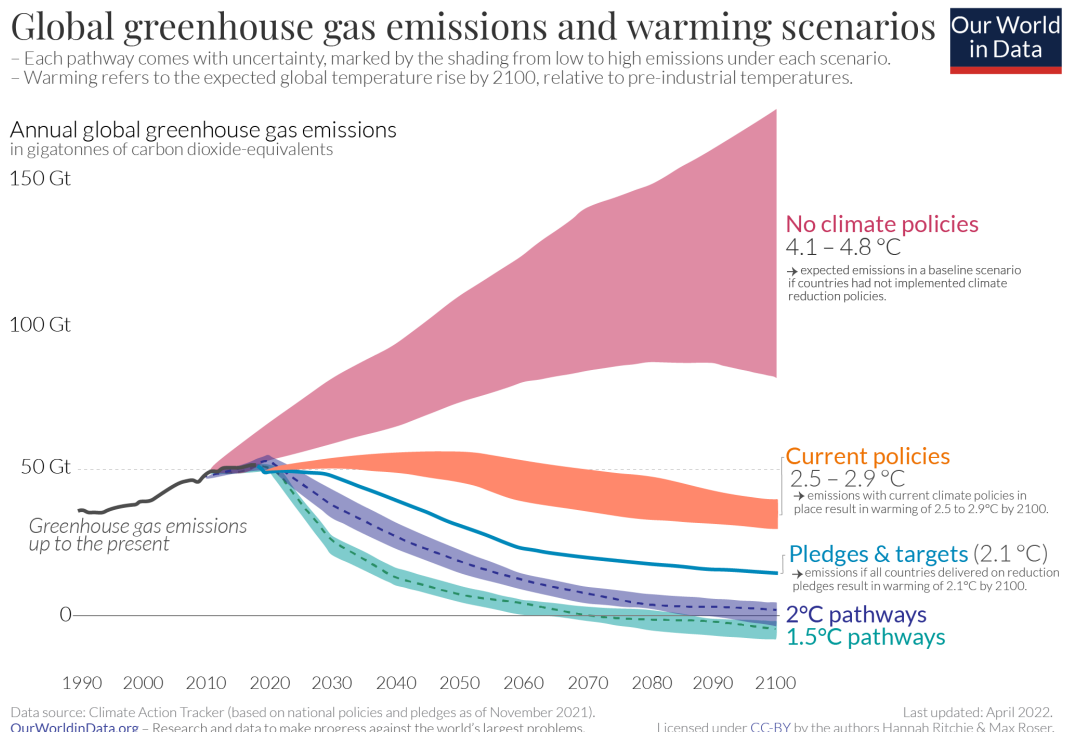


Figure 1.1: Global greenhouse gas emissions and warming scenarios
[32]

1.2. Research Question

Negative emission technologies such as carbon sequestration plays an important role in helping mankind mitigate the effects of global warming and climate change. Among them, CO₂ mineralization has the potential to be a viable countermeasure to combat climate change considering the vast amount of CO₂ that can be permanently stored. However, further research needs to be conducted to improve on its performance and capabilities. The reason being the mutual factor for deploying CO₂ sequestration on a large scale basis lies in its very high cost projections and very slow carbonation kinetics to which it subsequently dampers further technological developments in the field. Also, the logistical challenges and emissions associated with siting of the facilities and transportation of CO₂ gas and feedstock often render implementing mineral carbonation-based CO₂ capture processes impractical [120].

On the other hand, direct air capture technologies can alleviate this disadvantage. Its ability to extract CO₂ directly from the air offers flexibility in location selection as well as bringing production closer to the end user such as greenhouse markets which promotes more affordable CO₂ prices. When coupled with the permanency aspect of CO₂ mineralization, this combination presents an intriguing pathway for the development of a secure CO₂ storing system that bears further research. This led to the formulation of the main research question as follows:

- **What is the techno-economic feasibility of an integrated Direct Air Capture + Mineralization system?**

Several studies have explored the integration of direct air capture (DAC) systems with mineralization processes like the research that was conducted by Valentin Gutknecht et. al. [16] which combines direct air capture with in-situ CO₂ injection into basalts and by Raghavendra Ragipani et. al. [120] which focuses on direct air capture with mineralization using coal fly ash. Nevertheless, due to the constraints of identifying appropriate underground CO₂ injection sites and the limited global availability of fly ash, there is a need for further research in exploring alternative approaches. Specifically, investigating the utilization of abundant minerals and employing ex-situ methods that can expand mineralization capacities while also possibly introducing a business perspective to the end products.

Regrettably, there is a scarcity of available information that delve into these aspects. As a result, this knowledge gap has further motivated the development of the following sub-questions to be addressed:

- **What are the ideal characteristics of a mineralization process?**
- **What are the energy requirements associated with the DAC + Mineralization system?**
- **What are the possibilities of the mineralized end products?**
- **What are the optimization steps that can be taken to further improve the system in the future?**

This graduation project will therefore focus on developing a techno-economic analysis for a DAC + CO₂ mineralization system that will tackle the problems stated above. For this investigation to be useful, the integration of CO₂ captured from air via adsorption from direct air capture technologies followed by the subsequent mineralization process of the captured CO₂ is key. This thesis project will encompass how such a system would look like and also assess its performance and technical-economic feasibility.

1.3. Research Approach

To fully answer the posed research question above, the following outcomes are to be achieved:

- **Overview and analysis of existing CO₂ mineralization processes, reactors, operating conditions, energy requirements and scalability.**
- **Defining direct air capture (DDAC) to mineralization system.**
- **Design and partial modelling of DAC to mineralization system for specific, to be defined use case.**
- **System optimization and performance evaluation**

By the end of the graduation project, the following milestones are to be expected:

- **Design of a system to capture and mineralize CO₂ from ambient air.**
- **Equipment selection, mass and energy balance determination**
- **Techno-economic and performance evaluation of an integrated and non-integrated system**

A literature review will be conducted in Chapter 2 that provides a comprehensive summary and comparison of various developed mineralization concepts. Subsequently, considering these aspects, an evaluation of process selection will be undertaken in Chapter 3, focusing on feedstock selection, and carbonation methods.

Upon determining the system parameters, Chapter 4 will contain a more detailed process flow diagram, accompanied by energy consumption calculations. The energy assessment will encompass factors such as grinding energy, DAC modular requirements, heating/cooling demands, CO₂ compression, water pump usage, and more.

Subsequently, equipment selection and sizing followed by optimization steps will be undertaken in Chapter 5 to explore potential design improvements and further energy reductions. A preliminary economic analysis of the mineralization process as a whole will be conducted in this chapter as well to evaluate the associated costs from start to finish. Finally, a business case model will be formulated to assess potential opportunities for further exploration and development.

2

Direct Air Capture & Mineralization Framework

Chapter 1.1 provided an overview of the critical challenges our planet is currently facing and discussed potential solutions, including CO₂ mineralization. It also introduced the main research question and the research approach undertaken in this investigation. This chapter will dive into the framework of direct air capture and mineralization, exploring the underlying concepts, existing technologies, and presenting potential avenues for further exploration.

2.1. Direct Air Capture

DIRECT AIR CAPTURE

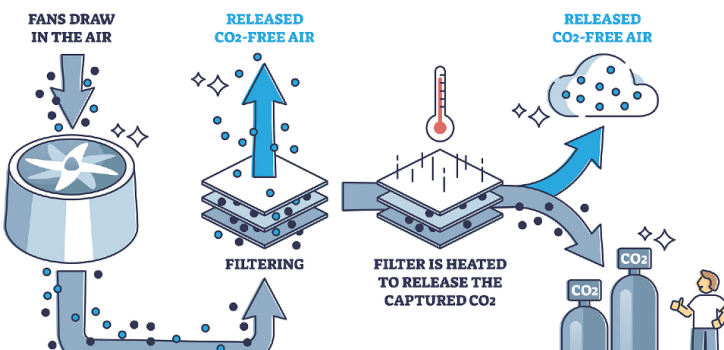


Figure 2.1: How direct air capture works
[92]

The act of capturing carbon dioxide at stationary point sources of emission (e.g., power plants) alone is expected to only slow down the increase of CO₂ concentration in the atmosphere [38] as this does not solve the problem of capturing carbon dioxide that is already present in the air. Therefore, developing methods to extract CO₂ directly from the atmosphere is critical to ensuring the collective goal of the Paris Agreement is achieved.

In response to this, in 1999 Klaus Lackner suggested the concept of direct air capture. Direct air capture (DAC) technologies extract CO₂ directly from the atmosphere. The CO₂ can then be either permanently stored in deep geological formations (carbon capture and storage), or recycled and reused (carbon capture and utilization). The applications of the captured CO₂ depends on the objectives of governments or industries involved.

Systems that already exist to capture CO₂ from ambient air works in two concepts:

- Adsorption
- Absorption

Each of the aforementioned concepts have their own respective traits and characteristics which leaves a lot of room for future optimization research opportunities.

2.1.1. Adsorption

The concept of adsorption is mainly used by solid sorbents. They are solid-based materials such as zeolites and amines that adsorb CO₂ on the surface of the material when it makes contact with air. It generally do not pose any health hazard and has a relatively smaller energy consumption than that of absorption technology [105]. However, the problem with using solid sorbent is the co-adsorption of water during the CO₂ capture process [1]. Adsorption can occur through various mechanisms such as chemisorption or physisorption. In physisorption, the molecules are attracted to the surface of the material through Van der Waals forces, whereas for chemisorption the target gas molecules undergoes a covalent chemical reaction to bind to the sites on the sorbent as shown in Figure 2.2.

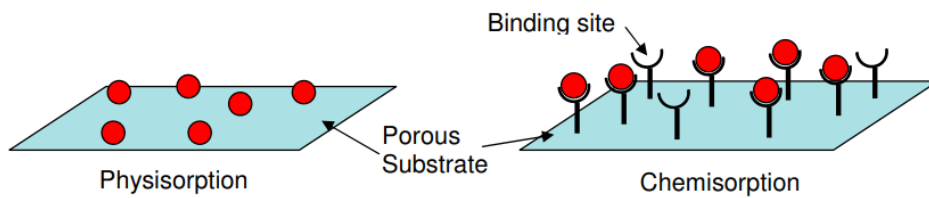


Figure 2.2: Physisorption and Chemisorption mechanisms
[8]

Temperature Swing Adsorption

The method of capturing CO₂ by the adsorption process using solid sorbents can be done through what is called a temperature swing adsorption (TSA) process. In temperature swing adsorption, the adsorbed gases are desorbed after adsorption steps by heating the adsorbent to a specific temperature. Figure 2.3 shows the example of what is called a "collector", which is a term coined for a device used to capture CO₂ from ambient air.

The solid sorbents are fitted to a filter in such a way that it has high surface area to volume ratio, to maximize the contact between the air and the sorbent material for efficient CO₂ capture. This filter is then places into the collector to be used for DAC applications. When air enters the air collector through the fans, it passes through the solid-sorbent filter located inside the collector which traps the carbon dioxide particles. When the filter is completely saturated with CO₂, the collector closes and the temperature inside gets heated to a certain temperature, which causes the filter to release the captured CO₂ to be used either for utilization or storage purposes [24].

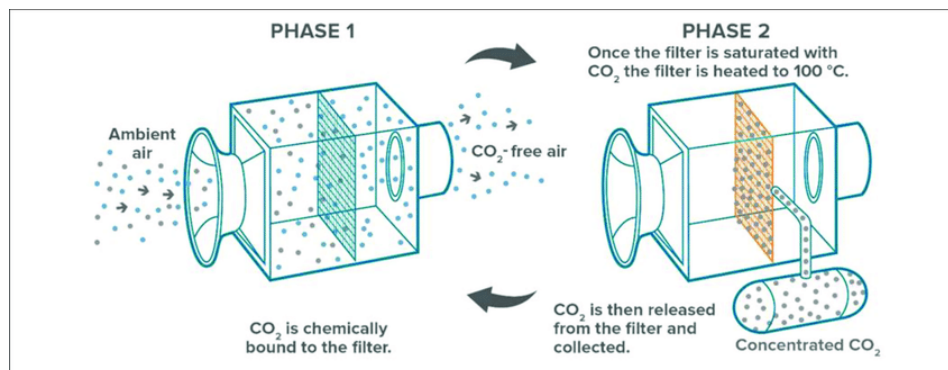


Figure 2.3: Collector for direct air capture process
[24]

Supercapacitive Swing Adsorption

Supercapacitive swing adsorption (SSA) is a newly discovered electrochemically driven CO₂ capture technology that promises significant efficiency improvements over traditional methods [69]. It is based on charging/discharging supercapacitors, where one electrode is fully submerged in electrolyte and serve as the anode and the other is partially submerged and serve as the cathode. When voltage is applied, this creates a potential difference of the electrodes that facilitate the charging/discharging mechanism of this process for CO₂ adsorption/desorption. This emerging technology gained attention in recent years due to the fact that they avoid the energy penalty associated with thermal and pressure cycling. Furthermore, SSA is significantly simpler than other electrochemical sorption techniques, where it only requires inexpensive, robust, and environmentally benign porous activated carbons and aqueous electrolytes. However, the current limitation of SSA is the low sorption capacity and the slow sorption kinetics compared to known amine sorbents [70].

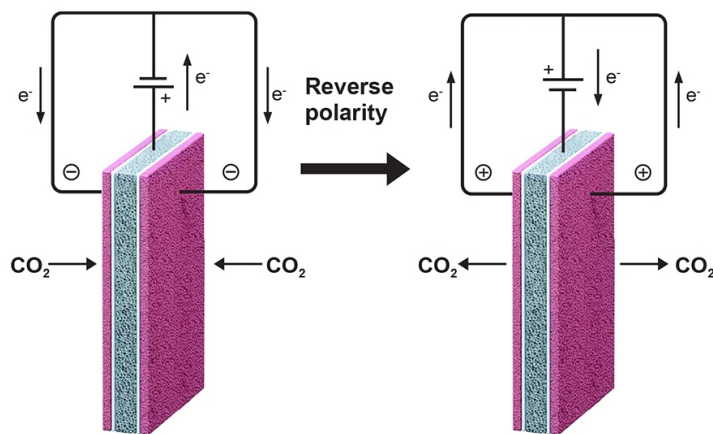


Figure 2.4: Supercapacitive swing adsorption direct air capture process
[112]

2.1.2. Absorption

A liquid based sorbent uses the concept of absorption, which involves passing ambient air over a chemical solution which can absorb CO₂. An example is the use of a potassium hydroxide solution where this non-toxic solution chemically binds with the CO₂ molecules, removing them from the air and trapping them in the liquid solution as a carbonate salt. The CO₂ contained in this carbonate solution is then purified and compressed to be delivered in gas form ready for use or storage [40]. An example of this process can be observed in Figure 2.5 where a capture solution passes through a collector, or in this case an "air contactor" and binds with the oncoming CO₂ from air. The CO₂ rich solution is then taken out to be further processed.

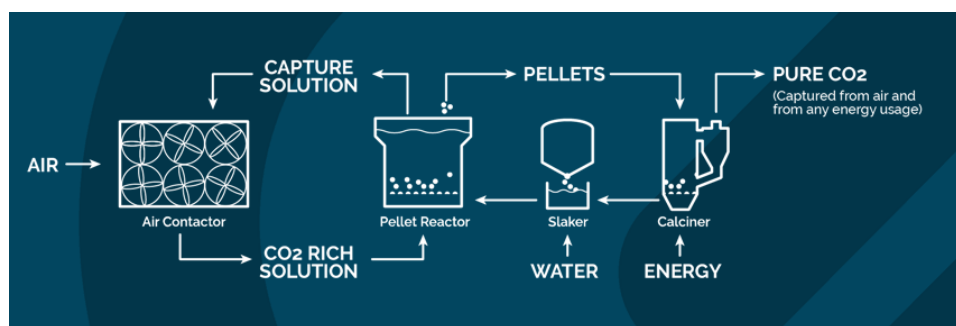


Figure 2.5: Absorption based direct air capture process
[40]

2.1.3. Cost

Despite the benefits and flexibility of applications methods mentioned above, direct air capture is currently more costly per tonne of CO₂ removed compared to many other mitigation approaches and natural climate solutions as it is energy intensive to separate carbon dioxide from ambient air. The range of costs for DAC vary between \$250 and \$600 depending on the technology choice, low-carbon energy source, and the scale of their deployment; for comparison, most reforestation costs less than \$50/tonne of CO₂ removed [11]. This shows how costly the process of direct air capture can become. However, depending on the rate of deployment, which could accelerate through supportive policies and market development, costs for DAC could fall to around \$150-\$200 per tonne over the next 5-10 years [11].

Another reason for high costs today is there are relatively few DAC companies and projects; developing more projects will provide learning knowledge that could reduce costs. And it is important to note that DAC offers quantifiable and permanent storage, whereas nature-based carbon removal solutions like reforestation/afforestation are at risk of deforestation and climate change induced threats like wildfires and drought. Ultimately, the greatest benefit for DAC comes when it is paired with geologic sequestration. However, there is unfortunately no revenue opportunity beyond public policy and public funding. Public investment and support of carbon removal technology has increased in the past few years, but more will be needed to scale sufficiently and avoid the worst impacts of climate change [11].

2.2. Carbon Capture and Storage (CCS)

The methods described in Section 2.1 provide valuable insights into the working concepts of capturing CO₂ from ambient air, as opposed to capturing it from point sources like flue gases. However, while there are various applications for the captured CO₂, such as fuel production, greenhouses, and the food and drink industry, this utilization approach only serves to slow down carbon emissions. At best, it can be considered carbon neutral if no additional CO₂ is added or removed from the atmosphere. Unfortunately, this approach alone is insufficient to achieve the target of limiting global warming to 1.5°C, as outlined in the Paris Agreement.

To address this limitation, the concept of carbon capture and storage (CCS) has been developed. CCS involves the separation, treatment, and transportation of a relatively pure stream of CO₂ from industrial sources or directly from the air to a long-term storage location, typically an underground geological formation (In-Situ) or above-ground facilities (Ex-Situ) before storage [80]. This process effectively reduces greenhouse gas emissions and helps mitigate climate change by permanently removing CO₂ from the atmosphere.

The development of CCS is a crucial step towards achieving the climate goals set forth in the Paris Agreement. By capturing CO₂ from industrial processes or directly from the air and securely storing it, CCS offers a more comprehensive and impactful approach to reducing greenhouse gas emissions. Implementing CCS technology at scale can significantly contribute to the global efforts to mitigate climate change and work towards a sustainable future.

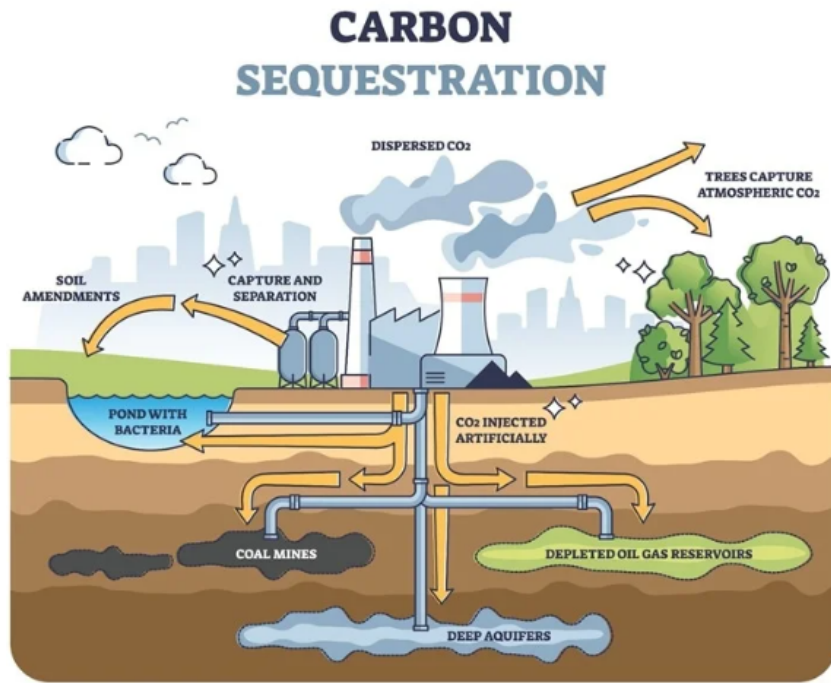


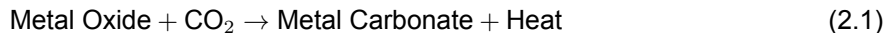
Figure 2.6: Different ways to sequester CO₂
[137]

As seen from Figure 2.6, the CO₂ is to be disposed of in the subsurface [88]. For effective climate change mitigation, it is crucial that CO₂ remains fixed in storage for long periods. Geological storage offers a favorable solution in this regard, as it is capable of achieving long-term fixation and can be implemented on a large scale, making it suitable for capturing emissions from major sources. However, there are two significant drawbacks associated with this method: the risk of CO₂ leakages and the requirement for rigorous site monitoring to ensure containment [3].

Moreover, the costs associated with the carbon capture process itself are already high [25], and geological storage further adds to the overall expenses. Unlike carbon capture and utilization, there are no viable options for generating additional revenue from CO₂ sequestration. Therefore, the widespread adoption of CCS relies heavily on government policies, subsidies, and public support as incentives. Unfortunately, these setbacks pose challenges to the technological advancement and wider implementation of the CCS process.

2.3. Mineral Carbonation

Mineral carbonation, which involves the accelerated weathering of naturally occurring silicate rocks, has been proposed as a potential approach for CO₂ sequestration since the 1990s [118]. This process entails the reaction of metal oxide-bearing materials with CO₂, resulting in the formation of insoluble carbonates. The reaction can be represented by the following equation:



This reaction can take place either below (*in situ*) or above (*ex situ*) ground. In *situ* mineral carbonation involves the injection of CO₂ into underground reservoirs to promote the reaction between CO₂ and alkaline-minerals present in the geological formation to form carbonates [59]. Ex *situ* mineral carbonation relates to above-ground processes, which requires rock mining and pre-treatments to the minerals involved [84]. Mineral carbonation have a large CO₂ sequestration potential (410 000 Gt C) across the globe due to the large abundance of silicates or feedstock available around the world, as can be seen in Figure 2.7.

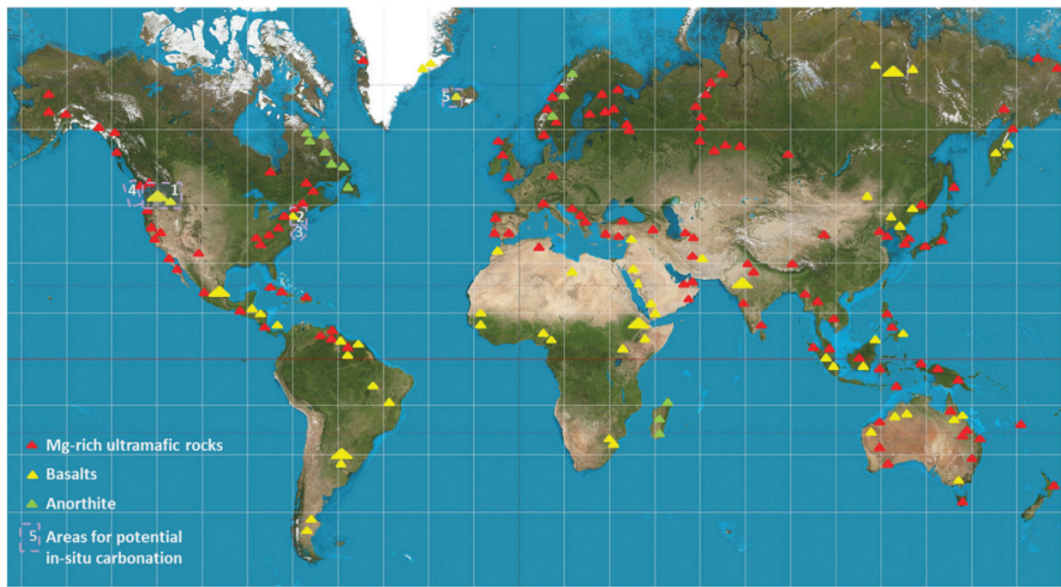


Figure 2.7: Available feedstock for mineral carbonation
[83]

The implementation of mineral carbonation for CO₂ mitigation is currently constrained by several challenges, which limit its widespread usage. These challenges include slow kinetics of CO₂-silicate reactions, energy-intensive pre-treatment requirements, the need for public support, logistical issues such as locating suitable mineral resources and CO₂ emitters, and the development of transport and storage facilities for waste carbonates on a large scale [74].

Figure 2.8 provides a comprehensive overview of the existing feedstocks and carbonation methods that are currently used and studied. The feedstocks encompass natural minerals available in the Earth's crust as well as industrial by-products obtained from nearby industrial processes. Carbonation routes can be categorized into direct carbonation and indirect carbonation. The variables depicted in Figure 2.8 will be further elaborated upon in the subsequent sections, offering a more detailed explanation of each aspect.

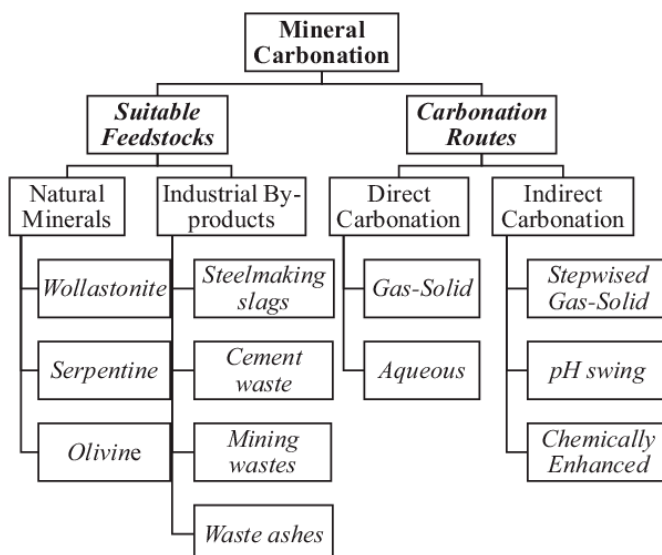


Figure 2.8: Summary of existing feedstocks and carbonation methods
[62]

2.4. Feedstocks

The selection of appropriate feed materials is a crucial aspect of mineral carbonation, as it directly impacts the efficiency of the mineralization process. Calcium and magnesium are the most abundant alkaline earth metals found in nature, making them the preferred choices for carbonate formation [42]. As shown in Figure 2.8, feed materials rich in calcium and magnesium can be classified into two categories: natural minerals and industrial by-products. Each category has its own specific requirements as well as advantages and disadvantages.

2.4.1. Natural Minerals

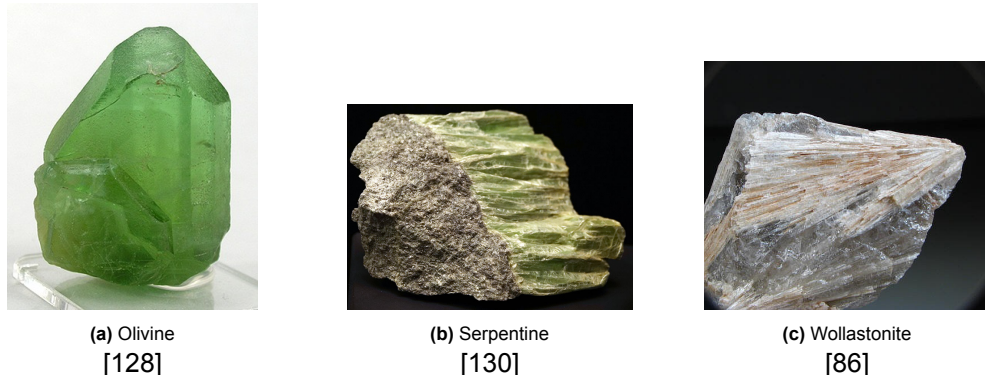


Figure 2.9: Olivine, serpentine, and wollastonite

Natural minerals encompass mineral deposits found in the Earth's crust, such as olivine, serpentine, and basalt. These minerals require mining or extraction processes to obtain and may require further processing or grinding to enhance their reactivity. The main advantage of natural minerals is their abundant availability [141], while the disadvantages include the energy and resource-intensive extraction processes and potential environmental impacts associated with mining operations. Furthermore, although these natural minerals are abundant in earth's crust, their respective conversion rates and reaction kinetics are relatively slow [104].

Silicate minerals such as olivine, serpentine and wollastonite are among the common natural minerals that have been chosen as feed materials across many mineralization investigations [94]. A description on each of these minerals can be seen below:

Olivine

Olivine is an abundant mineral found on Earth, comprising approximately 60 to 80 percent of the upper mantle. When olivine reacts with CO₂, it forms carbonate minerals. Remarkably, one ton of olivine has the potential to absorb nearly one ton of carbon dioxide from the air [23]. To fully utilize its carbon capture capacity, olivine needs to be crushed into fine particles, which increases its reactive surface area with the surrounding air.

During the natural weathering process, the surface of olivine reacts with CO₂ present in rainwater, effectively absorbing the carbon and forming new carbonate minerals. This unique property of olivine presents an opportunity for CO₂ capture. In small-scale applications, such as the civil construction projects in Rotterdam, it is estimated that over 853,000 tonnes of CO₂ could potentially be captured using olivine. Scaling up this approach to a national level could result in capturing a comparable amount of CO₂ to annual freight traffic emissions [100].

Table 2.1 shows the general information regarding olivine.

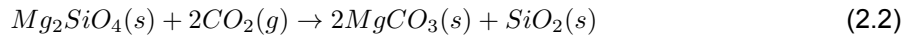
Parameters	Values
Chemical Formula	(Mg,Fe) ₂ SiO ₄
Molar Mass	153.31 g/mol
Species	Forsterite Fayalite
Density	3270-3370 kg/m ³
Mohs Scale	6.5-7

Table 2.1: General olivine information
[128]

According to the table, olivine crystals consist of a mixture of Mg₂SiO₄ and Fe₂SiO₄, with the magnesium component typically being more dominant [108]. This variation in composition within the crystal structure gives rise to different types of crystals in the olivine group. Forsterite represents the magnesium-rich member, while fayalite represents the iron-rich member of this crystal group.

The Mohs scale is a qualitative ordinal scale used to measure mineral hardness. It ranges from 1 to 10 and characterizes the scratch resistance of minerals based on the ability of harder materials to scratch softer ones [126]. Olivine has a Mohs hardness scale rating of 6.5-7.0. To put this into perspective, diamonds have a Mohs hardness rating of 10. Therefore, among the three natural materials suitable for CO₂ mineralization, olivine is the hardest mineral.

The general chemical reaction between forsterite and CO₂, leading to the formation of a mineral carbonate, can be represented by the following equation:



Serpentine

Serpentinites are metamorphic rocks primarily composed of polymorphs of minerals from the serpentine group. They consist of hydrated magnesium silicates and are formed through a process called serpentinization, which involves the reaction of olivine with water. Table 2.2 highlights the presence of different serpentine group minerals, including antigorite, lizardite, and chrysotile [89].

Similar to olivine, serpentinites also serve as a promising feedstock for carbonation reactions and possess the capacity to sequester carbon dioxide (CO₂) on a global scale. They present a promising avenue for carbon capture and storage efforts, contributing to the mitigation of greenhouse gas emissions.

Parameters	Values
Chemical Formula	(Mg,Fe,Ni,Al,Zn,Mn) ₂₋₃ (Si,Al,Fe) ₂ O ₅ (OH) ₄
Molar Mass	252.81 g/mol [122]
Species	Chrysotile Antigorite Lizardite
Density	2600 kg/m ³
Mohs Scale	3-6

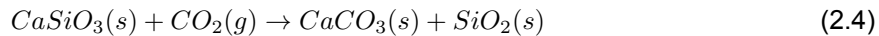
Table 2.2: General serpentine information
[130]

However, the carbonation process for serpentine is generally slower compared to olivine, but it can be enhanced [12]. One method to improve its reactivity is thermal pre-treatment, which involves dehydrating serpentine through heat. The temperature required to remove the -OH group from the serpentine lattice is approximately 630°C [79]. Pre-heated serpentine exhibits significantly higher reactivity compared to olivine, although the energy cost associated with achieving this level of reactivity must be taken into consideration for CO₂ sequestration applications. In terms of hardness, serpentine has a Mohs scale ranging from 3 to 6, making it slightly softer than olivine but still classified as a hard mineral. The chemical equation below illustrates the general reaction between a serpentine ore group and CO₂, leading to carbonate formation.



Wollastonite

Aside from the aforementioned Olivine and Serpentine, the other widely studied feedstocks for CO₂ mineralization is wollastonite, an earth-abundant calcium-rich silicate mineral with estimated global reserves of over 80 million tons. Because wollastonite contains high calcium (Ca) content, it was considered as a suitable feedstock in the mineral carbonation process [7]. However, the utilization of wollastonite is very limited, as it is much rarer than Mg-rich silicates of olivine and serpentine [94], corresponding to the annual production of only about 1.1 million tons [71]. The general reaction between CO₂ and wollastonite can be expressed as:



Ca-silicates like wollastonite have a comparatively weaker Ca-O bond rather than Mg-O bond in Mg silicates. This difference in bonding strength contributes to the faster dissolution rate of Ca-silicates, in comparison to Mg silicates [48]. The relatively rapid dissolution rate makes wollastonite an attractive candidate for CO₂ carbonation processes. Table 2.3 provides general information about wollastonite.

In addition, the lower Mohs scale hardness of wollastonite compared to olivine and serpentine is noteworthy. This characteristic makes wollastonite easier to grind, resulting in potentially lower energy consumption during pre-treatment processes.

Parameters	Values	
Chemical Formula	CaSiO ₃	
Molar Mass	116.16 g/mol [131]	
Species	Serandite	Pectolite
Density	2900 kg/m ³	
Mohs Scale	4.5-5	

Table 2.3: General wollastonite information
[86]

2.4.2. Industrial By-products

While natural minerals are abundant, as discussed earlier, they generally exhibit lower reaction rates for CO₂ mineralization and require pre-treatment processes to enhance their reactivity. This would result to a substantial energy penalty for the whole process. This is where industrial by-products are attractive to be utilized as feedstock. Industrial by-products are rich in calcium and magnesium and offer distinct advantages over natural minerals for mineral carbonation purposes. They do not necessitate pre-treatment processes and can exist in highly reactive forms such as MgO/CaO or Ca/Mg-(OH)₂.

Additionally, these industrial wastes are often cost-effective and conveniently located near industrial areas, reducing transportation costs. Moreover, they provide a readily used CO₂ containing stream from flue gas (slags) rather than ambient air, in which case the CO₂ content is more concentrated than ambient air [39]. Examples of industrial waste products used for mineral carbonation include steelmaking slag, waste cement and concrete, and coal fly ash.

However, one limitation of utilizing industrial wastes as feed materials is that, despite their high reactivity, they are available in much fewer quantities when compared with natural minerals, with a total annual production of only 7.1 Gt of waste [133]. In comparison, the total capacity of available natural minerals suitable for CO₂ sequestration, as mentioned in Section 2.3, is estimated to be 410,000 Gt. Moreover, industrial by-products can contain other gases other than CO₂ that may be harmful to people as well as affect the direct air capture or mineralization processes when compared using ambient air.

2.5. Carbonation Routes

As can be observed from Figure 2.8, the existing methods to speed up the carbonation process can be classified as direct carbonation and also indirect carbonation, respectively. Figure 2.10 shows the basic principles of direct and indirect carbonation. Direct carbonation involves a reaction that occurs in only one step or occurs in the same reactor whereas indirect carbonation involves multiple stages [3]

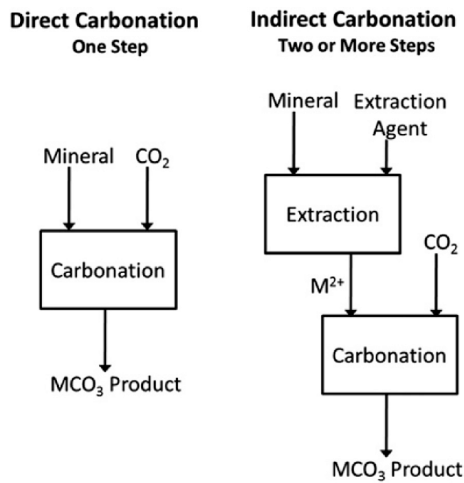
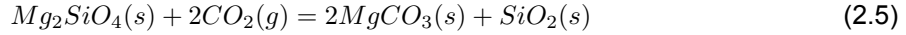


Figure 2.10: Basic principles of direct and indirect carbonation methods [3]

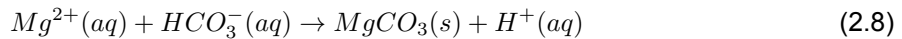
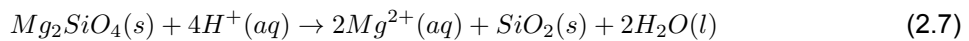
2.5.1. Direct Carbonation

Direct carbonation can be divided into two main methods: gas-solid carbonation and aqueous carbonation. Gas-solid carbonation is a straightforward and simple route. For instance, the direct gas-solid reaction between olivine and CO₂ can be represented as:



In this process, carbon dioxide gas is converted into a solid carbonate, simulating the natural weathering processes involving alkaline silicate minerals. However, in a dry environment, this reaction often requires high CO₂ partial pressures and temperatures to compensate for the slow reaction kinetics. Under appropriate conditions, as indicated in Equation 2.5, CO₂ is sequestered on the surface of the mineral ores as magnesium carbonates. Additionally, silica by-products form on the mineral surface, encapsulating the magnesite crystals [15]. The formation of a silica passivation layer restricts further carbonation reactions, leading to increased process costs for this type of reaction [136]. Overcoming the passivation layer and increasing carbonation rates pose challenges to the commercial viability of direct mineral carbonation processes [94].

Direct aqueous carbonation, on the other hand, involves the reaction of carbon dioxide gas with a feed material in an aqueous suspension, typically water, at high pressures [13]. By subjecting CO₂ to water at elevated pressures (usually 100-150 bar), the amount of dissolved CO₂ increases. This behavior follows Henry's law, which states that, at a constant temperature, the amount of gas dissolved in a liquid is directly proportional to the partial pressure of the gas in equilibrium with the liquid [35]. The direct aqueous carbonation process can be represented by the following equation:



First, the dissolved CO₂ will dissociate to form bicarbonate acid (HCO₃⁻) and hydrogen ions (H⁺). The hydrogen ions will react with the mineral, extracting the magnesium ions from its matrix and producing silica (SiO₂) and water (H₂O) as byproducts. In the final step, precipitation occurs between the magnesium ions and bicarbonate acid, resulting in the formation of magnesium carbonate (MgCO₃) and releasing another hydrogen ion.

In the direct aqueous mineral carbonation system, the dissolution of the mineral is the rate-limiting step, primarily due to the absence of protons at pH close to 7 [79]. After dissolution, product layer diffusion takes place, leading to the formation of a silica layer similar to direct gas-solid carbonation.

On the other hand, researchers have proposed combining direct aqueous carbonation with organic additives as a promising strategy for mineral carbonation. This approach is based on the idea that

catalyst-like additives can significantly accelerate silicate dissolution, thereby increasing the extent of carbonation [10]. In a study by W.K. O'Connor et al. [13], it was theorized that ions present in additives such as sodium chloride and sodium bicarbonate can hydrolyze the silicate, resulting in the formation of magnesium carbonate, hydroxide (OH^-) ions, and free silica (SiO_2), as shown in the following equation:



The formed hydroxide ion is believed to then react immediately with additional CO_2 that is injected into the solution to reform the bicarbonate acid. The paper stated that the pre- and post- pH test measurements that were carried out gave results of a pH range of between 7.7-8.0, which meant that the solution chemistry still remains relatively constant and therefore the sodium chloride and sodium bicarbonate addition to the water suspension is not consumed in the reaction but acts as a catalyst similar to water [13].

An example of a process flow diagram of a direct carbonation process can be seen from Figure 2.11. For this process, the feed material olivine undergoes the grinding process in a grinding reactor which reduces the particle size of the feedstock typically from initial sizes of more than 100 mm to less than 100 μm . Following that, 0.64 M NaHCO_3 were added to the solution to increase its reactivity. Later, it travels to the precipitation reactor and undergoes mineralization at 150-200°C and 100-150 bar. This process has reported to achieve 80% carbonation in 6 hours [79]. The process also reported that the feed material wollastonite achieved 70% in only 1 hour, and unlike the other minerals, the reaction proceeded rapidly in distilled water [107]. Therefore, this process shows that the grinding step speeds up the reaction rate of the direct carbonation method in exchange for higher energy requirements.

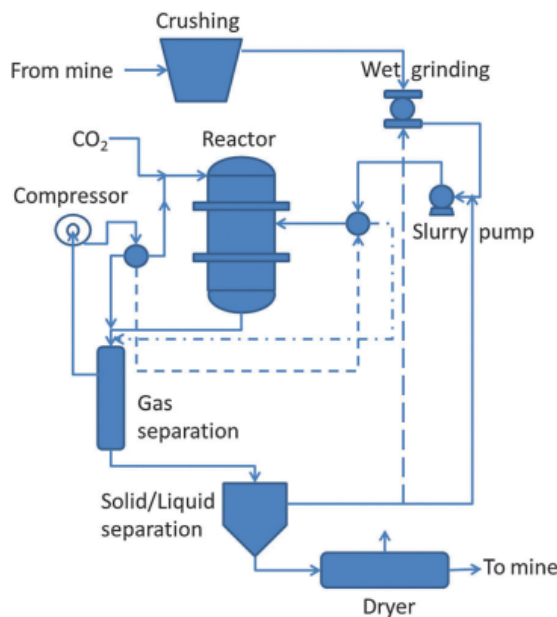


Figure 2.11: Example process flow diagram of direct carbonation
[107]

2.5.2. Indirect Carbonation

Indirect carbonation involves dividing the overall mineral carbonation technology process into multiple steps to enhance the reaction kinetics, particularly the dissolution of minerals, which is often the rate-limiting step in carbonation processes. One example of indirect carbonation is the stepwise gas-solid mineral carbonation method, which is an improvement over the direct gas-solid carbonation approach. This method was developed by Johan Fagerlund and involves several stages to overcome the slow reaction rate of the gas-solid process.

In the stepwise gas-solid mineral carbonation process, the first step is the extraction of magnesium from magnesium silicates, followed by the production of magnesium hydroxide ($Mg(OH)_2$), and finally, the carbonation process takes place in a fluidized bed reactor. This process maintains a gas-solid reaction state, allowing the exothermic heat released from the reaction to exist as a hot concentrated gas, rather than being diluted in water as in direct aqueous carbonation processes [43].

Figure 2.12 and 2.13 illustrate the complete process of stepwise gas-solid reaction for indirect carbonation. These figures provide a visual representation of the different stages involved in the process.

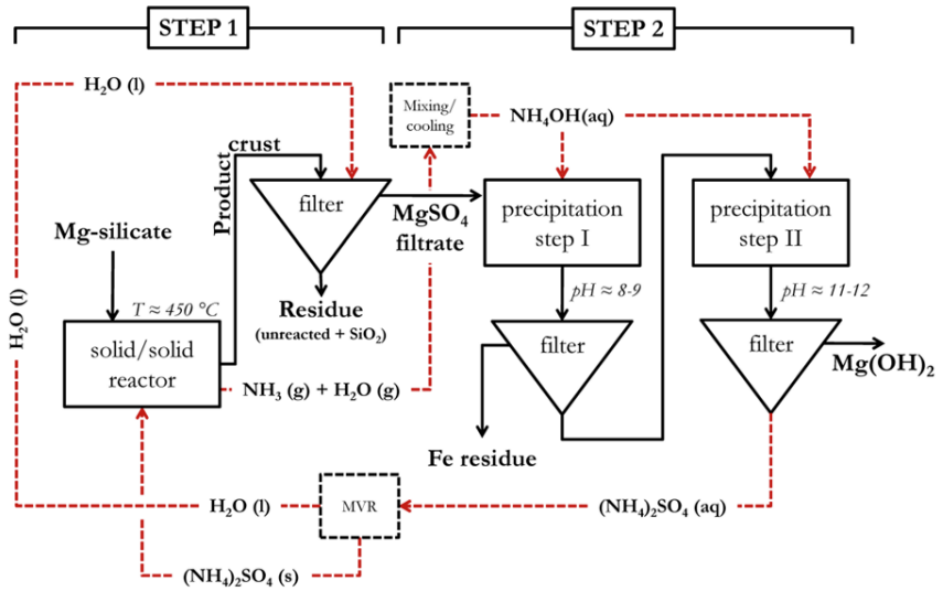


Figure 2.12: Schematic overview of magnesium extraction (step 1) and $Mg(OH)_2$ production (step 2) proposed by Fagerlund [43]

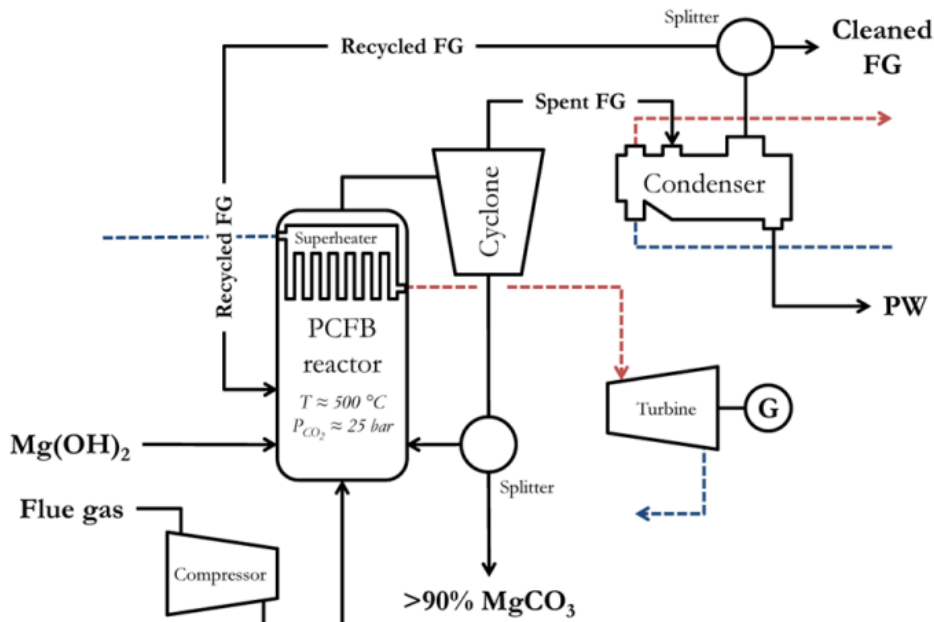


Figure 2.13: Schematic overview of a carbonation reactor operation by Fagerlund [43]

Furthermore, Figure 2.8 also provides an overview of many other indirect carbonation routes, includ-

ing the pH swing process and chemically enhanced processes such as the indirect aqueous carbonation using acetic acid [59]. These routes utilize different minerals and processes to achieve mineral carbonation through indirect methods. One of the advantages of indirect mineral carbonation is the production of higher purity products, as the multiple steps involved in the process allow for the removal of impurities and unreacted materials while also separating the carbonates from the process. Additionally, the conversion rate of calcium and magnesium to carbonates is generally higher in indirect methods.

However, it is important to consider the disadvantages associated with indirect mineral carbonation methods. One drawback is the higher energy and heat input required due to the additional steps involved in the process. Moreover, there can be regeneration issues with the chemical additives used, as some of them may not be easily regenerated, reused, or reproduced. This limitation adds to the cost of the carbonation process compared to direct carbonation methods and also its environmental impact.

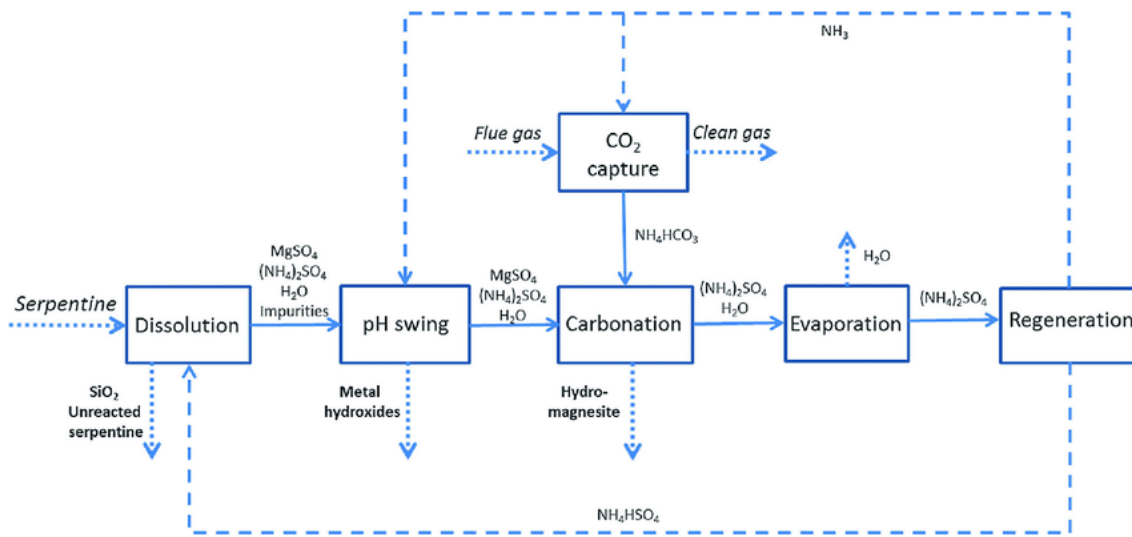


Figure 2.14: Process flow diagram of indirect carbonation
[79]

The process flow of indirect carbonation can be exemplified through the pH swing process as seen in Figure 2.14. The pH swing method takes advantage of the fact that a low pH environment promotes mineral dissolution, while a high pH environment facilitates carbonate precipitation [96]. In this particular method, serpentine is initially dissolved in a 1.4 M aqueous solution of NH₄HSO₄ to extract magnesium from its lattice. NH₃ is utilized to capture CO₂ from flue gas, generating NH₄HCO₃ as a product.

The Mg-rich solution obtained from the dissolution step is then neutralized with NH₄OH to remove impurities before proceeding to the carbonation step, where it reacts with NH₄HCO₃ obtained from the CO₂ capture phase. Furthermore, an additive regeneration step is employed, involving the decomposition of (NH₄)₂SO₄ at 300°C to produce ammonia, which can be reused for both the CO₂ capture step and the serpentine dissolution step.

The overall process has proven to be highly efficient, achieving a 90% capture rate of CO₂ from flue gas with a CO₂ content ranging from 3% to 15% [78]. However, a significant drawback of this indirect carbonation process lies in the substantial amount of water that needs to be separated from the salts during the regeneration step, leading to its energy-intensive nature.

2.6. Factors Affecting Mineralization

As discussed in Section 2.5, there are two methods of carbonation: direct carbonation and indirect carbonation. Direct carbonation is a straightforward process for mineralizing CO₂, but it suffers from slow reaction kinetics. However, there are several approaches that can be employed to accelerate the reaction in CO₂ mineralization. This section will explore some of the factors and methods that can enhance the reaction rate.

2.6.1. Feed Material

The choice of feed materials is a crucial factor in CO₂ mineralization. As discussed in Section 2.4, the carbonation process can utilize either natural minerals or industrial by-products as feed materials. Industrial by-products generally exhibit higher reactivity rates compared to natural minerals. However, their utilization in CO₂ sequestration is limited by the environmental impact of the material sources used and the limited capacity available worldwide.

Figure 2.15 provides a comparison of the reactivity of olivine, serpentine, wollastonite, and activated serpentine. Activated serpentine refers to serpentinite material that has undergone substantial heating to remove the -OH group from its crystal matrix. Figure 2.15 demonstrates that activated serpentine exhibits significantly higher reactivity compared to its parent mineral. However, the requirement for a high-temperature thermal pre-treatment, as mentioned in Section 2.4.1, makes activated serpentine unfavorable as an ideal candidate for the mineralization system due to the high energy input it necessitates.

On the other hand, both wollastonite and olivine demonstrate favorable reaction rates. Conversion results reported in the literature indicate over 80% efficiency in 6 hours for olivine, while wollastonite, being the most reactive, achieves over 70% carbonation in just 1 hour [107]. It should be noted that the particle size used for the comparison in Figure 2.15 is <75 µm.

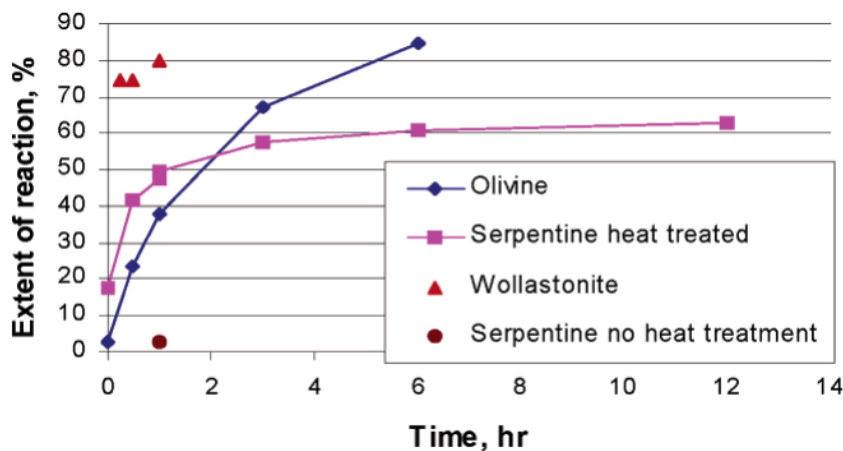


Figure 2.15: Comparison of olivine, serpentine, wollastonite and activated serpentine; extraction at 185°C, 150 atm CO₂ in NaCl NaHCO₃ solution [107]

The superior reaction rate of wollastonite in comparison to olivine results in a lower CO₂ partial pressure requirement, typically ranging from 10-40 bar instead of 100-175 bar [54]. Solely considering reaction rates, wollastonite appears to be the optimal choice as a feed material. However, based on the carbonation reaction presented in Section 2.4.1, it can be observed that wollastonite has a lower CO₂ sequestration capacity per unit of feedstock compared to olivine and serpentine. Furthermore, the global availability of wollastonite is limited compared to Mg-silicates, although the exact extent remains unknown. Limited research has been published on the carbonation of wollastonite [26], thus its effectiveness as a feedstock material remains unclear.

2.6.2. Particle Size

As discussed earlier, direct carbonation of silicate minerals leads to the formation of a passivating layer of silica on the exposed surface, which acts as a barrier hindering further carbonation reactions [136]. In order for the mineralization process to continue, this passivated layer needs to be eroded, exposing fresh and reactive surfaces to CO₂. If the passivated layer remains intact, it takes progressively longer for reactants to penetrate through and reach the reactive alkaline-earth metal oxides deeper within the mineral matrix [5].

To overcome this limitation and enhance reaction rates, various methods have been explored, with a focus on increasing the reactive surface area of the mineral rock. Mechanical treatment is one of

the widely studied approaches in the literature. It involves breaking down the mineral lattice into finer pieces to expose a larger cumulative surface area. This is achieved through a sequence of crushing and grinding processes, reducing the particle size of the rock to $<300\text{ }\mu\text{m}$ or smaller, which is necessary to liberate sufficient reactive surface area for reasonable reaction rates. Mechanical treatment equipment typically includes crushers and grinders. Crushers are employed to break large solid pieces into smaller lumps, while grinders further reduce the crushed feed into powders [50].

However, it is important to note that mechanical treatment, especially grinding, is an energy-intensive process. Achieving the required particle size for optimal conversion rates often requires a significant energy input for the entire mineralization system. Thus, a trade-off exists between enhancing the conversion rate of the process and the energy demand associated with grinding to reach the desired particle size [140].

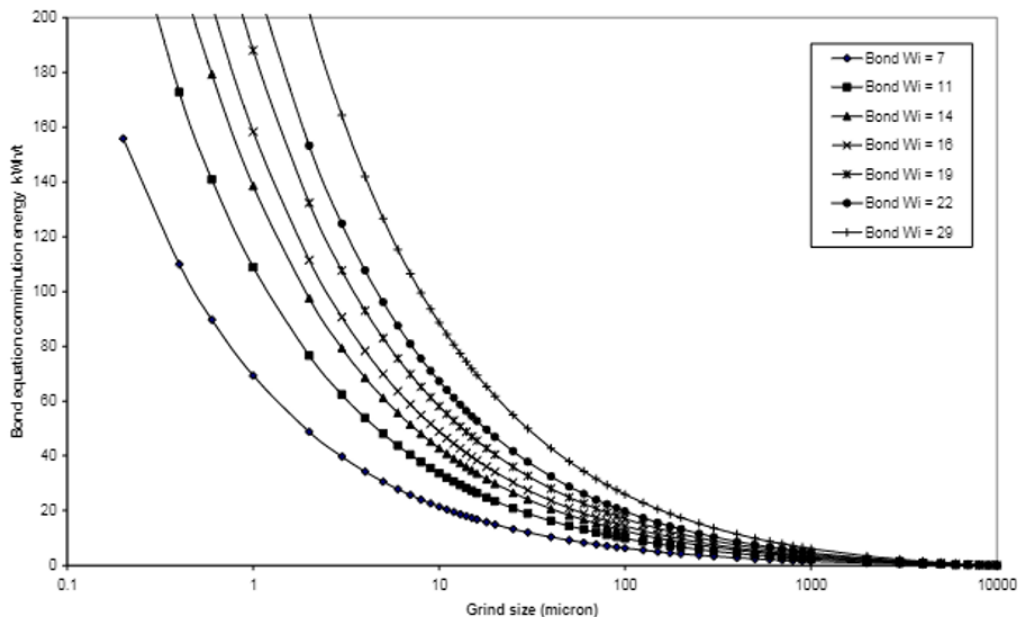


Figure 2.16: Particle grind size versus specific comminution energy
[30]

Figure 2.16 shows the relationship between the particle size and the comminution energy required for that particle size with varying bond working indexes. As one can see, the energy requirements increases exponentially below the $10\text{ }\mu\text{m}$ range.

2.6.3. Temperature and Pressure

Ex-situ carbon mineralization research often involves utilizing high pressure and temperature to accelerate the carbonation process. Figure 2.17 depicts the relationship between temperature and the partial pressure of CO_2 on mineral carbonation, as demonstrated in an experiment conducted by S.J. Gerdemann et al. using olivine [98]. Using Gerdemann's experimental model as an example, it is observed that the reaction extent increases exponentially for low to mid temperatures. However, beyond a certain temperature, the carbonation extent begins to decrease with further temperature increase. Most literature suggests that the ideal temperature range for carbonation falls around 185°C [106] [37]. There are two factors working against raising the temperature: (1) decreased carbon dioxide solubility, and (2) reduced thermodynamic favorability of the reaction. Consequently, beyond a certain temperature, the overall extent of reaction decreases.

However, a revelation was discovered in a study by Dea Hyun Moon et al. [60]. Under high pH conditions and in the presence of numerous cations in the solution, CO_2 is rapidly absorbed into the alkaline solution. Simultaneously, the dissolved CO_2 reacts with ions present in the solution. In cases where the chemical reaction between dissolved ions is more rate-determining than CO_2 solubility in

aqueous solution, the total reaction rate exhibits an opposite effect, where solubility of CO_2 increases with temperature.

Regarding pressure, increasing the partial pressure of CO_2 also enhances the extent of the reaction. This can be attributed to the increased activity of CO_2 , as pressure pushes the reaction towards completion due to the volume change caused by the consumption of gas as CO_2 is converted into solid carbonate. Figure 2.17 demonstrates that the rate of increase in carbonation extent diminishes at higher pressures, indicating that further increasing the pressure at already high levels will not significantly enhance the carbonation extent.

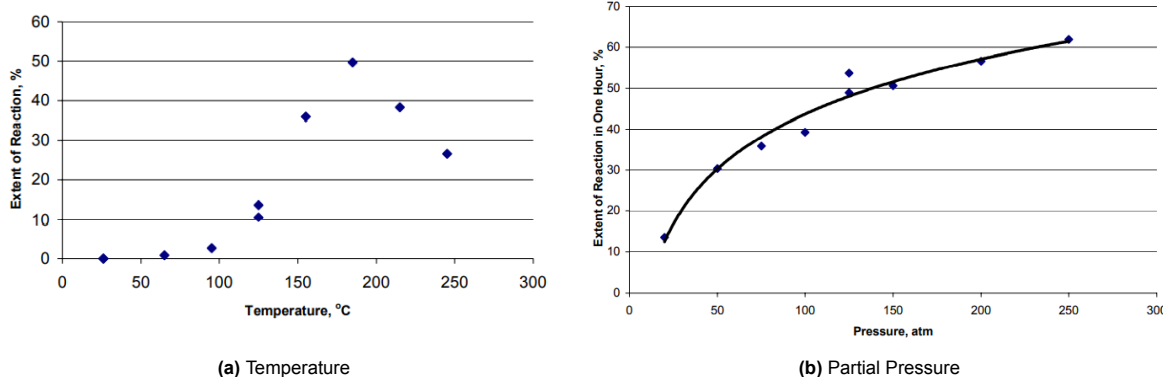


Figure 2.17: Effect of temperature and partial pressure of CO_2 on carbonation of Twin Sisters Olivine [98]

2.6.4. Water or Steam

In all the ex-situ mineral carbonation developments, direct aqueous route still provides one of the most promising and consistent carbonation conversion rates in literature to date [61]. This is due to the fact that the presence of water significantly enhances the dissolution rate of the minerals which subsequently increases its carbonation rate. As mentioned in Section 2.5.1, in the presence of water carbon dioxide dissolves resulting in a mildly acidic environment with HCO_3^- as the dominate carbonate species. The dissolved CO_2 can be further increased by increasing the pressure. Next, leached Mg/Ca ions from the silicates via the consequent reactions with the H^+ protons reacts with the carbonic acid and precipitates into magnesium/calcium carbonate. Aqueous mineral carbonation has been shown, in principle technically and energetically feasible thanks to the obtained acceleration of the reactions resulting in applicable reaction rates.

One of the studies that has been conducted in order to prove the effectiveness of water in facilitating CO_2 mineralization is through the works of Huijgen et. al. [134]. They studied the direct aqueous carbonation of finely grounded wollastonite mineral to particle size $38\ \mu\text{m}$ that was suspended in distilled water. A CO_2 stream was introduced into the reactor under continuous stirring to ensure dispersion of the gas. The carbonation reactions occur in the aqueous phase in two steps: calcium leaching from the CaSiO_3 matrix and nucleation and growth of CaCO_3 . A promising conversion of 75% was attained after 15 minutes residence time at 200°C and 20 bar CO_2 , with estimated costs of €102 per t- CO_2 sequestered, based on process simulation conducted in Aspen.

As mentioned in subsection 2.6.3, since higher temperatures and water are some of the critical factors in accelerating the carbonation process of carbon dioxide, the application of steam is ideal in this case as it fits these two criteria. Many researchers have reported significant improvements on the carbonation of CaO -based sorbents by adding steam [139] [75]. In a study investigating the effects of steam and simulated syngas on CO_2 capture, Symonds et.al. [75] found that steam significantly promotes absorption of CO_2 . The author hypothesized that the reaction is catalyzed by H_2O by means of formation of transient $\text{Ca}(\text{OH})_2$ which is more reactive than is CaO . In other words, they suggested that the fast reaction step, controlled by chemical reaction kinetics, is accelerated in the presence of H_2O . Similarly, in another study by Wei Liu et.al. [139] investigating the effects of steam for CO_2 sequestration of fly ash, it was discovered that steam has an activation effect on the pore structure of fly ash thus increasing the pore volume, BET surface area and consequently the carbonation of fly ash.

2.6.5. pH

Traditional mineralization processes was studied at high temperatures with the acidifying help of pressurized CO₂ to accelerate the overall rate limiting step, namely the dissolution of the feed material [134]. Such operating conditions entails substantial costs increase, as well as careful consideration of the mineralization plant's design to handle such extreme conditions.

In Section 2.5.2, it was mentioned that pH is one of the methods that exist for indirect carbonation method. This is due to the fact that different pH environments favors different processes for CO₂ mineralization. Figure 2.18 shows a simple representation of a temperature-pressure two step carbonation process. This process is attractive in the fact that it avoids high temperature and pressure and instead utilises a pH-swing concept and is being developed to avoid the large CO₂ and energy penalties associated with high-pressure carbonation.

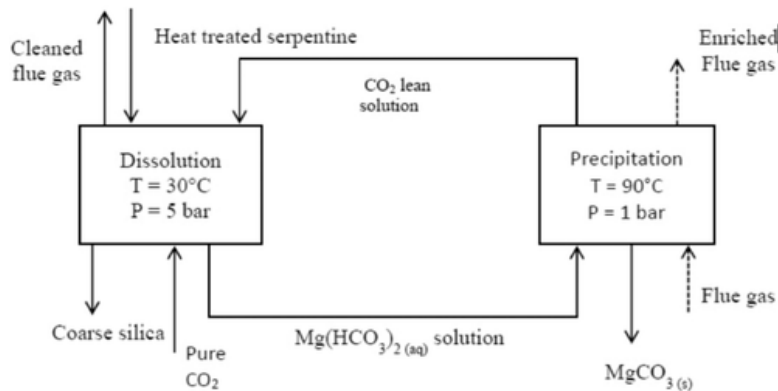
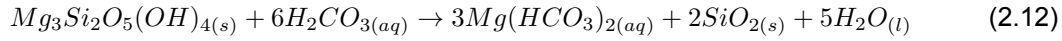
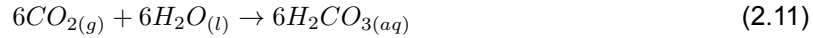


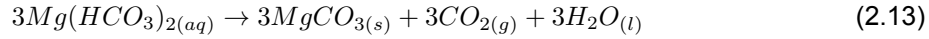
Figure 2.18: Temperature-Pressure Swing Process
[140]

The two-step carbonation process uses two reactors, the first is a low-temperature, high-pressure reactor in which dissolution of magnesium from the mineral ore occurs and the second is a high-temperature, low pressure reactor in which precipitation occurs. The dissolution and precipitation are favored in their respective working conditions due to the change in pH associated with the temperature and pressure changes. In more detail, the process consists of a dissolution reactor (R1) operating at 30°C (sometimes higher or a reactor under changing temperature conditions)with a CO₂ pressure of 5 bar and the precipitation reactor (R2) operates at 90°C and 1 bar [140]. The chemical reactions that occur in the process are described below:

Dissolution (R1):



Precipitation (R2):



However, for this particular process only the usage of serpentine was reported. In addition, the serpentine was first pre-heated to 630°C to gain a reasonable reaction rate before undergoing mineralization using the system above. Therefore, although the process in itself is not energy intensive due to the low working pressures and temperatures, the pre-treatment of serpentine is highly energy demanding. Furthermore, there are no existing literature that conducted the same process using other available feedstock which makes its effectiveness remain unclear.

2.7. Cost of Mineralization

In order to meet the 1.5°C target of the Paris agreement, 125 GtCO₂ has to be removed from the air and permanently stored by 2100 [109]. As mentioned in Section 2.3, mineralization reactions can take place either below (in situ) or above (ex situ) ground. In situ mineral carbonation is estimated to cost around \$7-\$30 per ton of CO₂ sequestered (storage costs only). Storage of a total of 125 Gt CO₂ would result in a capital input of approximately 1-4 trillion dollars in total and 10-50 billion dollars per year until 2100. To put it into perspective, the total cost of the energy transition, i.e. decarbonizing the energy sector was estimated to be 1.6-3.8 trillion dollars until 2050 [4].

For ex situ carbon mineralization, although it has the potential to carbonate many GtCO₂/year when using industrial waste, wollastonite and olivine [29], the process is more expensive than the projected cost of direct air capture of CO₂, and significantly more expensive than CO₂ storage via in situ method. The projected cost is about 10 times higher than CO₂ injection and sequestration into subsurface reservoirs [109], depending on the reactants and the mineralization technique. The reason being the extra costs associated with heating and transportation of the minerals from mine tailings etc.

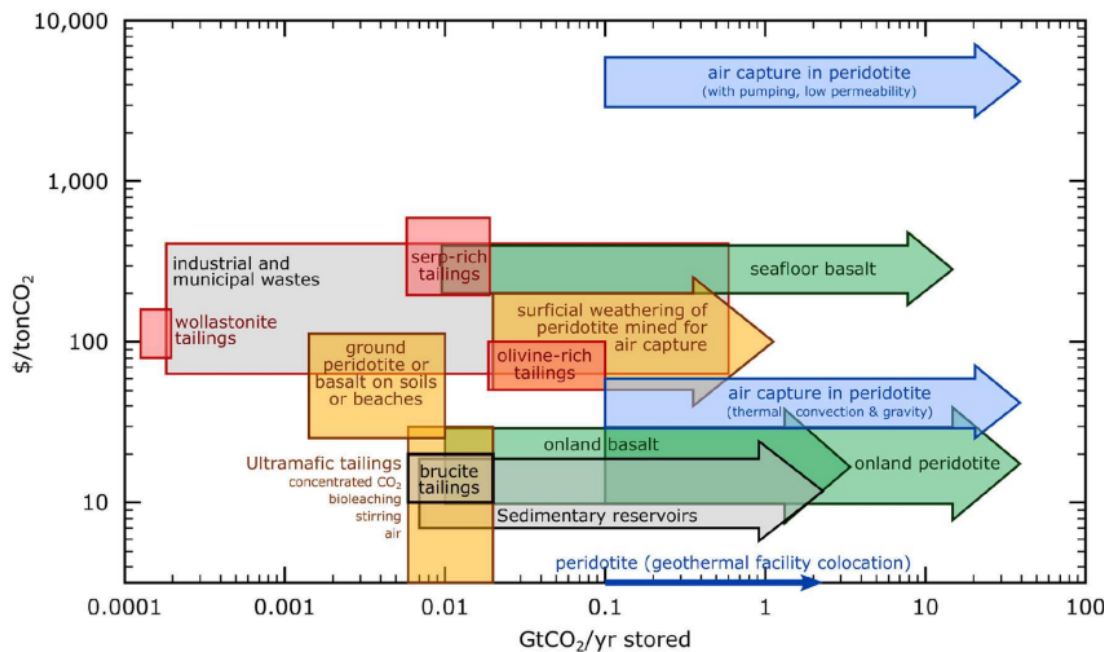


Figure 2.19: Summary of cost of CO₂ stored vs. storage potential of CO₂ per year in Gt
[133]

Figure 2.19 shows the summary of the cost of CO₂ stored in US\$/t-CO₂ to the storage potential of CO₂ in Gt-CO₂/year. The red boxes illustrate costs and rates for ex-situ CO₂ mineralization using heat and concentrated CO₂. Yellow boxes are for surficial CO₂ mineralization of mine tailings, of ground peridotite added to soils or beaches, and of peridotite mined and ground for the purpose of CO₂ removal from air with solid storage. Green arrows are for in-situ carbon storage by injection of CO₂-enriched fluids into mafic and ultramafic formations. Blue arrows are for in-situ carbon sequestration by circulating water saturated in air into peridotite formations, for CO₂ removal from air with solid storage. Gray arrow is for in-situ carbon sequestration by injecting supercritical CO₂ into subsurface sedimentary formations [133]. Given that ex situ carbon mineralization is still under development, there are still plenty of research gaps in the field that needs to be optimized before carbon mineralization can be deployed on a commercial scale.

3

Design Selection

Chapter 2 delves into a comprehensive exploration of the pertinent knowledge and information concerning the CO₂ mineralization process. Additionally, Section 1.2 outlines the particular aim and objectives of the research project. Building upon these foundational chapters, the current chapter directs its attention toward the approach used to evaluate various criteria crucial for an efficient CO₂ mineralization system. Parameters such as process type, feedstock used, pressure, temperature, particle size, as well as flow concentrations will be taken into account.

3.1. Feed Mineral Selection

As discussed in Section 2.4.1, three natural minerals, namely olivine, serpentine, and wollastonite, have been commonly used for CO₂ mineralization. These minerals need to be studied to determine which one exhibits the most desirable characteristics for the CO₂ capture and mineralization system. Table 3.1 presents a comparison of these minerals based on parameters such as abundance, price, reactivity, and pre-treatment processes.

Upon examination from literature, it was deduced that serpentine is not suitable to be used as a feedstock for this system due to its requirement for pre-heating at temperatures as high as 630°C, which is not favorable from an energy perspective. On the other hand, both olivine and wollastonite demonstrate favorable characteristics for some of the specified parameters, making it difficult to make a clear distinction between the two. Therefore, a more comprehensive analysis is necessary to determine which mineral is best suited for the system. This analysis was carried out in Section 3.4.

Parameters	Olivine	Serpentine	Wollastonite
Abundance	High	Moderate	Low
Price	Low	Moderate	High
Reactivity	Low	Low	High
Pre-Treatment	Grinding	Grinding	Grinding
	-	Pre-Heating	-
	High P & T	High P & T	Low P & T

Table 3.1: Comparison between natural minerals

3.2. Direct Carbonation vs Indirect Carbonation

Next, it is important to determine the suitable process or mineralization method for the CO₂ capture + mineralization system. As discussed in Section 2.5, there are two main types of processes: direct carbonation and indirect carbonation. Indirect carbonation is known to have higher reaction efficiency compared to direct carbonation, achieved through the use of acids and bases. However, the regeneration of these chemicals poses challenges in terms of implementation and energy requirements, as

illustrated in Figure 2.12 and Figure 2.13 in Section 2.5.2. A summary of the comparison between direct and indirect carbonation based on knowledge retrieved from literature can be found in Table 3.2.

Considering the simplicity of direct carbonation, where reactions occur in a single reactor (one-step process), and the potential to compensate for slow reaction rates through various pre-treatment processes, this carbonation method was chosen for further exploration. As a result, focus will be solely on direct carbonation and exclude indirect carbonation from the subsequent investigation. As mentioned in Section 2.5.1, direct carbonation can be classified into gas-solid carbonation and direct aqueous carbonation. Both processes will be evaluated to assess the ideal process to be used for the system.

Parameters	Direct Carbonation	Indirect Carbonation
Reaction Step	Single	Multiple
Carbonation Efficiency	Moderate	High
Additives	No	Yes
Complexity	Low	High

Table 3.2: Comparison between carbonation routes

3.3. Design Methods

This chapter aims to construct process models that simulate reactions and their energy consumption based on existing literature. For this purpose, the "Aspen Plus V12" software is employed due to its suitability with the parameters under comparison and the process used. In addition to technical considerations, economic factors, including feedstock costs and transportation costs, are also taken into account to facilitate decision-making. In this section, the design methods that are considered to develop the process model are outlined.

3.3.1. Boundary Conditions

In this chapter on design selection, in order to make a valid comparison between different processes it is crucial to identify the elements that are being considered and calculated, as well as those that are neglected. Figure 3.1 illustrates the boundary conditions set for this chapter, with the primary focus placed on the internal aspects of the mineralization process. Comparison of the different processes will encompass elements such as compression energy, the mineralization reactor and subsequent reaction, grinding energy, and pumping energy are being taken into account, while the remaining elements are neglected.

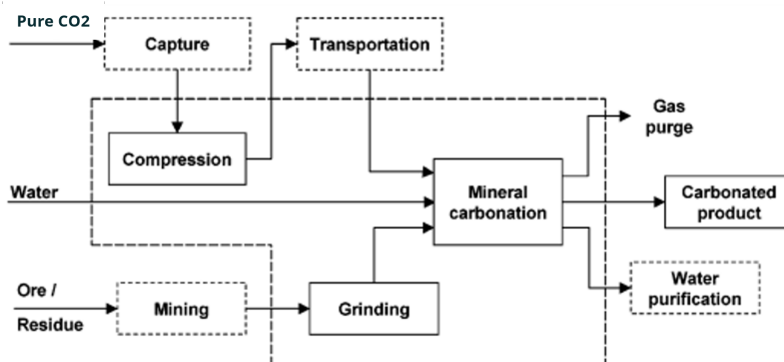


Figure 3.1: Boundary conditions for design selection
[134]

3.3.2. Partial Pressures

In the process described in Section 3.4 for the olivine feedstock, the pressure, temperature, and reaction efficiency data were obtained from the study by DaCosta et al [101]. However, it should be noted that the

author used a composition of flue gas, whereas this system involves capturing carbon dioxide directly from ambient air (i.e., pure CO₂). Therefore, adjustments need to be made to the partial pressures of CO₂ used to account for the use of pure CO₂. This adjustment can be made using Dalton's Law, also known as the law of partial pressures, which states that the total pressure exerted by a gas mixture is equal to the sum of the partial pressures of the individual gases in the mixture [72]. The application of Dalton's Law can be expressed as follows:

$$P_{total} = P_A + P_B + \dots \quad (3.1)$$

to which assuming a working pressure of 100 bar for DaCosta's method, at 15% CO₂ and 8.3% H₂O would yield 15 bar of pressurized CO₂ and 8.3 bar of water vapor. In total this would give an approximate total pressure of around 24 bar. Furthermore, for the data involving wollastonite as the feedstock for the gas-solid carbonation comparison, since the reference data uses a pure CO₂ stream, Dalton's law is therefore not needed.

3.3.3. Grinding Energy

The grinding energy required for the energy consumption comparison can be calculated by using Bond's equation [9]:

$$W = \frac{10W_i}{\sqrt{P}} - \frac{10W_i}{\sqrt{F}} \quad (3.2)$$

with F being the original particle size of the feedstock, P being the imaginary sieve size through which 80% of the ground feedstock passes, and W_i the standard Bond's working index. In the case of a grinding step with a final particle size requirement of < 70 µm, an extra multiplier of:

$$\frac{(10.6 \times 10^{-6} + P)}{1.145 \times P} \quad (3.3)$$

will be applied, as used by Aspen [134]. The standard Bond's working index (W_i) for olivine was set at 18.9 kWh/ton, considering that olivine is commonly found in basaltic rocks, which have a Bond's working index value of 18.9 kWh/ton [81]. On the other hand, the Bond's working index for wollastonite was set at 14 kWh/ton, based on the average working indices of limestone (11.6 kWh/ton) and silica sand (16.5 kWh/ton) [134].

Following the approach used by the Albany Research Center [90], it was assumed that both olivine and wollastonite ores were firstly ground to a particle size of <200 mesh (approximately 75 µm) from an initial size of 0.1m. Following this, they underwent a second grinding step to achieve the desired particle size. An energy penalty of 4 kWh/ton was considered for the beneficiation step.

3.3.4. Equation of State

The gas-solid reactions in Section 3.4 for both olivine and wollastonite, as well as the direct aqueous carbonation in Section 3.5 for olivine, were modeled using the Peng-Robinson equation of state. This choice of model in the Aspen Plus process simulation was based on three goals [103]:

- The parameters should be expressible in terms of the critical properties.
- The model should provide reasonable accuracy near the critical point, particularly for calculations of the compressibility factor and liquid density.
- The mixing rules should utilize a single binary interaction parameter that remains independent of temperature, pressure, and composition.

Considering that some of the processes mentioned in the literature operate at critical pressures and temperatures, the Peng-Robinson equation of state can provide a near-accurate representation of the specified values. For the properties of free water, the SteamNBS model was employed due to its suitability for the desired working conditions of the system, as well as its reliable convergence and extrapolation properties at high pressures and temperatures [95].

In the case of direct aqueous carbonation, the Peng-Robinson equation of state with Modified Huron-Vidal mixing rules (PRMHV2) is the chosen property method, as suggested by Wouter J. J. Huijgen [134]. This selection was based on the consideration of a polar non-electrolyte system operating at pressures above 10 bars. The decision to treat the system as a polar non-electrolyte was made because of the motivation that the influence of ions leached from solids and the dissolution of gaseous CO₂ and salt additives on the system's thermodynamic properties will be neglected for the simulation. Huijgen also neglected this consideration in his paper. However, the effects of dissolved ions on the carbonation reaction are implicitly taken into account in the definition of conversion in the carbonation reactor.

The decision-making process for choosing this property method can be summarized from an article by Eric C. Carlson on selecting appropriate property methods for simulations [14]. A segment of the decision tree is shown in Figure 3.2. As depicted in the figure, for polar non-electrolyte systems operating above 10 bars, PRMHV2 is deemed a suitable option.

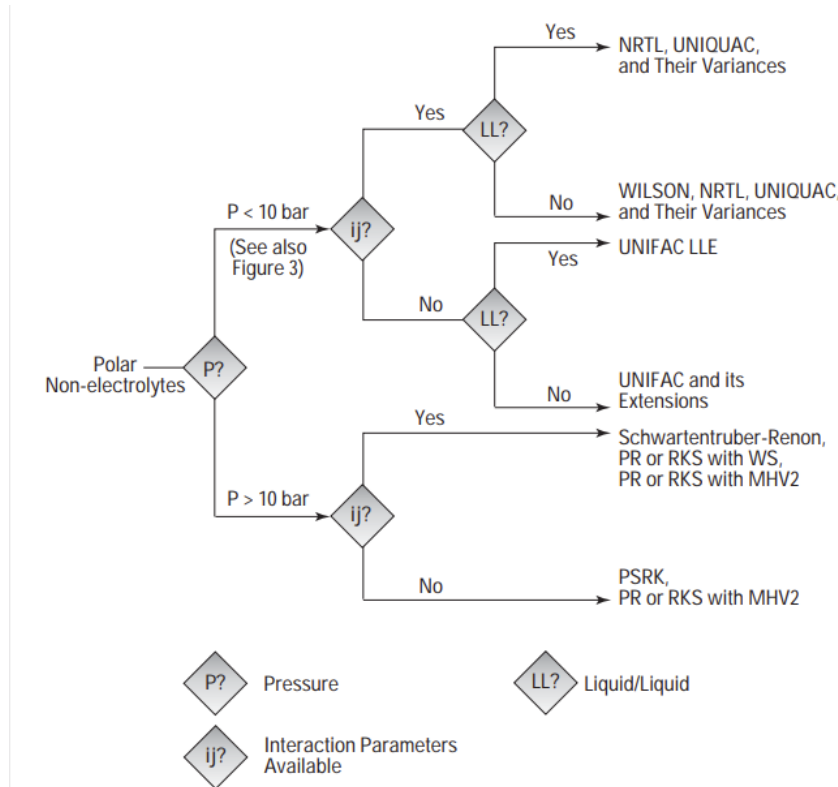


Figure 3.2: Proceeding for polar and non-electrolyte components
[14]

3.3.5. Reaction Kinetics

The rate of CO₂ mineralization is influenced by various kinetic factors, such as the CO₂ concentration, reactivity of the mineral reactants, and availability of reactive surface area. Understanding and optimizing these kinetics is crucial for the efficient implementation of CO₂ mineralization as a carbon capture and storage (CCS) technique. Kinetics play a key role in determining the rate at which CO₂ is converted into solid minerals. Faster reaction kinetics can result in higher carbon sequestration rates, leading to a more efficient process [51]. The rate of the mineralization process, denoted as r , can be determined using the following equation:

$$r = k(T)f(x) \quad (3.4)$$

where $k(T)$ is the rate constant, T is the reactor temperature, and $f(x)$ is a kinetics-model-dependent function [60]. For this investigation, first-order reaction kinetics will be employed due to the unavailability of certain parameters specific to the chosen working conditions based on literature, as discussed in

Section 3.4 and Section 3.5. Moreover, considering the concentration of CO₂ plays a significant part in how well the system performs, the function f(x) was set to be the CO₂ concentration parameter, denoted as α . As a result, the reaction rate can be expressed as:

$$r = k(T)[\alpha] \quad (3.5)$$

The rate constant k is expressed using the Arrhenius equation,

$$k = A \exp\left(-\frac{E_a}{RT}\right) \quad (3.6)$$

where A, E_a, and R are the pre-exponential factor, apparent activation energy, and universal gas constant, respectively. It is important to note that the data obtained from the two papers in literature for gas-solid carbonation and direct aqueous carbonation correspond to different working pressures (i.e., 24 bar and 36 bar; 150 bar and 115 bar, respectively). Therefore, prior research is necessary to determine the extent to which these pressure differences influence the overall performance of the system and whether they may affect the integrity of the comparison of these processes.

3.4. Gas-Solid Carbonation Comparison

To ensure the validity of the comparison between gas-solid carbonation and direct aqueous carbonation, it is essential to investigate the potential impact of different working pressures on the reaction rate. Understanding the influence of varying pressures is crucial, as significant differences in reaction rates could undermine the validity of the comparison.

In this analysis, the rate constant equation described in Section 3.3.5 is considered. The activation energy (E_a = 43.2 kJ/mol), pre-exponential factor (A = 2.30E+06), and universal gas constant (R = 8.314 J/(K mol)) are assumed to be fixed values [116] which subsequently makes pressure and temperature as the manipulated variables. In the rate constant equation, the temperature (T) is the variable that affects the rate constant (k).

The graph below depicts the relationship between k and ln(k):

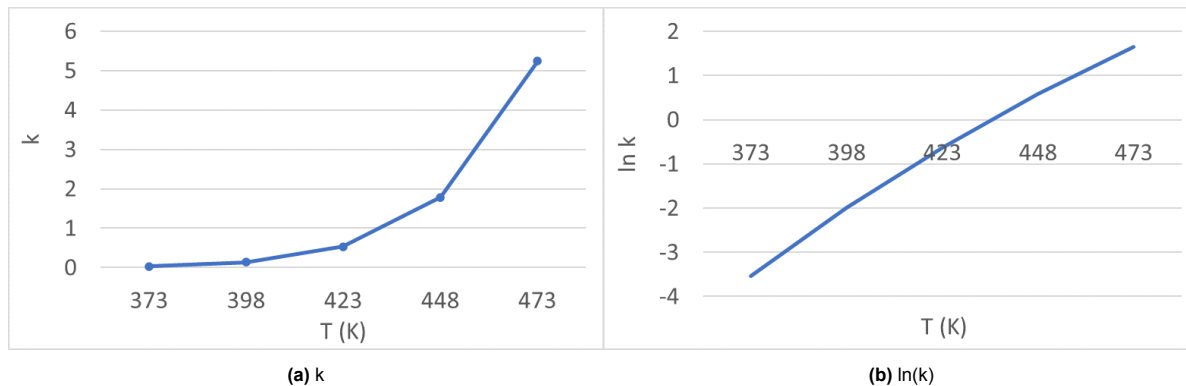


Figure 3.3: Rate constants k and ln(k) as a function of temperature

The graph above clearly demonstrates the exponential growth of the reaction constant as temperature increases. By utilizing the varying reaction constants and the parameters outlined in Section 3.3.5, the reaction rate can be determined.

As discussed in Section 2.6.3, increasing CO₂ pressure enhances carbonation efficiency. This correlation is further supported by Henry's Law, which is briefly explained in Section 2.5.1. Since the concentration of CO₂ is directly proportional to the pressure of the solution, the CO₂ concentration parameter, denoted as α , can also be expressed in terms of pressure.

This analysis results in the generation of reaction rate graphs, as depicted in Figure 3.4. The graph on the left shows the trend line of the reaction rate at a pressure of 1 bar, indicating that increasing the reaction temperature exponentially enhances the reaction rate, consistent with the reaction constant (k). On the other hand, the graph on the right presents the natural logarithm, ln(r), as a function of

temperature with varying pressures (CO_2 concentrations). It is evident that $\ln(r)$ increases with higher pressures. However, the rate of increase diminishes as the pressures approach higher values.

Based on this data, it can be inferred that comparing mineralization processes using different pressure values is valid given the pressures are high enough, as to not significantly influence the reaction extent. Consequently, this would make the energy requirements associated with the various working pressures would play a more dominant role in determining the effectiveness of the processes in terms of overall costs.

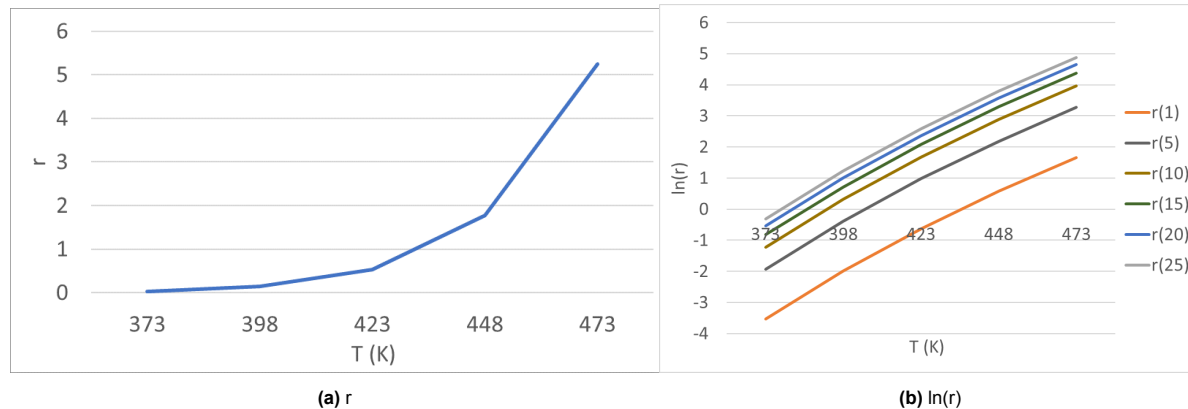


Figure 3.4: Reaction rate as a function of temperature with varying pressures

Direct carbonation can be mainly distinguished into two main processes, gas solid carbonation and direct aqueous carbonation. Various research has been conducted based on literature to improve on these methods while still aligning with their main carbonation characteristics. To facilitate a comparison, the initial calculation phase in this study aims to provide a preliminary estimation of the numbers and values, which should already demonstrate significant differences between the processes. The following is a summary of the property settings configured in Aspen Plus for the development of a simulation model.

Parameters	Specifications
Components	$\text{CO}_2, \text{H}_2\text{O}, \text{Mg}_2\text{SiO}_4, \text{MgCO}_3, \text{CaSiO}_3, \text{CaCO}_3, \text{SiO}_2$
Property Method	Peng-Robinson Equation of State
Free Water Method	Steam NBS
Reaction	$\text{Mg}_2\text{SiO}_4(\text{s}) + 2\text{CO}_2(\text{g}) \rightarrow 2\text{MgCO}_3(\text{s}) + \text{SiO}_2(\text{s})$ $\text{CaSiO}_3(\text{s}) + \text{CO}_2(\text{g}) \rightarrow \text{CaCO}_3(\text{s}) + \text{SiO}_2(\text{s})$
Heat of Reaction	-89 kJ/mol [3] -87 kJ/mol [134]

Table 3.3: Properties for gas-solid carbonation

Now that the properties of the system has been specified, the simulation model can be developed. Below is the overview of the process flowsheet of a gas-solid carbonation used for both olivine and wollastonite.

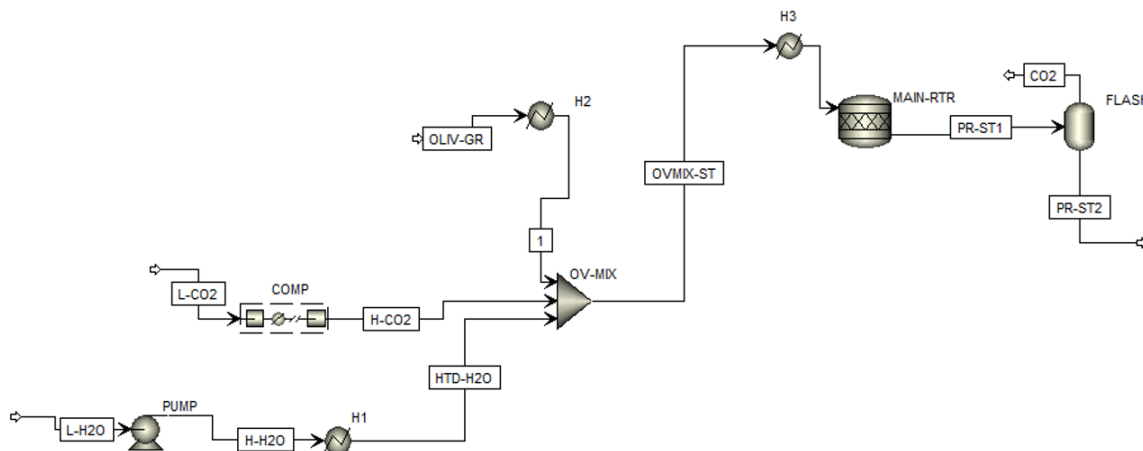


Figure 3.5: Gas-solid carbonation process flowsheet from Aspen Plus

The functions of each unit operation depicted in Figure 3.5 are summarized in Table 3.4. Additionally, Table 3.5 provides information on the working conditions and flow rate requirements of the system, based on literature data.

Regarding reactor selection, since the literature data already includes the reaction efficiency for each specified reaction, using a stoichiometric reactor would provide a straightforward representation of the reactor's behavior in terms of the resulting end products and the amount of generated exothermic heat that can later be considered.

Unit Operation	Specifications
Pump	Efficiency = 0.8
Compressor	Isentropic; 3-stage compressor with intermediate cooling to 20°C
Reactor	Stoichiometry reactor; Isothermal operation;
Flash Drum	Assumes perfect separation of streams
Mixer	Pressure drop = 0 bar

Table 3.4: Unit operations for gas-solid carbonation

Olivine		Wollastonite	
Parameters	Specifications	Parameters	Specifications
Pressure	24 bar	Pressure	36 bar
Temperature	150°C	Temperature	200°C
CO ₂ Flow	158 kg/day	CO ₂ Flow	158 kg/day
Olivine Flow	252 kg/day	Wollastonite Flow	252 kg/day
H ₂ O Flow	184 kg/day	H ₂ O Flow	184 kg/day
Mineralization Capacity	18%	Mineralization Capacity	75%

Table 3.5: Material specifications and working conditions for gas-solid carbonation

From the table above, for the gas-solid carbonation of olivine, the data provided by DaCosta et.al. [79] was used to simulate this mineralization process. In their work, it was specified that a flue gas composition of 15% CO₂ and 8.3% H₂O vapor at a pressure range of 100-150 bar and temperature 150°C was used that reported a mineralization capacity of 18% (0.18g of CO₂ per gram olivine).

For the gas-solid carbonation of wollastonite, data was retrieved from the paper published by Wouter J. J. Huijgen et. al. [134]. In this process, CO₂ is subjected to a pressure of 20 bar and water vapor at

16 bar, which according to Dalton's law explained in Section 3.3 would give the overall working pressure of 36 bar, as outlined in Table 3.5. The temperature was set at 200°C and the overall efficiency that was reported for this process is 75%. It is worth noting that Huijgen also made a model constructed in Aspen Plus as seen in Figure 3.6 below:

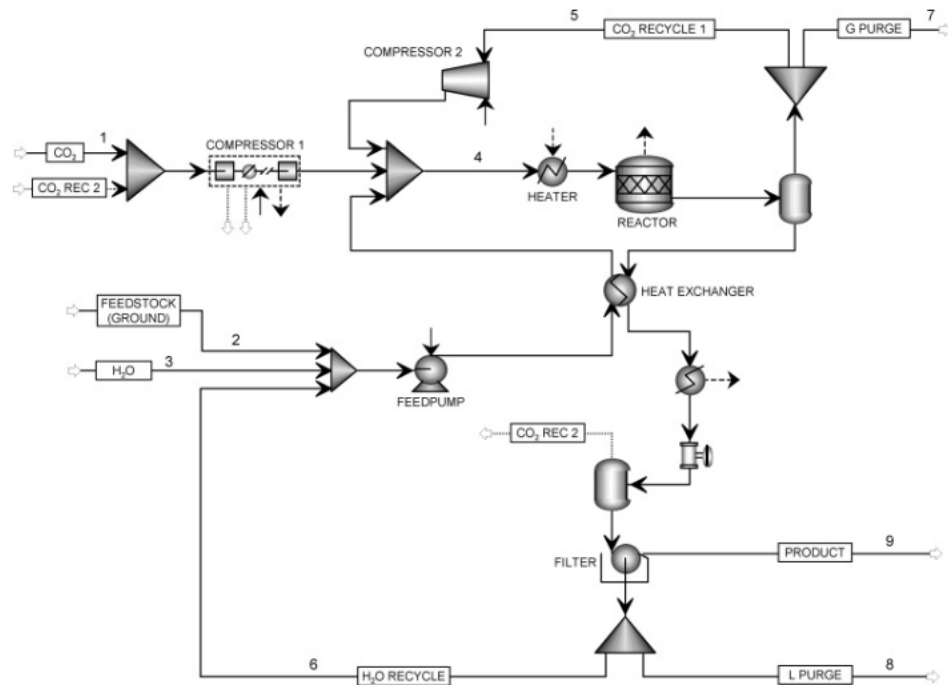


Figure 3.6: Huijgen's model for gas-solid carbonation using wollastonite

However, for the comparison of these two natural minerals, a different model was used. The model proposed by Huijgen is already optimized in terms of heat integration and recycled streams. In contrast, the initial comparison conducted here is a simplified calculation that does not take these components into account. Therefore, a modified version of the model shown in Figure 3.5 was adapted and adjusted based on the specifications outlined in Table 3.5 specifically for wollastonite.

The results of the process simulations for olivine and wollastonite are presented in Figure 3.7. Mineral heating refers to the mineral being heated to the desired reaction temperature as well as removing impurities from the mineral whereas water heating refers to water being heated up to become steam. The units of the figures below are per ton of CO₂ sequestered.

In this analysis, the units for electrical energy and thermal energy were defined as kWh per ton of CO₂ sequestered (mineralized), with an energy price set at €0.08 per kWh. This pricing approach allows for a better assessment of the differences between the systems, as the primary objective of an efficient mineralization plant is to sequester the maximum amount of CO₂ at the lowest possible cost. The results reveal a significant disparity in total energy consumption between the olivine-based system and the wollastonite-based system. This difference arises from the varying efficiencies of the two processes.

However, evaluating the overall performance of the systems based solely on energy requirements is insufficient. Other factors such as transportation costs and feedstock prices must also be considered. In this analysis, the feedstock prices were set at €70/ton-mineral for olivine [91] and €273/ton-mineral for wollastonite [28]. Regarding transportation, both minerals are assumed to be transported to the Netherlands via cargo ship from Finland, taking into account the availability of resources in both countries [28] [67]. The transportation costs are assumed to be included in the mineral prices. However, for the transportation of the plant's products, a rough estimation was made using truck transport with a cost of €0.11/km [97] over a distance of 150 km.

With consideration of these transportation aspects, an assessment of the costs is presented in Figure 3.8. It can be observed that despite wollastonite's high carbonation efficiency which is shown in terms of low total energy requirements from Figure 3.7a, its overall costs exceed those of olivine. The

high price of wollastonite overshadows its high carbonation efficiency and supports the information mentioned in Section 2.4.1 that its abundance is still uncertain, where the mineral's price reflects this uncertainty. Based on this comparison, it can be concluded that olivine is the preferable choice of feedstock.

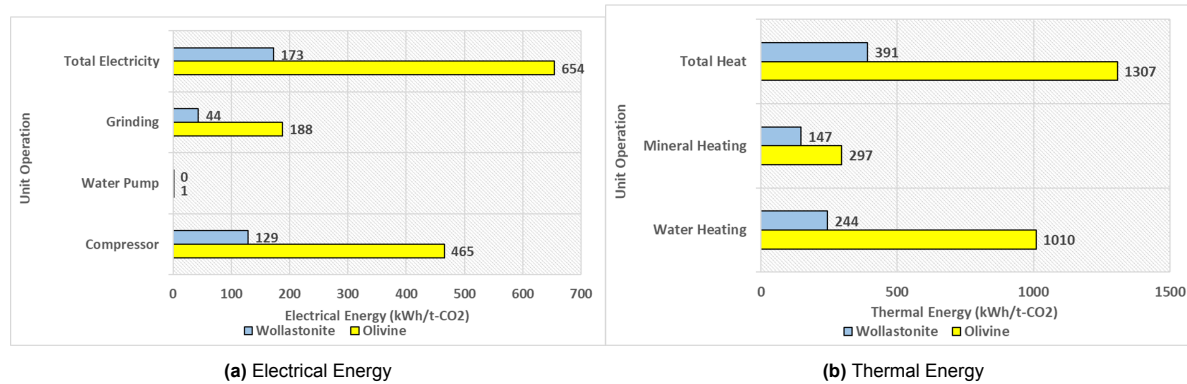


Figure 3.7: Electrical and thermal energy for olivine vs wollastonite

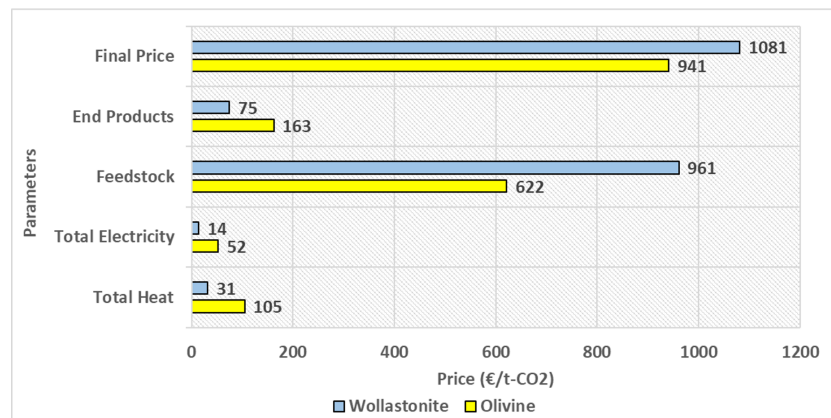


Figure 3.8: Price comparison for olivine vs wollastonite

3.5. Direct Aqueous Carbonation Comparison

Having established olivine as the more cost-effective mineral choice despite its lower reaction rate, the next step is to determine the preferred process within direct carbonation. In the previous section, the calculations for direct gas-solid carbonation were presented. Building on this, the focus will shift to investigating direct aqueous carbonation. As described in Section 2.5.1, this method involves dissolving the mineral in water to form a slurry, which is then combined with CO₂ in a reactor in a single step. The parameters and specifications for direct aqueous carbonation are outlined in Table 3.6.

Parameters	Specifications
Components	CO ₂ , H ₂ O, Mg ₂ SiO ₄ , MgCO ₃ , SiO ₂
Property Method	Peng-Robinson Equation of State with Modified Huron-Vidal mixing rules (PRMHV2)
Free Water Method	Steam NBS
Reaction	Mg ₂ SiO ₄ (s)+2CO ₂ (g) → 2MgCO ₃ (s)+SiO ₂ (s)

Table 3.6: Properties for direct aqueous carbonation

For the material components, it consist of the same compositions as direct gas-solid carbonation except that wollastonite related components have been left out and PRMHV2 is used instead of Peng-Robinson. The unit operation of this carbonation process can be observed in Figure 3.7.

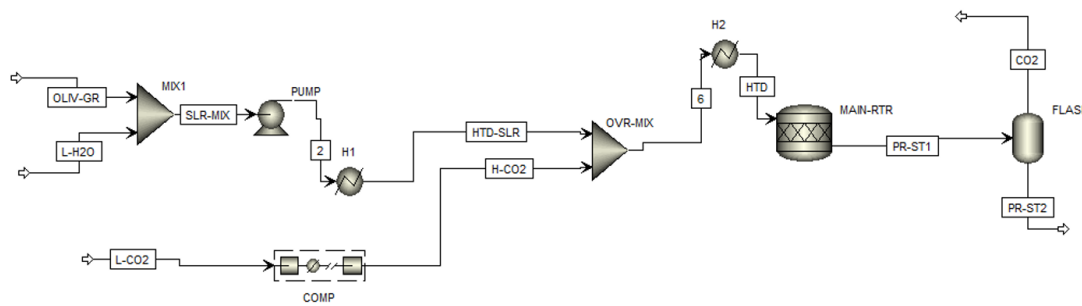


Figure 3.9: Direct aqueous carbonation process flowsheet from Aspen Plus

Unit Operation	Specifications
Pump	Efficiency = 0.8
Compressor	Isentropic; 5-stage compressor with intermediate cooling to 40°C
Reactor	Stoichiometry reactor; Isothermal operation;
Flash Drum	Assumes perfect separation of streams
Mixer	Pressure drop = 0 bar

Table 3.7: Aspen flowsheet components description for direct aqueous carbonation

In the case of direct aqueous carbonation, two comparisons are being made: one using distilled water and the other involving salt additives such as NaCl and NaHCO₃. Data for direct aqueous carbonation using distilled water was obtained from a study conducted by Pavan Kumar Naraharisetti et al. [140]. Their research reported a mineral conversion efficiency of 61% achieved under a pressure of 150 bar, a temperature of 185°C, and a particle size of 38 µm.

On the other hand, data for direct aqueous carbonation with salt additives was obtained from the work of W.K. O'Connor et al. [13]. In their study, a 15% slurry concentration was subjected to pressures up to 115 bars and a temperature of 185°C, using a solution containing 1M NaCl and 0.5M NaHCO₃. This process achieved a conversion rate of 84% with a particle size of 37 µm. The utilization of salts in the slurry solution for this process, which was explained in Section 2.5.1, has been shown to provide significant benefits, as supported by W.K. O'Connor's work.

Furthermore, the choice of similar particle sizes and temperatures in these two processes allows for a more accurate comparison, as particle size and temperature significantly influences the efficiency of mineralization processes. Also, as outlined in Section 3.4, although the two processes employ different working pressures, it should not have a significant influence on the validity of the comparison between these two systems.

By considering these factors and the respective studies, a comprehensive comparison can be made between direct aqueous carbonation using distilled water and direct aqueous carbonation with salt additives. A summary of the parameters and conditions for the process flowsheet in Aspen Plus can be found in Table 3.8. In direct aqueous carbonation, higher pressure levels are employed due to the low solubility of CO₂ gas in water. Consequently, a 5-stage compressor is utilized instead of the 3-stage compressor employed in gas-solid carbonation, with intermediate cooling between stages at 40°C. The mass flows of olivine, CO₂, and water are set based on a 15% liquid-to-solid ratio and following the chemical reaction of the process.

DAC - Without Salts		DAC - With Salts	
Parameters	Specifications	Parameters	Specifications
Pressure	150 bar	Pressure	115 bar
Temperature	185°C	Temperature	185°C
CO ₂ Flow	200 kg/day	CO ₂ Flow	200 kg/day
Olivine Flow	319 kg/day	Olivine Flow	319 kg/day
H ₂ O Flow	233 kg/day	H ₂ O Flow	233 kg/day
Mineralization Capacity	61%	Mineralization Capacity	84%

Table 3.8: Aspen plus parameters for direct aqueous carbonation of olivine

The results of both processes are presented in Figure 3.10. Due to its higher mineralization capacity, it is evident that direct aqueous carbonation with salt additives offers an advantage over using distilled water in terms of total energy consumed per CO₂ sequestered. To assess the transportation costs, the same approach used in comparing direct gas-solid carbonation is applied. Consequently, the total cost of the systems becomes €227 and €306, respectively. The significant price change highlights the difference adding salt additives can make to the overall system.

Figure 3.12 shows the summary of the price comparison conducted in this chapter. It is evident from this figure that direct aqueous carbonation with salt additives is a more favorable process and will be chosen for further research in the following chapter.

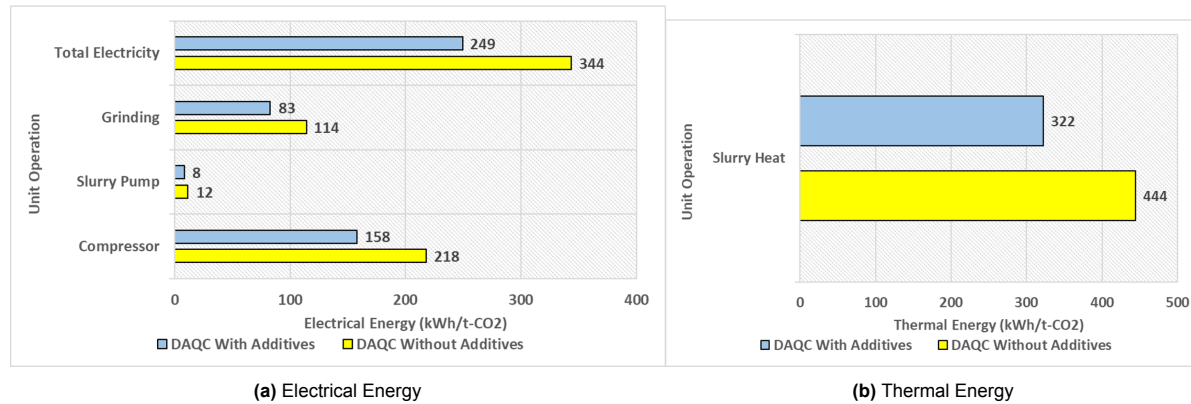
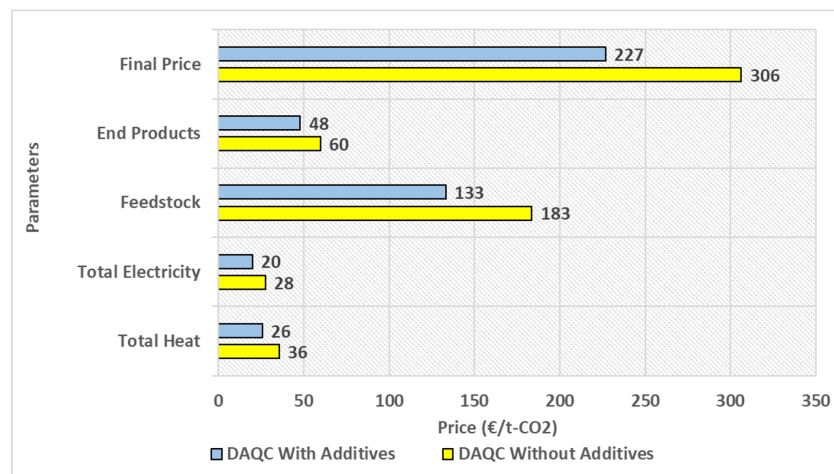
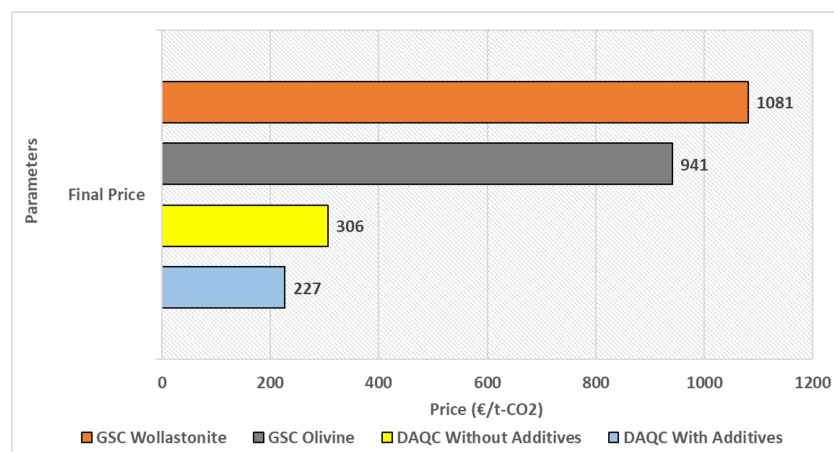


Figure 3.10: Electrical and thermal energy for direct aqueous carbonation

**Figure 3.11:** Price comparison for direct aqueous carbonation**Figure 3.12:** Summary of price comparison for mineralization processes

4

Process Design

Chapter 3 dove into the various criteria associated with an ideal mineralization system, ultimately leading to the decision to adopt a direct aqueous carbonation process with the utilization of salts additives and olivine as the preferred feedstock. In this chapter, the focus will be on evaluating the performance of both the non-integrated system and the integrated system. In order to do that, the final model will be developed in which integration elements such as heat integration and recycled streams will be implemented. The inclusion of a direct air capture unit to the mineralization system will also be assessed.

4.1. Non-Integrated and Integrated System

4.1.1. DAC Unit

The first aspect to be investigated in both the non-integrated and integrated mineralization systems is the direct air capture unit. This unit is responsible for supplying a continuous stream of CO₂ to the system, which can then be used to convert the feedstock into carbonates. It is assumed that the CO₂ supply is sourced from one of Skytree's modular units and is of 100% purity. The desorption of CO₂ from the modular units requires heat energy for the sorbent to release the captured CO₂.

To enable a fair comparison between the two systems, an energy consumption value of 1000-2000 kWh per ton of CO₂ (t-CO₂) will be used.

4.1.2. Final Model

To establish a comparison between the integrated and non-integrated systems, it is essential to outline all the key components present in the final mineralization system model. The process design model for the integrated system is based on the publication by W.K. O'Connor [119]. In this model, a slurry is subjected to pressures of up to 115 bar and temperatures of 185°C. It has been reported that this system achieves an efficiency of 84% when 1M NaCl and 0.5M NaHCO₃ are added to the process.

This section will provide a detailed analysis of each of the main components, including their specifications and performance, in order to gain a comprehensive understanding of their roles within the system.

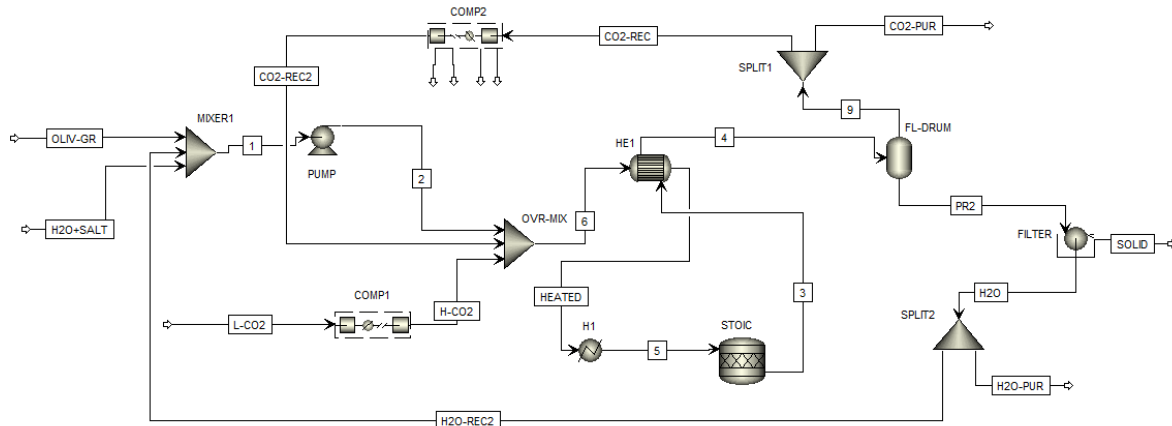


Figure 4.1: Schematic of a heat integrated mineralization system with recycled streams modelled in Aspen

Unit Operation	Description
CO ₂ Flow	200 kg/day
Pump	Efficiency = 0.8
Compressor	Isentropic; 5-stage compressor with intermediate cooling to 40°C
Heat Exchanger	Efficiency = 0.72; Included for integrated system; Removed for non-integrated system
Reactor	Stoichiometry reactor; Isothermal operation
Flash Drum	Isothermal and isobaric; Assumes perfect separation
Splitter	80% purge fractions for both CO ₂ and H ₂ O recycled streams
Filter	Solid separator model; Separation efficiency = 100%
Others	All streams enter the process at 25°C and 1 atm; Product streams and purge streams leave the process at 1 atm

Table 4.1: Aspen flowsheet components description for an integrated direct aqueous carbonation

Figure 4.1 illustrates the final model of the integrated direct aqueous carbonation method, which incorporates heat integration and recycled streams modeled in Aspen. The initial CO₂ stream is modeled at 1 atm and 20°C and is heated in a heater to simulate the desorption temperature.

The heated CO₂ stream is then introduced to a 5-stage compressor with intermittent cooling at 40°C between each stage (except the final stage). The cooling stages help to maintain the temperature within an acceptable range for the compressor's functionality. However, in the last stage, no cooling is applied, allowing the heat generated from the gas compression to contribute to the heating of the slurry mixture in the mixer. This configuration is further discussed in Section 5.6.

The compressed CO₂ stream is combined with the pressurized slurry mixture, consisting of finely ground olivine mixed with water. The slurry mixture is pressurized to the desired temperature before entering the mineralization reactor.

Within the reactor, the reaction mixture is further heated to the designated reaction temperature of 185°C using a heater. The resulting mixture then undergoes separation in a flash drum, assuming perfect separation in the model. However, it is important to note that achieving perfect separation is not possible in real-world scenarios, and optimization of the flash drum is necessary to maximize separation efficiency between the unreacted CO₂ gas, water, and the solid products. Further details on optimization strategies will be covered in Section 5.6. The separated solid products and water then proceed to a filter for additional separation, with a separation efficiency of 100%. The final products obtained from this process include a mix of magnesium carbonate (MgCO₃), silica (SiO₂), and any remaining unreacted olivine (Mg₂SiO₄) in the system.

Recycled Streams

In contrast to the process flow diagram presented in Chapter 3, the process design in this model incorporates recirculated streams for both unreacted CO₂ gas and water, which act as catalysts to enhance the reaction rate. The CO₂ released from the slurry in the flash drum is redirected back to the compressor, where it is recompressed to the reaction pressure. Similarly, water is separated from the solid products through the filtration system and also recycled.

To prevent the accumulation of impurities in the unreacted CO₂ and water streams, purge systems are implemented in the plant design. The CO₂ purge fraction is typically determined based on the composition of the captured gas stream, while the H₂O purge fraction depends on the composition of the water recycle stream. Since specific values are not provided in the reference literature, for this particular case, both purge streams will be set to 0.

It is worth mentioning that for the second compressor, water vapor may be present in some cases. Therefore, as seen in Figure 4.1, the condensed water from recompression (represented by the four arrowed lines) is added to the process water recycle stream. This ensures that any water vapor present in the CO₂ stream is captured and recycled within the system.

Heat Integration

Heat integration is a crucial aspect in optimizing the performance and energy efficiency of a CO₂ mineralization system. It involves effectively managing and utilizing the heat generated during various stages of the process to minimize energy consumption, reduce costs, and improve sustainability. Heat exchangers play a vital role in facilitating heat transfer between different mediums, such as gases and liquids, either through direct contact or via a solid wall to prevent mixing. These heat exchangers enable efficient heat exchange and transfer in the system [57]. Pinch analysis, which is based on fundamental thermodynamics, is a systematic technique used to achieve heat integration and analyze heat flow within industrial processes [58].

In the mineralization system, two key elements contribute to heat integration: the use of a heat exchanger and the utilization of the exothermic heat generated during the mineralization reactions. Mineralization reactions are known for their exothermic nature, meaning they release heat as a byproduct. This excess heat can be captured and effectively utilized within the system for other purposes.

To demonstrate the impact of heat integration, a heat exchanger model was incorporated into the integrated system calculations, whereas it was not included in the non-integrated system calculations. This difference allows for a comparison of the effects of heat integration on the system's performance. The specifications of the heat exchanger used in the integrated model were determined using Aspen Plus software and are presented in the table below:

Parameters	Description
Model	Shortcut
Flow Direction	Counter Current
Specification	Exchanger Duty
Value	1.8 kW
Min. Approach Temperature	5°C
Efficiency	0.72
Hot Stream In	185°C
Hot Stream Out	101°C
Cold Stream In	95°C
Cold Stream Out	156°C

Table 4.2: Heat exchanger parameters

To expedite the process, a shortcut model was employed in Aspen instead of modeling the entire heat exchanger unit. Counter-current flow was selected due to its higher transfer efficiencies compared to parallel flow. The minimum approach temperature, which signifies the minimum permissible temperature difference between a heat source and a heat sink in designing an energy-efficient heat exchanger network [115], was set to 5°C as to prevent costly over-design associated with very low

approach temperatures [138]. The Aspen simulation showed heat transfers that resulted in the cold stream being heated up to 156°C and the hot stream being cooled down to 101°C. The efficiency of the heat exchanger was not explicitly specified but after running the simulation, it was shown to have an efficiency of 72%.

In addition to the utilizing residual heat with a heat exchanger, there is also excess heat available from the reactor that can be effectively utilized. The stoichiometry reactor used in the model generated a total exothermic heat of -4.129 kW based on the calculations computated in Aspen, with the negative sign indicating heat release from the reaction. Since this reaction has a residence time of 6 hours, this means that for an hour it has an exothermic heat value of 0.69 kW per hour. From Figure 4.1, it can be seen that there are two main components that require heat supply: the direct air capture unit for CO₂ desorption and the second heater (H1) used to raise the temperature of the slurry + CO₂ mixture to the reactor temperature. The heat duty for H1 is estimated at 0.846 kW. This implies that the exothermic reactor heat can cover a significant amount of the heat requirements of H1. Excess heat can also be retrieved from the purge streams of both CO₂ and water as these streams have a temperature of 98°C when exiting the flash drum and filter which should contribute to a portion of the DAC unit's heat requirements. For estimation, it is assumed the heat recovery from the purge stream is able to support around 10% of the DAC's heat requirements.

4.2. Comparison

As previously mentioned, one of the advantages of CO₂ mineralization is the exothermic nature of the reaction, which results in the generation of excess heat. This excess heat can be effectively utilized by implementing heat integration techniques in the integrated model. Heat integration allows for the redistribution of this excess heat to other components of the system, improving overall energy efficiency.

By incorporating heat integration into the model, a comprehensive comparison between the two systems can be conducted, providing a more accurate assessment of their respective performance. This analysis will consider the efficient utilization of excess heat, enabling a thorough evaluation of the overall energy consumption and cost-effectiveness of the mineralization processes.

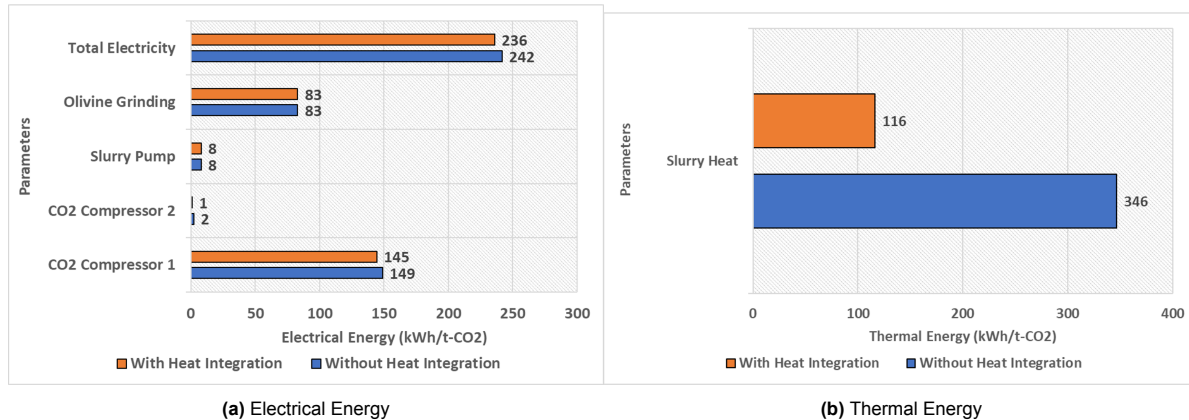


Figure 4.2: Electrical and thermal energy for non-integrated and integrated system

Figure 4.2 provides a comparison between the components of both the non-integrated and integrated systems. The impact of heat integration can be observed in Figure 4.2b, where a significant thermal energy reduction of 66.5% is achieved by utilizing the heat exchanger and harnessing the exothermic heat from the reactor. This integration allows for the efficient utilization of excess heat generated during the mineralization process, resulting in lower energy requirements.

It is also important to note that the utilization of heat integration has a slight influence on the energy requirements of other components within the system. This is primarily due to the temperature variations of the streams as they traverse through the system. For instance, in the integrated system in Figure 4.1, the end product stream labeled "4" exits the heat exchanger with a lower temperature compared to the non-integrated system. This lower temperature leads to reduced energy requirements for re-

compressing the gas to the desired pressure in the second compressor, as higher temperature gases require more energy for compression due to their increased enthalpy.

Overall, the incorporation of heat integration not only improves energy efficiency but also has a ripple effect on the energy demands of various components, resulting in a more optimized and sustainable mineralization system.

5

Equipment Selection & Economic Analysis

In the previous Chapter, the comparison between the integrated and non-integrated systems have been compared and the final model has been presented. In this chapter, the aspects of optimization and equipment selection based on the final model will be further discussed. Optimizing the process parameters and selecting suitable equipment play a vital role in maximizing efficiency, minimizing costs, and ensuring successful implementation to a real world application. This chapter explores the key steps involved in optimizing the components involved in the system and highlights the factors to consider when selecting equipment for each stage of the process.

5.1. Scaling

In order to accurately determine parameters such as pressure drop, equipment sizes, and equipment selection, it is essential to establish the scale of the mineralization system. In this section, the final model developed in Section 4.1.2 will be used and three different scales will be considered, which will be referenced throughout the rest of this chapter.

In Chapter 4, the flow rates were determined to be at 73 tons/year. However, for this chapter, we will explore three distinct scaling factors: 500 tons, 5 kilotons, and 50 kilotons of CO₂ sequestered annually.

The following summary outlines the flow parameters corresponding to these different scales:

Parameters	Value		
	0.5 ktons/year	5 ktons/year	50 ktons/year
CO ₂ Flow	1632 kg/day	16308 kg/day	163079 kg/day
H ₂ O Flow	1891 kg/day	18902 kg/day	189023 kg/day
Mg ₂ SiO ₄ Flow	2596 kg/day	25944 kg/day	259444 kg/day

Table 5.1: Flow Parameters for 3 different scaling options

It is important to acknowledge that the stoichiometry reactor assumes complete conversion of reactants in a single pass based on the reaction efficiency. Therefore, the values presented in the table above has already taken into account the reaction efficiency of the reaction which is 84%. Another aspect of interest is the quantity of reactants used in the system for each component, as it influences the price of the materials and the equipment costs. Specifically, the grinding equipment, compressor, reactor, and heat exchanger contribute significantly to the overall costs of the mineralization plant, while the other components are considered negligible [135]. This can already be seen in Figure 4.2 from

Chapter 4 where the energy requirements of the aforementioned equipment contribute significantly to the overall costs of the system (excluding equipment purchasing costs).

As for the material costs, as the scale for the system gets larger, it is evident that the purchasing price of materials or services gets cheaper according to the economies of scale concept [63]. However, there is no known equation or formula to forecast how much the price decreases. Therefore, further analysis is required to estimate how much the price of materials and feedstock decreases with varying plant scales.

5.2. Pressure Drop

With the scaling of the mineralization system determined, it is possible to calculate the pressure drop that occurs within the system. The final model, developed in Section 4.1.2, was constructed using Aspen Plus software. It provided information on the properties of reactants and products as they flow through the various components, accounting for changes in pressure and temperature. However, the model did not consider the parameter of pressure drop during the movement of the mixture stream within the system. Consequently, an optimization step is required to obtain a more precise representation of the pressure losses incurred when operating the CO₂ mineralization system using Aspen. For the representation of the pressure drop calculations, the 500 tons/year system will be used. The pressure drop calculations can be accomplished using Fanning's equation, which is expressed as follows:

$$\Delta P_t = \frac{2f \rho v^2 L}{d_{ti}} \quad (5.1)$$

where, ΔP_t is the pressure loss inside pipe for the fluid (Pa), f is the Fanning friction coefficient, ρ is fluid density (kg/m³), v is the mean velocity of fluid inside pipe (m/s), L is the pipe length (m), and d_{ti} is the inner diameter of the operating pipe string (m). By employing Fanning's equation, the pressure drop within the system can be determined, allowing for a more comprehensive analysis of the CO₂ mineralization process.

First the density of the slurry was calculated via the weighted average of the 3 different streams present in the slurry composition given by the following:

$$\rho_{slurry} = (V_{CO_2})(\rho_{CO_2}) + (V_{H_2O})(\rho_{H_2O}) + (V_{Mg_2SiO_4})(\rho_{Mg_2SiO_4}) \quad (5.2)$$

The volume fraction can be determined by analyzing each flow stream and dividing each individual stream with the total flow entering the system. Using the above equation, the weighted density of the system falls at 446 kg/m³. Next, the Fanning Friction factor is needed, which is given by [34]:

$$f = \frac{a}{Re_n^b} \quad (5.3)$$

where a and b are constants, given as follows:

$$a = \frac{\log_{10}n + 3.93}{50} \quad (5.4)$$

$$b = \frac{1.75 - \log_{10}n}{7} \quad (5.5)$$

To calculate the Fanning friction factor (f), it is necessary to determine the Reynolds number (Re) for the flow. However, a careful consideration needs to be made regarding whether the slurry behaves as a Newtonian fluid or a non-Newtonian fluid, as it influences the formulation of the Reynolds number to be used. According to an article published by Pump Fundamentals [46], the slurry is considered to behave as a Newtonian liquid under the following conditions: when the slurry contains particles smaller than 150 microns and the particle concentration is low, with the fluid velocity being sufficiently high to ensure uniform particle distribution.

Considering that the mineralization system operates with particle sizes of around 37 microns, it satisfies the first condition mentioned above. Regarding the fluid velocity and uniform particle distribution, it is important to ensure that the particles do not settle down while flowing through the stream. This can be verified by employing the settling velocity formula, also known as the sedimentation velocity formula, as provided by [36]:

$$v_{settling} = \frac{\rho_{particle}gd^2}{18\mu} \quad (5.6)$$

where g is gravity, ρ is the particle density, d is the particle diameter and μ is the viscosity of the medium. It is worth mentioning that for the viscosity, a weighted approach similar to the calculation of the density of the slurry was adapted. The result shows that the settling velocity falls to around 0.11 m/s. To make sure the velocity of the slurry is well beyond the settling velocity, the pipe diameter was selected to be 0.025 m. This would give a velocity of 0.32 m/s. Figure 5.1 shows the correlation between varying pipe diameters and its effects towards pressure drop and slurry velocity. It can be observed that when the pipe diameter is above 0.045 m, the slurry velocity will be less than the settling velocity and therefore the solid particles in the system will not move through the pipe.

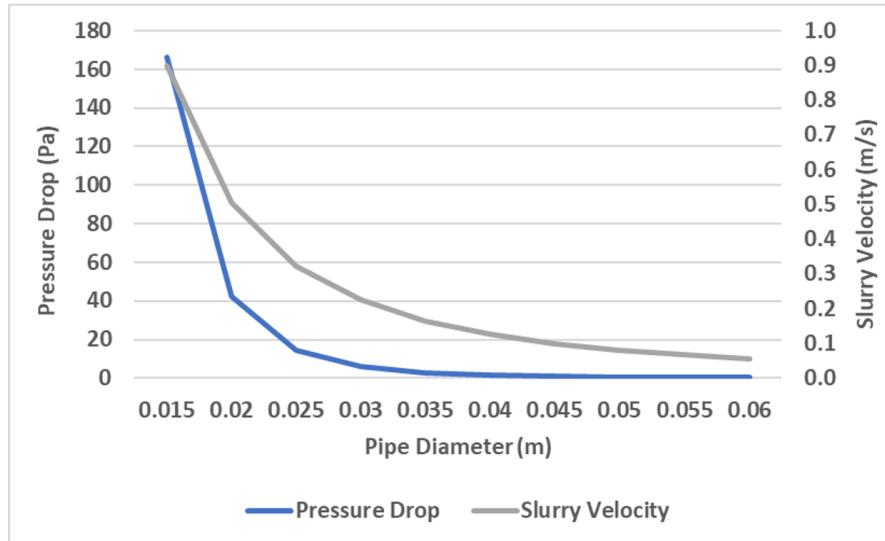


Figure 5.1: Pressure drop and slurry velocity with varying pipe diameter

Following this, the Re number can be calculated using the equation below:

$$Re = \frac{\rho v D}{\mu} \quad (5.7)$$

where ρ is the slurry density, v is the slurry velocity, D is the pipe diameter and μ is the viscosity of the medium. This can also be derived from using the generalized Reynolds number for non-Newtonian fluids given below:

$$Re_n = \frac{d_{ti}^n v^{2-n} \rho}{K^{8n-1}} \left(\frac{4n}{3n+1} \right)^n \quad (5.8)$$

where K is a consistency index, $\text{Pa} \cdot \text{s}^n$, and n is a flow behavior index. For Newtonian fluids, K is equal to viscosity, and n is equal to 1. This would make this equation similar to the one above. Calculating the Re number would give a value of 1.599E+05 which shows turbulent characteristics. Next, using the equations provided for a and b would give values of 0.0786 and 0.25 respectively. This then would make the friction factor equates to 0.00393. With all the parameters specified, the pressure drop can be calculated and gives a value of 14.67 Pa/m. This pressure drop is quantitatively very small and therefore it should not pose a problem for further consideration of the system.

It is essential to recognize that the pressure drop value mentioned earlier only accounts for the slurry traveling through the pipe within the system and does not consider the pressure drop occurring at various components such as the compressor, heat exchanger, and others. In a realistic plant design, it is reasonable to expect that pressure drops will also occur within these components, and they must be taken into consideration for the overall calculations.

5.3. Grinding

One crucial aspect of the optimization process is the grinding step for the feedstock. This step is often recognized as one of the most energy-intensive stages within the mineralization process, emphasizing the importance of selecting the most suitable equipment. Previous chapters have established that the particle size is reduced to approximately 37 µm, indicating the presence of very fine particles. To achieve uniform particle sizes, multiple grinding steps are recommended. The relationship between particle size and energy comminution values is explored in Section 2.6.2, while Section 3.3.3 provides approximate energy consumption values for the system.

This section focuses on equipment selection for the grinding process. Crushers and grinders are both involved in the process to finely tune the feedstock to the desired particle size. Crushers can be classified as either jaw crushers or gyratory crushers. In a jaw crusher, the feed is introduced between two jaws that form a "V" shaped opening at the top. One jaw remains fixed while the other jaw rotates in a horizontal plane, applying compressive force to the feedstock lumps trapped between the jaws. Gyratory crushers can also be regarded as jaw crushers but with circular jaws that continuously crush material between them. A comparison between the two types of crushers is presented in Table 5.2.

Crushers	Jaw	Gyratory
Capacity	1200 ton/hr	4500 ton/hr
Speed	Jaws open and close 250-400 /min	Gyrations 125-425 /min
Discharge	Intermittent	Continuous
Maintenance	High	Low
Power Requirements	High	Low

Table 5.2: Comparison of jaw and gyratory crushers
[50]

The data demonstrates that gyratory crushers possess several favorable characteristics for the grinding requirements of the mineralization system. These include a higher capacity of 4500 tons/hr, a continuous discharge rate, and lower maintenance and power requirements. To provide a visual representation, refer to Figure 5.2, which illustrates the appearance of a gyratory crusher.

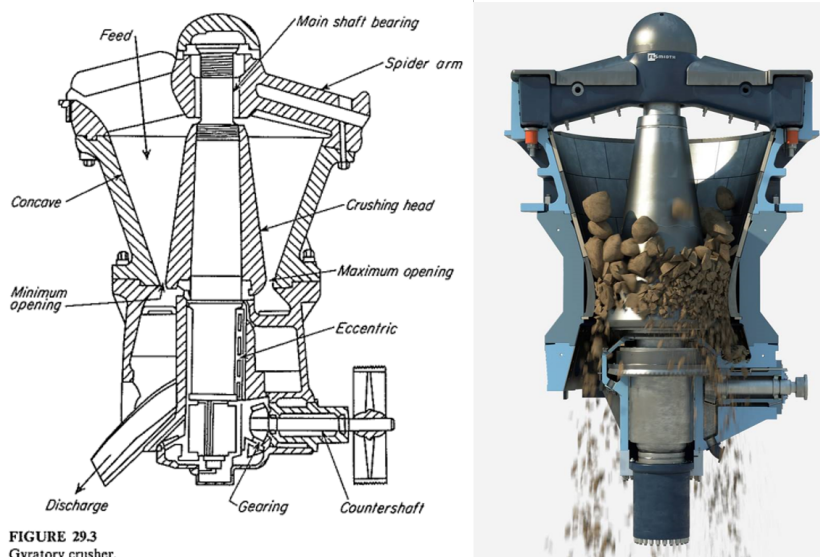


Figure 5.2: Representation of a gyratory crusher
[50]

Crushers are initially employed as mechanical tools to break down large feedstock lumps into

smaller sizes. However, to achieve a powder-like consistency, the use of grinders becomes necessary. Grinders are classified as intermediate duty size-reduction machines and play a crucial role in further reducing the size of the product obtained from crushers to the desired particle size in powder form.

Several types of grinders are available for this purpose, including hammer mills, impactors, rolling-compression machines, attrition mills, and tumbling mills [76]. Each machine has its own unique characteristics and suitability for specific applications. A comprehensive overview of the features and performance data for each type of grinder can be found in Table 5.3. This table provides valuable information for selecting the most appropriate grinder based on the specific requirements of the mineralization system.

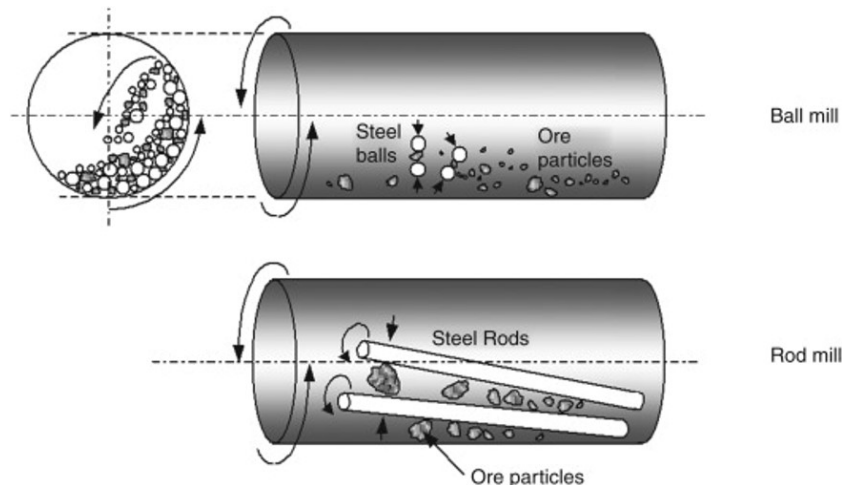


Figure 5.3: Representation of ball/rod mills
[76]

Grinders	Hammer Mills/ Impactors	Attrition Mills	Tumbling Mills
Capacity	0.1-15 ton/hr (HM) 600 ton/hr (I)	0.5-8 ton/hr	5-200 ton/hr (Rod) 1-50 ton/hr (Ball)
Speed	Hammer tips 110 m/s	350-700 r/min (single) 1200-7000 r/min (double)	-
Discharge	Continuous	Continuous	Continuous/ Batch
Power Requirements	4.17-16.7 kWh/ton product	8-80 kWh/ton product	4 kWh/ton product (Rod) 16 kWh/ton product (Ball)

Table 5.3: Comparison of grinders

Based on the information presented in the aforementioned table, it becomes evident that tumbling mills exhibit the lowest energy demands among the three types of grinders, while still maintaining satisfactory grinding capacities. Notably, tumbling mills offer the advantage of both continuous grinding and batch grinding options, which enhance process flexibility. Additionally, specific to rod mills, they have the ability to produce a 10-mesh product during the grinding process. Considering these favorable characteristics, rod mills emerge as the preferred choice of grinder. To provide a visual representation, Figure 5.3 depicts both ball mills and rod mills, illustrating their respective configurations and designs.

5.4. Heat Exchanger

Section 4.1.2 briefly mentioned that the heat exchanger used in the system was not specified, and instead, a shortcut model was employed to provide values for the heat exchanger without modelling

the actual component. However, this section will delve into the topic of the actual heat exchanger in more detail.

The classification of heat exchangers depends on various factors, including flow configuration, construction, and heat transfer mechanism [99]. Some commonly available types of heat exchangers include shell and tube heat exchangers, plate type heat exchangers, spiral heat exchangers, and finned tube heat exchangers. Among these options, shell and tube heat exchangers are typically the most widely used, accounting for approximately 50% of applications [99]. Therefore, given the various options to choose from, careful consideration must be given to selecting the most suitable type of heat exchanger for the mineralization system.

Figure 5.4 illustrates the selection of heat exchangers based on working pressure/temperature conditions. By referring to this figure, it becomes apparent that both the spiral heat exchanger and the double pipe heat exchanger are well-suited for the working conditions of the mineralization system.

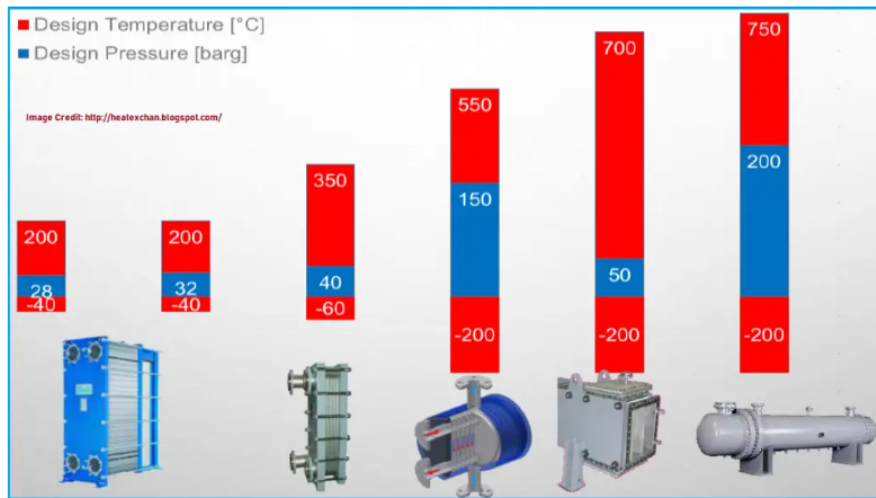


Figure 5.4: Selection of heat exchangers with respect to design temperature and pressure [99]

The mineralization system involves the flow of a slurry stream with a solid concentration of 15%, which needs to be heated to the desired reaction temperature. During the transportation of slurry through a piping system, fouling can occur, referring to the unwanted accumulation and formation of materials on the equipment surfaces during heating and cooling processes [55]. This becomes particularly relevant for recycled streams, where solid particles may be present in the recycled CO₂ and H₂O stream in real-world scenarios.

The selection of heat exchangers always involves a trade-off. Opting for higher performance, such as a smaller gap channel, may result in a shorter operational lifespan due to the fouling effect. On the other hand, choosing a wider gap channel can extend the operating cycle but compromises thermal performance [114]. However, spiral heat exchangers possess an intriguing characteristic in this context. They feature a single-channel design with high-velocity turbulent flow, which can generate a self-cleaning effect, making it more resistant to fouling occurrences. Furthermore, as indicated in Table 4.2, counter-current flow is recommended for more efficient heat transfer between the two fluids, and this can be achieved using a spiral heat exchanger.

Considering the presented information, spiral heat exchangers exhibit ideal characteristics for the mineralization system. They can effectively mitigate fouling concerns due to their self-cleaning capabilities and facilitate efficient heat transfer through the implementation of counter-current flow. Figure 5.5 illustrates the schematic of a spiral heat exchanger.

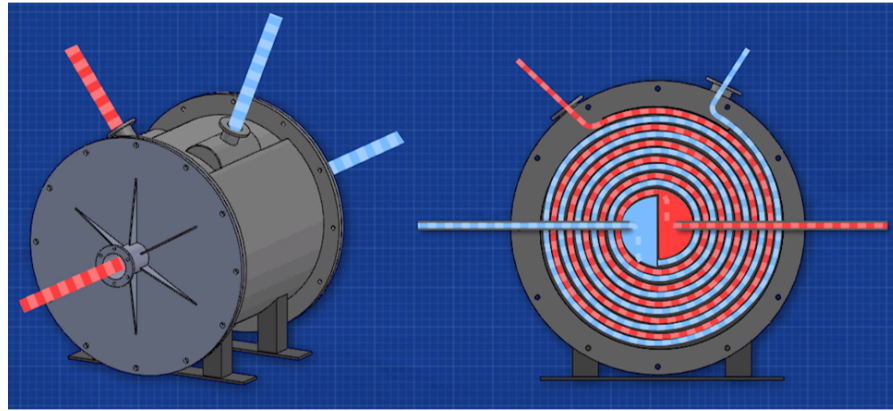


Figure 5.5: Schematic of a spiral heat exchanger
[85]

To determine the appropriate size of the selected heat exchanger, the heat transfer formula for a heat exchanger can be utilized. Again, the 500 tons/year mineralization system will be used to illustrate the calculation procedure. The formula is expressed as follows:

$$Q = U * A * (\text{LMTD}) \quad (5.9)$$

where Q is exchanged heat duty (W), A is the exchange area (m^2), U is the heat transfer coefficient ($\text{W}/(\text{K}\cdot\text{m}^2)$), LMTD is the logarithmic mean temperature difference [125], given by:

$$\text{LMTD} = \frac{\Delta T_A - \Delta T_B}{\ln(\Delta T_A) - \ln(\Delta T_B)} \quad (5.10)$$

where ΔT_A is the temperature difference between the two streams at the hot side, and ΔT_B is the temperature difference between the two streams at the cold side. The heat duty for the 500 tons/year mineralization system is 14.8 kW and the LMTD was retrieved from Aspen with a value of 13.8°C . This heat exchange duty value was attained via trial-and-error to max out the heat transfer between the hot and cold streams conducted in the Aspen simulation just before a temperature crossover error occurs.

Regarding the heat transfer coefficient, this can be calculated using the Nusselt number [127]:

$$Nu = \frac{hd}{k} \quad (5.11)$$

where h is the heat transfer coefficient, d is the characteristic diameter (m), and k is the thermal conductivity of the fluid ($\text{W}/(\text{K}\cdot\text{m})$). Another derivation is given for Nusselt's number as follows [121]:

$$Nu = 0.565 Re^{0.5} Pr^{0.5} \quad (5.12)$$

where Re is the Reynold's number for the fluid, and Pr is the Prandtl's number. This Nusselt's number is derived from the condition that a low Prandtl's number is obtained ($Pr < 0.6$) and $Re < 500,000$. The Prandtl's number is given by [129]:

$$Pr = \frac{c_p \mu}{k} \quad (5.13)$$

where c_p is the specific heat capacity ($\text{J}/(\text{kg}\cdot\text{K})$), μ is the dynamic viscosity ($\text{Pa}\cdot\text{s}$), and k is the thermal conductivity of the fluid ($\text{W}/(\text{K}\cdot\text{m})$). The specific heat capacity, thermal conductivity and dynamic viscosity were calculated using the weighted average method using the volume fractions of the 3 separate streams and consequently gave a Prandtl's number of 0.129. Subsequently, substituting the respective values of Re and Pr would then give a Nusselt's number of 14.63. Using this value would then give the heat transfer coefficient of $153.81 \text{ W}/(\text{K}\cdot\text{m}^2)$ is obtained. Finally, going back to the heat transfer formula, substituting all these values will then give the heat exchanger area of 7.0 m^2 . The same procedure was applied to the other two scales. A summary of the calculations for the 3 scales is listed in Table 5.4.

Scale (ktons/year)	Exchange Duty (kW)	Exchanger Area (m ²)
0.5	14.8	7
5	148.3	22.5
50	1484	71.37

Table 5.4: Heat exchanger details for mineralization system at different scales

5.5. Reactor

In Chapter 3 and Chapter 4, the comparison of different CO₂ mineralization methods, as well as the final model, employed a stoichiometry-based reactor. This assumption implies complete conversion of the reactants in a single pass without considering the element of time. However, it is important to account for the reaction kinetics and the desired reaction efficiency over a specific duration.

According to a paper by W.K. O'Connor et al. [13], the direct aqueous carbonation reaction reaches an approximate rate of 84% after 6 hours. While this finding is valuable, the subsequent reactions that occur with different hourly intervals were not specified in O'Connor's study. Consequently, for a comprehensive understanding of how the mineralization process behaves in the reactor, it is essential to evaluate the reaction rate per hour.

To achieve this, the design and specifications of the reactor should incorporate a detailed analysis of the reaction kinetics over time. By monitoring the reaction rate at regular hourly intervals, insights into how the carbonation process progresses, how quickly it reaches its peak, and whether there are any potential variations or limitations in the reaction rate can be known.

This information is crucial for optimizing the reactor's performance and efficiency. It can help identify potential bottlenecks, determine the most favorable operating conditions, and assess the overall feasibility of the mineralization process. Additionally, understanding the reaction rate per hour can aid in predicting the reaction's completion time and provide valuable data for scale-up considerations in real-world industrial applications.

One commonly used reactor type for chemical reactions is called Continuous Stir Tank Reactors (CSTRs) [123]. CSTRs operate by continuously introducing CO₂ and mineral feedstock into a well-mixed tank reactor. The reactants are thoroughly mixed, therefore ensuring uniform concentrations and reaction conditions throughout the reactor. Figure 5.6 depicts the schematic representation of a CSTR reactor.

This reactor was selected based on Le Chatelier's Principle [19], which states that if a chemical reaction at equilibrium experiences a change in pressure, temperature, or concentration of products or reactants, the equilibrium will shift in the opposite direction to counteract the change. In the context of CO₂ mineralization, the reactions involved are exothermic, meaning they release heat. As a result, the temperature of the slurry in the reactor increases as the reaction progresses.

According to Le Chatelier's Principle, this temperature increase would inhibit further reactions. The mixing properties of the CSTR illustrated in Figure 5.6 can mitigate this by maintaining a low temperature by ensuring an even dispersion of the mixture throughout the entire reactor. By keeping the temperature low through efficient mixing, this allows for a higher conversion rate to be attained in the CO₂ mineralization process. Furthermore, Mattila et al. [142] found that effective mixing would significantly reduce the reaction time to reach equilibrium and therefore would be beneficial to be applied in this case.

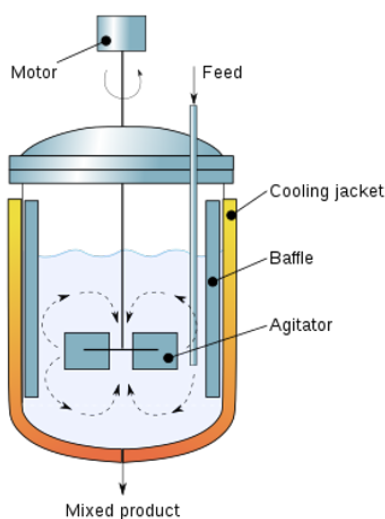


Figure 5.6: Continuous Stir Tank Reactor (CSTR)
[124]

Using the simulation in Aspen, a CSTR reactor model was adapted and replaced the stoichiometry reactor. In order to compute the reaction, information such as reaction constant needs to be known. These data can be obtained from a paper published by Fei Wang et. al. [52]. The kinetics based on Fei Wang's model does not have the same working conditions as the one proposed in the system. Therefore, this kinetics calculation is serve only as an initial estimation and evaluation of the CSTR reactor in comparison with the stoichiometry reaction. As for the CO₂ flow of the model, the 500 tons/year scale will be adapted to illustrate the data evaluation of the process.

In the paper published by Fei Wang [52], it was mentioned that mineral carbonation is limited by kinetics mainly by one of three possible steps: the dissolution of CO₂ into aqueous solution (mass transport control), the dissolution of Mg-silicates (chemical reaction control), or the formation of solid products (product layer diffusion control). At relatively high pressures, it was shown that reactions were controlled by particle chemical reactions. Therefore the reaction constant should be estimated keeping this control mechanism in mind.

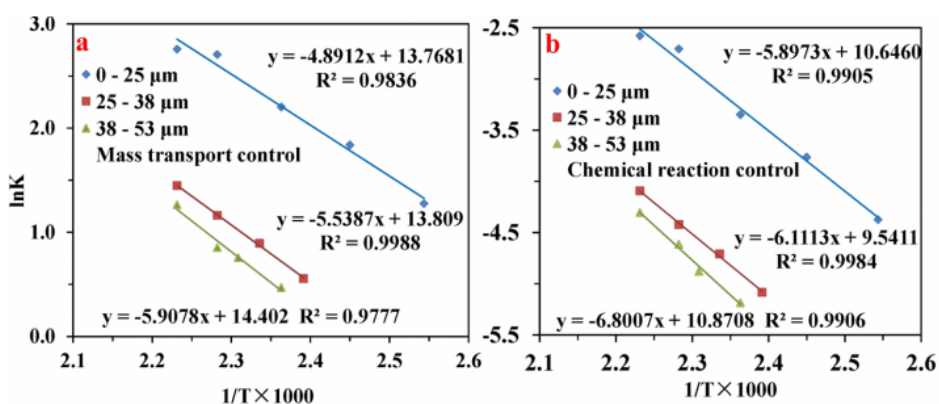


Figure 5.7: Relationship between ln(k) and 1/T × 1000 according to the mass transport control and chemical reaction control
[52]

The reaction constant calculated by Fei Wang's team is visualized in Figure 5.7. In the Aspen model, the reaction efficiency is associated with the particle size of olivine, which is determined to be 37 μm, and the temperature set at 185°C. Based on these parameters, the approximate ln(k) value is calculated to be -4.0, resulting in a reaction constant of 0.017.

This reaction constant is utilized in the simulation to determine the consumption of CO₂ (in mols) with respect to residence time (in hours). The corresponding graph in Figure 5.8 illustrates the relationship between CO₂ consumption and residence time. It shows that the consumption of CO₂ levels off after a certain period, indicating a significant slowdown in the mineralization reaction (equilibrium). Based on the graph presented in the figure, the CSTR reactor would have a final carbonation efficiency of 60.24% in 6 hours compared to 84% by the stoichiometry reaction.

To further analyze the reaction kinetics, the simulation breaks down the reaction into 1-hour intervals. Table 5.5 provides a clear overview of the CO₂ consumption per hour using the CSTR reactor model in Aspen. It is evident from the table that the majority of the reaction occurs within the first hour.

In summary, the calculation of the reaction constant and its incorporation into the simulation using Aspen allows for the analysis of CO₂ consumption in relation to residence time. The results demonstrate a gradual decrease in reaction rate over time, and the breakdown of the reaction into hourly intervals highlights the significant contribution of the initial hour to the overall reaction in the CSTR reactor model. Therefore, for the following evaluation, the first interval of the reaction for the CSTR will be considered.

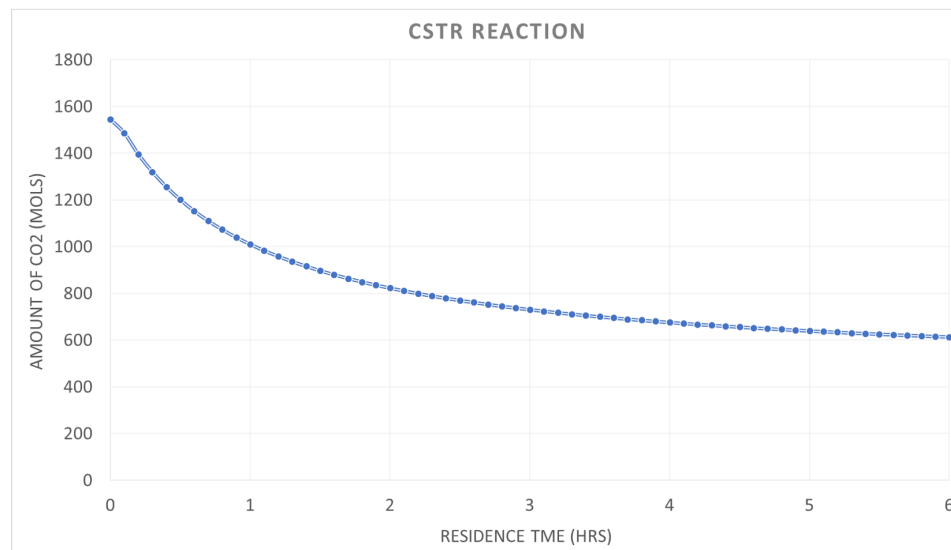


Figure 5.8: Sensitivity analysis of a CSTR reactor with respect to residence time

Hour	CO2 Consumption (%)
1	34.59
2	12.11
3	5.96
4	3.55
5	2.35
6	1.67

Table 5.5: CO₂ consumption per hour in a CSTR reactor

Expanding upon the provided information, a comparison between simulations conducted using a stoichiometry reactor and a CSTR reactor was performed, as illustrated in Figure 5.9. It is important to note that considering the time difference between the two reactors, with the CSTR reactor completing the reaction in 1 hour compared to 6 hours for the stoichiometry reaction. This means that the CSTR reactor produces a larger quantity of end products within the same timeframe, resulting in a greater amount of CO₂ sequestered.

Additionally, from Figure 5.9, the exothermic heat generated by the CSTR reactor is nearly five times higher than that of the stoichiometry reactor. This is advantageous as the excess heat can be utilized to meet the requirements for the desorption of CO₂ from the DAC unit and the heating of the slurry. This offers potential energy savings and operational benefits.

However, further research is required to validate and confirm these findings regarding the use of CSTR reactors for mineralization as previously mentioned the data of which the reaction kinetics were obtained did not match the working conditions set in the mineralization system.

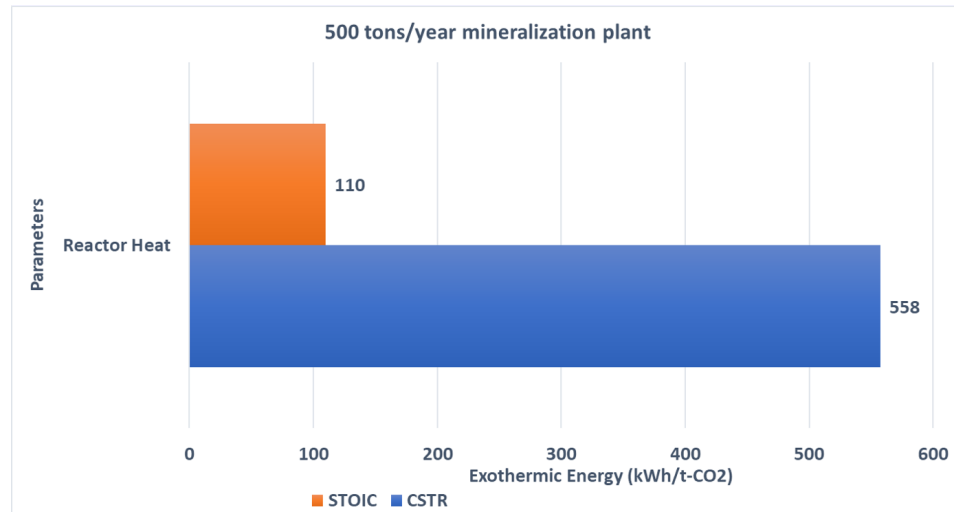


Figure 5.9: Exothermic heat comparison

From the data presented above and using the formula mentioned below for the residence time, the appropriate reactor volume can be calculated.

$$\text{Residence Time} = \frac{\text{Reactor Volume}}{\text{Flow Rate}} \quad (5.14)$$

Utilizing the residence time for 1 hour and the flow rate of $0.000158759 \text{ m}^3/\text{s}$, this results in a reactor volume for each of the 3 scales as shown in Table 5.6. It is worth mentioning that only one CSTR reactor was adopted for each scale considering the low residence time.

Scale (ktons/year)	Volume of Reactor (m^3)
0.5	0.57
5	5.71
50	57.13

Table 5.6: Final reactor volumes

While the reactor volumes for each scale have been determined, it is important to note again that the chosen reaction kinetics data used to represent the CSTR simulation in Aspen does not accurately reflect the working conditions of the system. This indicates that further experimental research is necessary to assess the reactor's performance and obtain more precise values for the Aspen simulations.

Considering this limitation, the economic analysis that will be conducted in Section 5.7 will still utilize the calculated reactor volumes from the table above but regarding the data related to the mineralization system, such as electricity, transportation, and feedstock costs etc, data related to the stoichiometry reactions with an efficiency of 84% will still be used to represent a best case scenario.

By using the reactor volumes determined and an ideal stoichiometry reaction efficiency, the economic analysis can still provide valuable insights into the potential profitability and viability of the mineralization system.

5.6. Pump, Compressor, Filter, & Flash Drum

When selecting an appropriate compressor for pressurizing CO_2 gas to the required pressure, it is crucial to consider operational efficiency and safety aspects. Three common types of compressors used

in small to medium industries are screw compressors, reciprocating compressors, and centrifugal compressors [102]. Screw and reciprocating compressors fall under the category of positive displacement compressors, while centrifugal compressors are classified as dynamic compressors. Dynamic compressors, such as centrifugal compressors, are typically preferred for large-scale operations, making them a suitable choice for the mineralization system considering its scale.

Centrifugal compressors offer significant energy efficiency advantages when handling large gas volumes, as their impellers are designed to match the required airflow and pressure, resulting in additional energy savings [53]. When it comes to compression stages, it is important to consider the discharge temperature of the compressor. To prevent degradation of the compressor materials, components, and lubricating oil, the discharge temperature should not exceed certain limits, typically around 148.9°C or 176.7°C [27]. However, in the model simulated in Aspen, where the discharge temperature of the last stage of the initial CO₂ compressor is 253°C, this exceeds the recommended temperature limit. To address this, countermeasures can be implemented, such as increasing the number of stages in the compressor or implementing cooling mechanisms to keep the temperature within an acceptable range.

In terms of pumping the slurry to a pressure of 115 bar, a centrifugal pump is commonly employed for this purpose. These pumps utilize a rotating impeller to move the slurry, similar to the operation of a standard centrifugal pump handling water-like liquids [56]. Moving on to filter selection, during the simulation process, a solid separator model with a solid-liquid separation fraction of 1 was assumed. Belt filtration, disk filtration, and drum filtration (centrifugal filtration) are among the commonly used filter types in industries. Figure 5.10 illustrates suitable filter types based on particle sizes. Given that the mineralization system operates with particle sizes of 37 microns, sedimentation filters and pressure filters are viable options worth considering.

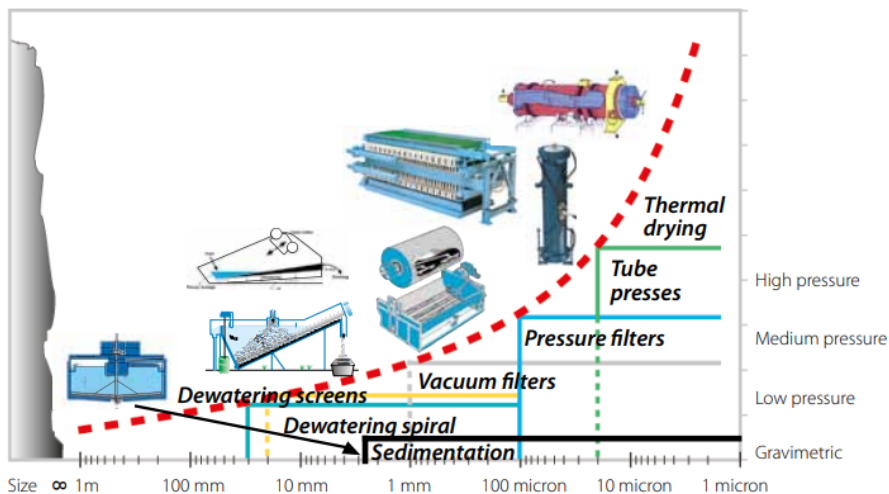


Figure 5.10: Type of suitable filtration types wrt particle sizes

[82]

However, operating at medium pressure ranges would result in additional energy consumption. In this case, sedimentation filters are considered the optimal choice as they utilize gravimetric force, possibly leading to lower energy requirements. Based on this consideration, a centrifugal filter has been selected as the preferred filtration method. Centrifugal filtration employs centrifugal force to exert pressure on a solids suspension against a filter medium, allowing the liquid to pass through while retaining the solid particles. One example of a centrifugal filter is the basket centrifuge, which can also operate at elevated temperatures to facilitate the drying process of solid cakes [22].

A flash drum operating in a real world scenario cannot perfectly separate the 3 different streams of solids, water, and CO₂. Therefore, optimization steps are necessary to estimate the extent of how much residual CO₂ can be extracted and recycled to the mineralization reactor. When the product stream enters the flash drum at a constant temperature, depressurization can enable the release of more CO₂ gas into the recycled stream, which can then be re-pressurized by the second compressor and reused again for the mineralization process. However, careful consideration must be given to determine the ideal pressure that maximizes the recovery of CO₂ gas back into the system without compromising

excessive energy consumption during the re-pressurization process. Thus, a trade-off exists between these two aspects.

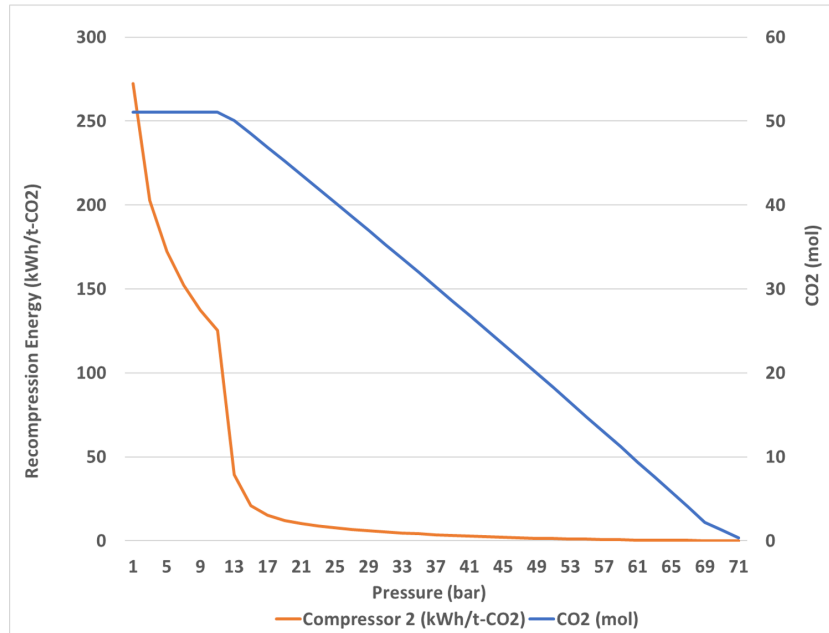


Figure 5.11: Recycled CO₂ stream and re-compression energy wrt to varying pressure

The sensitivity analysis was conducted using the sensitivity function in Aspen Plus and is depicted in Figure 5.11. This analysis was run using the final model with a CO₂ flow of 200 kg/day. This graph illustrates the relationship between the amount of recycled CO₂ stream and the corresponding compression energy, considering different pressures in the flash drum. The analysis reveals that the quantity of CO₂ being recycled starts to decrease significantly after reaching 13 bars, whereas the re-compression energy experiences a steep decline before leveling off around 17 bars. Based on this sensitivity analysis, it was determined that a flash drum pressure of 13 bars is optimal. This pressure allows for the effective recovery of most unreacted CO₂ gas back into the system, while maintaining relatively low compression energy requirements. A summary of this analysis is provided below:

Parameters	Ideal Characteristics
Flash Drum	13 bar pressure
Recycled CO ₂ Stream	50.1 mol/hr
Compression Energy	39.5 kWh/t-CO ₂

Table 5.7: Summary of sensitivity analysis of flash drum and re-compression energy

5.7. Economic Analysis

In this section, an economic analysis of the CO₂ mineralization system that has been implemented will be conducted. The objective is to evaluate the economic feasibility of the integrated DAC + mineralization system, taking into account the equipment selection and specifications outlined in previous sections. Various factors, including capital costs, operational expenses, energy requirements, and feedstock inputs, will be considered to assess the viability of the system in each of the 3 scales presented.

5.7.1. Carbon Footprint

It is vital to first assess the mineralization system's net CO₂ sequestration as it is undesirable to have a plant that emits more CO₂ into the air than the amount it sequesters. For this assessment, the paper

published by Pavan Kumar Naraharisetti [140] has provided percentage values of different unit operations for the direct aqueous carbonation system that contributes to the CO₂ emission penalties. This values can be used as a guideline to estimate the amount of CO₂ that is emitted during the sequestration process. The percentage values are given for natural gas and coal based on the paper provided by Pavan. For wind energy and solar energy, a ratio was taken based on their respective emission rates compared to the emission rates of natural gas. A summary of CO₂ emitted by different unit operations can be seen from Table 5.8.

Parameters	Natural Gas	Coal	Wind Energy	Solar Energy
	Weight (%)	Weight (%)	Weight (%)	Weight (%)
Pre-treatment	11.6	26.8	0.9	1.3
Compression	5.7	13.2	0.5	0.7
Pumping Water	1.7	1.6	0.1	0.2
Slurry Heating	7.7	12	0.6	0.9
TOTAL	26.7	53.6	2.1	3.1

Table 5.8: Summary of CO₂ penalty fractions for different energy sources

Next, a comparison was conducted with different energy sources to highlight how significant the difference would be. The energy sources used for this comparison are renewable sources like wind energy (CO₂ emission rate of 0.034 kg/kWh) and solar energy (CO₂ emission rate of 0.050 kg/kWh) [110], and also non-renewable sources like natural gas (CO₂ emission rate of 0.43 kg/kWh) and coal (CO₂ emission rate of 0.996 kg/kWh) [140]. Taking into account the fractional values listed above as well as the energy requirements for the mineralization system, the total amount of CO₂ being emitted per t-CO₂ sequestered can be seen in Figure 5.12.

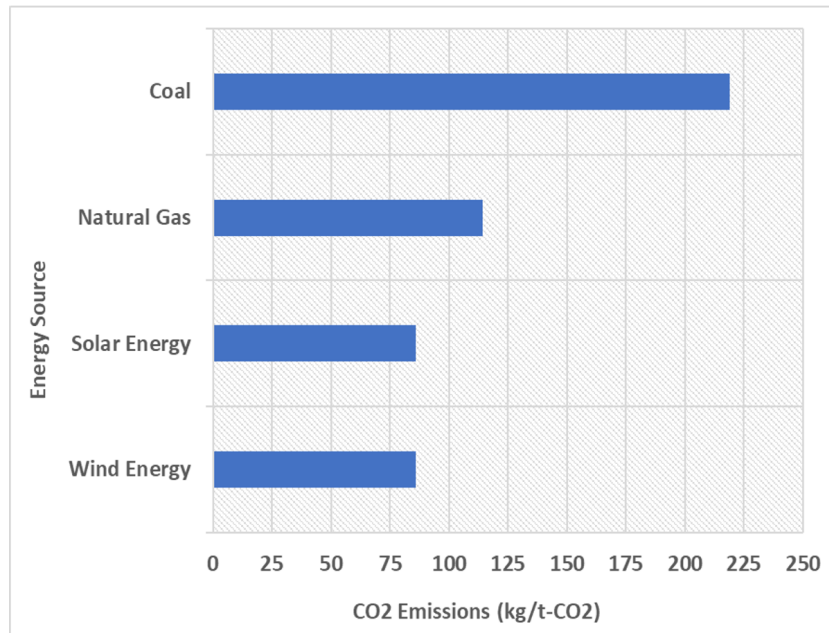


Figure 5.12: CO₂ emitted during the mineralization process with varying energy sources

For the emissions regarding transportation, an emission rate of 0.016 kg/t-goods per km for freight transport [64] and 0.057 kg/t-mineral per km for trucks [66] has been chosen. From Section 3.4 it has been specified that the distance for the trucks is assumed to be 150 km. Therefore, this value was used for the CO₂ emissions calculations in addition to the mass of the end products being transported. For the freight transport, a distance of 2013 km was taken which corresponds to the distance from Finland to The Netherlands. This value also took into account the ratio of how much olivine was used per ton CO₂ that is sequestered divided by the mineralization efficiency to get the overall amount of

feedstock needed to be brought in from Finland. This results in values of 61.3 kg/t-CO₂ sequestered for the transportation of minerals to the system and 24.3 kg/t-CO₂ sequestered for the transportation of end products out of the system.

Summing up the emissions from transportation with the emission values from the mineralization plant will give the values corresponding to the figure above.

5.7.2. CapEx and OpEx

Calculating capital expenditures (CapEx) for a CO₂ mineralization system involves estimating the costs associated with acquiring, installing, and commissioning the system. The capital costs will be estimated by using a cost-to-capacity method and scale factors which is a useful tool when developing elements of the cost approach in many valuations. It is an order-of-magnitude cost estimation tool that uses historical costs and capacity in order to develop current cost estimates for an entire facility or a particular piece of machinery or equipment [41]. The fundamental concept behind the cost-to-capacity method is that the costs of facilities of similar technology but with different sizes vary non-linearly. More specifically, cost is a function of size raised to an exponent or scale factor [41]. The governing equation is as follows:

$$\frac{C_2}{C_1} = \left(\frac{Q_2}{Q_1}\right)^X \quad (5.15)$$

where C_2 is the cost of facility 2 that is to be estimated with known capacity Q_2 , C_1 is the known cost of facility 1 with a known capacity of Q_1 , and X is the scale factor for technology of facility 1 and 2. The scale factor was taken based on the "Product and Process Design Book [49]" and also the sixth-tenth rule [73]. As mentioned in Chapter 5, the main contributors of the cost associated with the mineralization system are the grinding equipment, compressors, reactor, and heat exchanger. Therefore the pricing will only focus on these equipments. Table 5.9 shows the typical size exponents associated with equipment sizing. Once the base purchased equipment cost has been estimated, it has to be multiplied by multiple correction factors given the fact that the cost literature contains equipment cost at base conditions, such as being at low pressures and temperatures, carbon steel construction and a specific design [49]. The correction factors consist of material factor, F_M , temperature factor F_T , and pressure factor, F_P . The values set for each factor can be summarized in Table 5.10 which was calculated based on reference values provided in [49].

Equipment	Exponent
Crusher	0.6
Grinder	0.6
Compressor 1	0.69
Compressor 2	0.69
Reactor	0.55
Pump	0.6
Heat Exchanger	0.44
DAC Unit	0.6

Table 5.9: Typical size exponents for equipment costs
[49]

$$PEC = PEC_{Base} * F_T * F_P * F_M \quad (5.16)$$

Correction Factor	F_M	F_P	F_T
Value	1.3	1.15	1.06

Table 5.10: Correction factors used for purchased equipment cost

Following this, the corrected purchasing costs of equipment were then multiplied by the Lang Factor [49] to get the estimated total capital investment (TCI). The estimation of the Lang Factor includes

specific factors such as direct and indirect associated costs involved in the system process and has an accuracy of +/- 35%. Some of the direct associated costs taken into account were equipment installation, piping, utilities, and instrumentation whereas the indirect associated investments involved were design and engineering, contractor's fee, and contingency. The Lang Factor was set to 5.0 based on a typical value used for a fluid-solid plant [49]. The results of the calculation can be seen in Table 5.11.

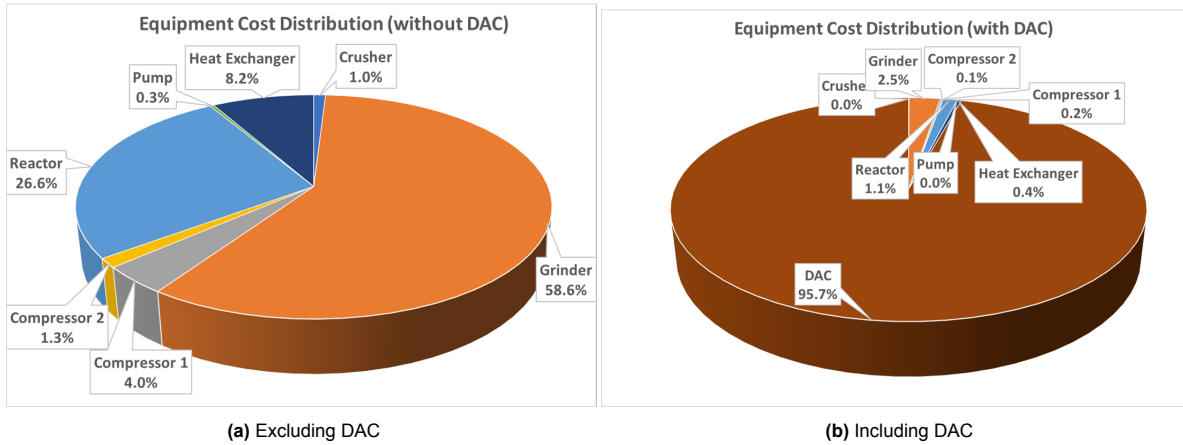


Figure 5.13: Equipment cost distribution

Scale (ktons/year)	Equipment (€)	Lang Factor	CapEx (€)
0.5	500,000-900,000	5.0	2,500,000-4,500,000
5	2,000,000-5,000,000	5.0	10,000,000-25,000,000
50	10,000,000-15,000,000	5.0	50,000,000-75,000,000

Table 5.11: CapEx cost estimations

Calculating operating expenses (OpEx) for a CO₂ mineralization system involves considering various factors and costs associated with the system's operation during the sequestration process. This consist of depreciation costs, variable costs, and fixed operating costs. The variable operating costs consist of costs for the acquisition of feedstock and other utilities. For feedstock, the price for olivine was assumed to be the same as mentioned in Chapter 3. As for the utilities, this consist of elements required for the mineralization process which involves electricity used to power the components such as crushers/grinders, compressors, heat exchangers, pumps, and reactors.

As for the fixed operating costs, it consisted of costs for operating labour, and maintenance. In order to determine the total sequestration costs, the depreciation costs, the variable and fixed operating costs were summed up resulting in the costs per ton CO₂ sequestered in the carbonation reactor. These aspects can be seen in Figure 5.14 and the final operating costs can be seen in Table 5.12.

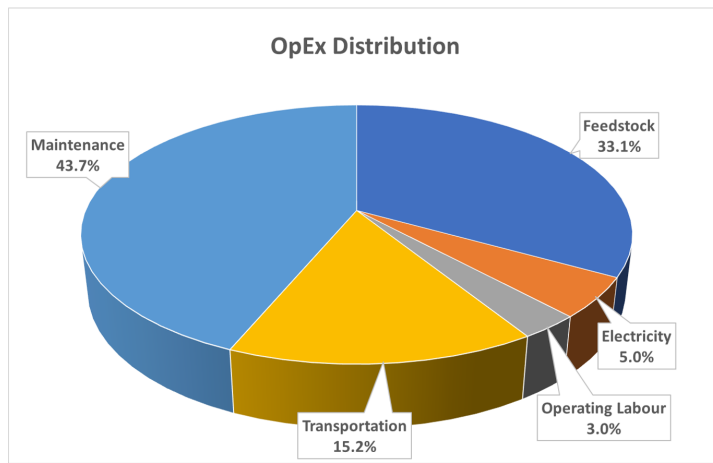


Figure 5.14: Variable cost and fixed cost distribution

Scale (ktons/year)	OpEx (€)
0.5	200,000-500,000
5	1,000,000-3,000,000
50	11,000,000-15,000,000

Table 5.12: OpEx cost estimations

Now that the capital costs (CapEx) and operating costs (OpEx) have been determined, the cash flow of the system can be calculated by using the following formula [49]:

$$CF = (1 - t)(S - VC - FC - D) + D \quad (5.17)$$

where CF is cash flow, t is taxation rate, S is annual sales, VC and FC are variable costs and fixed costs that make up the operating costs, and D is the annual depreciation. The taxation rate was set to 0.37 and the annual sales was based on the carbon credit price per ton of CO₂ removed. The annual depreciation can be obtained by dividing the total depreciable capital by the depreciation period in years, typically between 25-50 years for a typical chemical plant [117]. For this plant, the lifetime was set to 30 years. The results of the CF calculations can be seen in Figure 5.15a, Figure 5.16a, and Figure 5.17a respectively.

From the acquired cash flow, the Net Present Value (NPV) can be calculated using the following equation:

$$NPV_N = \sum_{n=1}^N \frac{CF_n}{(1+r)^n} \quad (5.18)$$

where N is the period of years (lifetime), CF is the cash flow, and r is the discount rate. The period of years is given to be 30 years and the discount rate was set to be 20%, given a typical value used for projects that is considered high risk. Using these values to calculate the NPV, it can give an insight on whether or not it is feasible to go forward with the investment of the plant. However, when it comes to estimating the cash flow for calculating the NPV, there is currently no established framework for carbon credits specifically for carbon mineralization. As of 2022, neither Verra nor any other third-party carbon standards have incorporated carbon mineralization into their systems [68]. Furthermore, the price of carbon credits can vary significantly depending on market conditions and various factors, including regulatory frameworks in different countries [65].

Consequently, predicting the price of carbon credits for CO₂ mineralization is challenging. To address this issue, an analysis was conducted to determine the potential range of credit prices that would yield a positive NPV. The results of this analysis are presented in Figures 5.15b, Figure 5.16b, and Figure 5.17b. This analysis provides a visualization of the relationship between the credit price and the

resulting NPV. By examining the range of credit prices that lead to a positive NPV, it becomes possible to make informed decisions regarding the economic feasibility of the project.

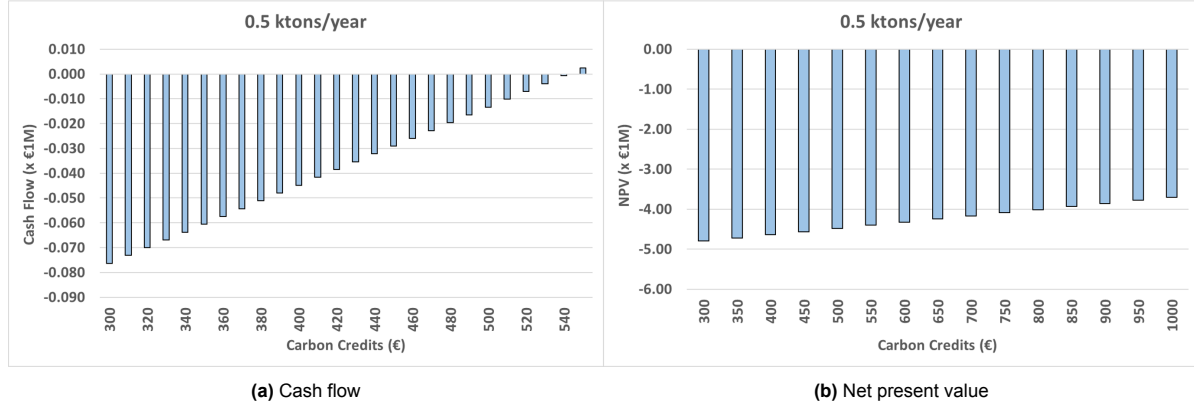


Figure 5.15: Cash flow and NPV of 0.5 ktons/year mineralization plant

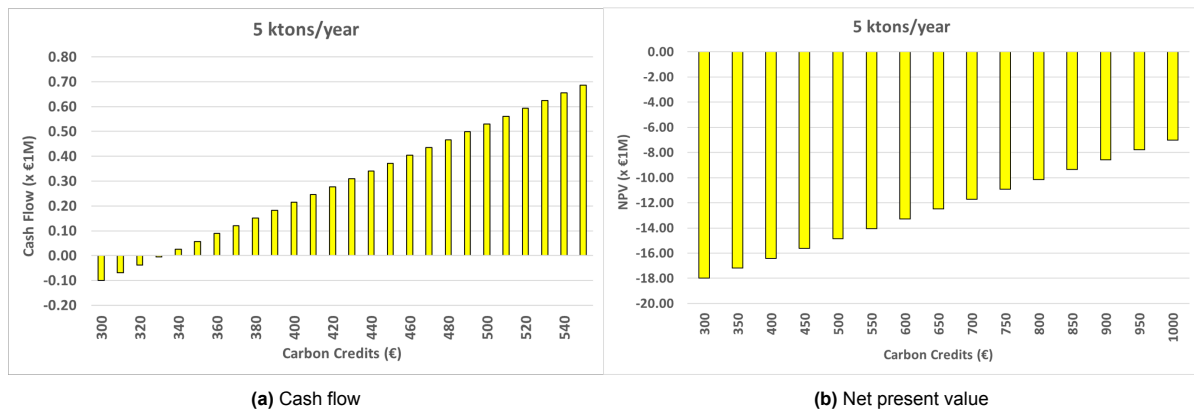


Figure 5.16: Cash flow and NPV of 5 ktons/year mineralization plant



Figure 5.17: Cash flow and NPV of 50 ktons/year mineralization plant

Based on the above results, it can be concluded that the 0.5 ktons/year and 5 ktons/year plants do not yield a positive NPV even with a high carbon credit price of €1000/t-CO₂, which is utilized by Climeworks for their direct air capture plant [47]. However, for the 50 ktons/year scale, both show feasibility in terms of generating a revenue stream for the mineralization plant.

To achieve a positive NPV for the 50 ktons/year plant, the carbon credit price required is around €700-750/t-CO₂, respectively. The values indicate the minimum carbon credit prices needed to offset the costs and generate a positive return on investment.

The analysis suggests that, compared to the smaller-scale plants, the larger-scale plants have a higher potential for profitability due to economies of scale and increased production capacity. The lower carbon credit prices required for positive NPV in the larger-scale plants indicate a more favorable financial outlook.

5.7.3. Sensitivity Analysis

In the preceding section, the minimum carbon credit price required for achieving an NPV>0 was determined. This section expands on that analysis by assessing the variables within the mineralization system that have the greatest impact on the NPVs. Figure 5.18 illustrates the results of a sensitivity analysis conducted on various factors, including olivine price, transportation costs, carbon credits, and other variables, to determine their influence on the NPV of the plant. The 50 ktons/year plant will be used as reference to assess this analysis.

The sensitivity analysis from the figure below highlights that changes in carbon credits, internal rate of return (IRR), and olivine price have a significant impact on the NPV of the mineralization system. These variables play a crucial role in determining the financial viability and profitability of the project. Therefore, careful evaluation and consideration of these factors are essential for making informed decisions. The carbon credit price, as established in the previous section, is a critical determinant of the NPV. Changes in carbon credit pricing have a direct effect on the revenue generated and, consequently, the profitability of the mineralization system. Monitoring and responding to fluctuations in carbon credit markets are therefore crucial for optimizing the financial performance of the project.

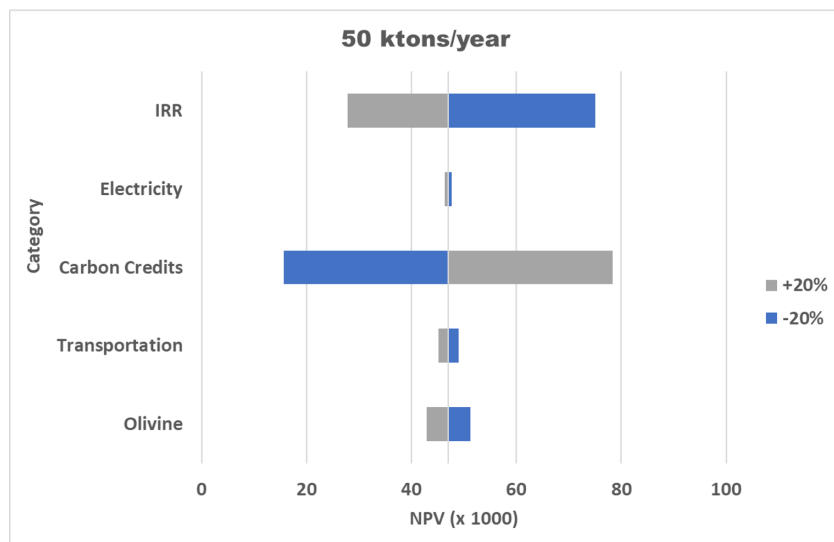


Figure 5.18: Sensitivity analysis on mineralization system

5.8. Business Case Opportunities

In the previous section, the economic evaluation of storing mineralized CO₂ was explored, revealing the potential for net profits through direct air capture + ex-situ mineralization. However, this section will focus on an alternative approach for utilizing the end products of CO₂ mineralization, namely through a business case model. Carbonated minerals have a potential of wide range of industrial applications, presenting attractive business opportunities for potential investors.

Figure 5.19 showcases the diverse industrial applications of carbonated products derived from CO₂ mineralization. These applications span various sectors, including construction, agriculture, water, manufacturing, and more. The versatility of carbonated minerals opens up avenues for innovation and commercialization, creating opportunities for entrepreneurs and investors to tap into.



Figure 5.19: Industrial applications of carbonated minerals
[6]

5.8.1. Building Materials

The cement industry is responsible for approximately 7% of anthropogenic CO₂ equivalent emissions and holds the highest carbon intensity of any industry per unit of revenue [111]. Given that the use of cement is fundamental to economic development, reducing its embodied emissions is considered essential. One of the ways this is dealt with is the application of natural minerals into cement in the concrete industry.

Although calcium carbonate (CaCO_3) derivatives are used extensively in the construction industry to reduce their carbon footprint [17], there exist some companies that created "olivine concrete" that has the capacity to store 0.133 tons of CO₂ per ton of concrete [2].

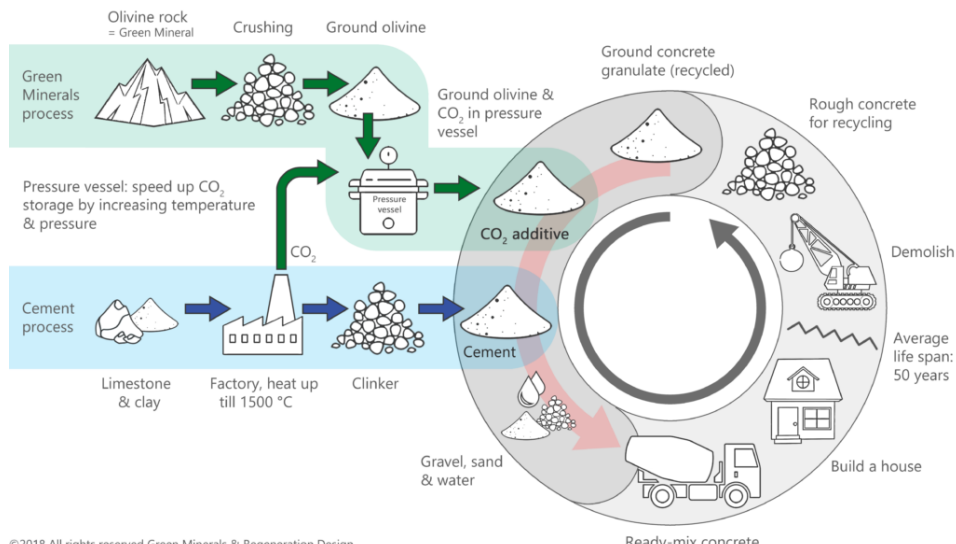


Figure 5.20: CO₂ based concrete and circular economy
[87]

The process can be depicted in Figure 5.20 where crushed olivine is grinded, reacted with CO₂ and used to replace cement in the concrete recycling process. This process is usually done by using industrial wastes products as CO₂ is captured directly from the concrete factory and used in the circular economy process [87]. Therefore, further investigations are required to assess the feasibility of using direct air capture and ex-situ mineralization with the application of this supplementary cementitious material (SCM).

The expected additional revenue that can be generated from this business case is €32 per tonne of cement (or €34 per ton CO₂ sequestered) in addition to additional CO₂ emission reductions of 8-33% [111]. Figure 5.21 shows the comparison of the NPV of a 50 kton/year mineralization plant with storage versus implementing a business case scenario. It can be seen that implementing a business case gave the plant a fixed difference in NPV of 0.53 million in revenue with varying carbon credit prices. Consequently, this amount to a lower carbon credit price needed to achieve a NPV>0. It can also be observed that when the carbon credit price hits around €650-700, implementing a business case model is enough to overturn a negative deficit in the storage case scenario into a positive outlook.

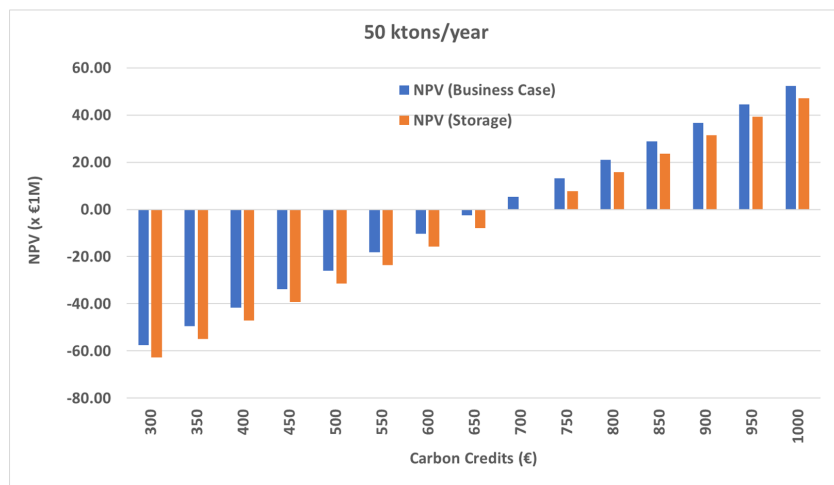


Figure 5.21: NPV comparison for 50 ktons/year mineralization plant

5.8.2. Asphalt Mixtures

The majority of European road and highway pavements are constructed using asphalt mixtures, with around 90% of them comprising natural aggregates. However, the extraction and consumption of these aggregates have a significant environmental impact [21]. To address this issue, researchers have investigated the use of low-grade Magnesium Carbonate (LG-MC) as a filler material in asphalt mixtures.

Low-grade Magnesium Carbonate refers to a product that contains not only magnesium carbonates but also unreacted olivine and silica, all of which are by-products of the mineralization system. Fortunately, these products have been proven to be beneficial in the road construction industry, as supported by literature [18, 21, 113].

A study conducted by Lopez-Montero et al. focused on replacing conventional calcium carbonate filler and a portion of the fine aggregates with LG-MC using the UCL (Universal de Caracterizacion de Ligantes) method in the manufacturing process of asphalt mixtures [20]. The evaluation considered various factors such as moisture sensitivity, cracking resistance at different temperatures, cohesion loss, and different mixture conditions [21].

The research findings indicate that LG-MC offers a protective effect to the asphalt mixture, enhancing its resistance to cracking. This demonstrates the suitability of magnesium carbonate as a partial substitute for the fine fraction of aggregates and as a filler in asphalt mixture manufacturing for road pavements. Utilizing this by-product would help reduce the use of natural aggregates, addressing the depletion of non-renewable resources and reducing waste that ends up in landfills, indirectly leading to a decrease in CO₂ emissions.

In addition, an article by Agro&Chemistry [18] mentioned a specific case where a 60-meter-long road constructed on the Zernike Campus in Groningen's Climate Adaptation Living Lab "captured" over 20

tonnes of CO₂. This road, when pulverized, exhibited an accelerated mineralization process. When the road surface gets wet, magnesium silicate in the stone initiates a chemical reaction, resulting in the formation of magnesium bicarbonate, which captures CO₂ from the air. Approximately 1 kg of this material can absorb about 1.25 kg of CO₂. Furthermore, the presence of silica in the mineralization process improves the bitumen (asphalt) resistance against aging, damages such as rutting and fatigue, and enhances the rheological behavior of bitumen [113].

To summarize, the end product stream consisting of magnesium carbonate, olivine, and silica offers several benefits to the road construction industry, including improving the durability and resistance of road surfaces. By incorporating these by-products, the industry can contribute to reducing the use of natural aggregates, minimizing the depletion of non-renewable resources, and reducing waste while indirectly lowering CO₂ emissions.

6

Conclusion & Recommendations

6.1. Conclusion

This investigation focused on the evaluation of an integrated direct air capture + mineralization system. Chapter 2 provided a literature review comparing different mineralization concepts, methods, and processes, ultimately selecting a base design with ideal characteristics for further analysis. The system design was modeled and simulated with varying flow rates to assess its performance. Optimization techniques, such as heat integration and recycling of streams were implemented along with the inclusion of a direct air capture unit to provide quantitative results regarding the mass and energy requirements of a complete system. A techno-economic evaluation was then conducted to determine the profitability of the process under specific assumptions.

With this in mind, the research questions posed in Section 1.2 were addressed as follows:

The techno-economic feasibility of the integrated Direct Air Capture + Mineralization system was assessed through a step-by-step comparison of existing processes, revealing that direct aqueous carbonation with salt additives showed the lowest price point amongst the presented options of €227/t-CO₂ sequestered.

Later, a more detailed design simulation was conducted which comprised of heat integration and recycled streams with the inclusion of a direct air capture unit. Comparison between an integrated and non-integrated process showed that the heat requirements of the system decreases 66.5% and also affected the energy requirements of other unit operations within the system.

Optimization steps and subsequent equipment selection were then conducted to be able to conduct an economic analysis for various plant scales, revealing that small-scale systems would not generate a net profit stream, while larger scales showed positive potential (NPV>0), warranting further research to validate this finding. A sensitivity analysis conducted in Chapter 5 highlighted the significant roles played by the carbon credit price, olivine price, and internal rate of return (IRR) in determining the plant's performance in the CO₂ market.

The mineralization process generated end products consisting of unreacted olivine, magnesium carbonate, and silica which are then either stored or utilized for business case models. It was revealed that in the cement making industry, additional revenue of €34 per ton CO₂ sequestered can potentially be made on top of further CO₂ reductions of 8-33%.

In summary, this investigation encompassed the design, simulation, and evaluation of a direct air capture + mineralization system. It addressed research questions, assessed techno-economic feasibility, and provided insights into the energy requirements, and carbon credit pricing. The investigation also explored the potential revenue streams and business opportunities associated with the mineralized end products.

6.2. Recommendation

Despite providing valuable insights into the behavior and feasibility of the direct air capture + mineralization system, this investigation raises unanswered questions that require further research. One area

that warrants more detailed investigation is the reaction kinetics of direct aqueous carbonation under specific pressure and temperature conditions set in the simulation. Obtaining accurate values through experimental work would enable the development of a more precise simulation model for using a CSTR reactor and subsequently gain a more accurate representation of the behavior of the whole system.

Moreover, due to the complexity of the system in terms of regeneration of acids and bases as well as the assumed negative implications from a life cycle assessment (LCA) perspective led to the exclusion of the indirect carbonation route in this investigation. However, exploring a comprehensive simulation of the indirect carbonation route and later comparing it with the direct aqueous carbonation simulation from this study would provide a clearer understanding of the limitations within CO₂ mineralization and improvements or the possible solutions that can be tackled in regards to the challenges associated with both routes.

Furthermore, the business case for the end products of CO₂ mineralization is only briefly discussed in this investigation. To fully evaluate its validity and attractiveness in a business case scenario, a comprehensive techno-economic evaluation should be conducted that includes more detailed information regarding the whole cement and concrete making industry and how it affects the mineralization process.

References

- [1] Carsten Drechsler; David W. Agar. *Investigation of water co-adsorption on the energy balance of solid sorbent based direct air capture processes*. 2020. URL: <https://www.sciencedirect.com/science/article/pii/S0360544219322820>.
- [2] AIREAL. *Olivine Concrete*. 2021. URL: <https://aireal-materials.com/Olivine-Concrete-8>.
- [3] Amin Azdarpour et. al. *A Review on Carbon Dioxide Mineral Carbonation Through pH-swing Process*. 2015. URL: https://www.researchgate.net/publication/277774057_A_Review_on_Carbon_Dioxide_Mineral_Carbonation_Through_pH-swing_Process (visited on 02/06/2023).
- [4] David L. McCollum et. al. *Energy investment needs for fulfilling the Paris Agreement and achieving the Sustainable Development Goals*. 2018. URL: <https://www.nature.com/articles/s41560-018-0179-z>.
- [5] HKaralee Jarvis; R. W. Carpenter; Todd Windman; Youngchul Kim; Ryan Nunez; Firas Alawneh. *Reaction Mechanisms for Enhancing Mineral Sequestration of CO₂*. 2009. URL: <https://pubs.acs.org/doi/10.1021/es8033507>.
- [6] Abdulaziz Alturki. *The Global Carbon Footprint and How New Carbon Mineralization Technologies Can Be Used to Reduce CO₂ Emissions*. 2022. URL: https://www.researchgate.net/publication/361396529_The_Global_Carbon_Footprint_and_How_New_Carbon_Mineralization_Technologies_Can_Be_Used_to_Reduce_CO2_Emissions.
- [7] M. Zuhaili Kashim; Haylay Tsegab; Omeid Rahmani; Zainol Affendi Abu Bakar; Shahram M. Aminpour. *Reaction Mechanism of Wollastonite In Situ Mineral Carbonation for CO₂ Sequestration: Effects of Saline Conditions, Temperature, and Pressure*. 2020. URL: <https://pubs.acs.org/doi/10.1021/acsomega.0c02358>.
- [8] Adam Hughmanick Berger and Abhoyjit S. Bhowm. “Comparing physisorption and chemisorption solid sorbents for use separating CO₂ from flue gas using temperature swing adsorption”. In: *Energy Procedia* 4 (2011). 10th International Conference on Greenhouse Gas Control Technologies, pp. 562–567. ISSN: 1876-6102. DOI: <https://doi.org/10.1016/j.egypro.2011.01.089>. URL: <https://www.sciencedirect.com/science/article/pii/S1876610211000919>.
- [9] Fred C. Bond. *Crushing and Grinding Calculations Part 1*. 1961. URL: <https://www.911metallurgist.com/blog/wp-content/uploads/2015/11/Bond-F-C-1961-Crushing-and-Grinding-Calculations.pdf>.
- [10] Benjamin Bonfils; Carine Julcour-Lebigue; Francois Guyot; Francoise Bodénand; Pierre Chiquet; Florent Bourgeois. *Comprehensive analysis of direct aqueous mineral carbonation using dissolution enhancing organic additives*. 2012. URL: <https://www.sciencedirect.com/science/article/pii/S1750583612001120>.
- [11] Katie Lebling; Haley Leslie-Bole; Zach Byrum. *6 Things to Know About Direct Air Capture*. 2022. URL: <https://www.wri.org/insights/direct-air-capture-resource-considerations-and-costs-carbon-removal>.
- [12] Balucan RD; Dlugogorski BZ. *Thermal activation of antigorite for mineralization of CO₂*. 2013. URL: <https://pubmed.ncbi.nlm.nih.gov/23215352/>.
- [13] W.K. O'Connor; William K. Dahlin; David C. Nilsen; David N. Rush; G E. Walters; Richard P. Turner; Paul C. *Carbon Dioxide Sequestration by Direct Mineral Carbonation: Results from Recent Studies and Current Status*. 2001. URL: <https://www.osti.gov/biblio/897125>.
- [14] Eric C. Carlson. *Don't Gamble With Physical Properties For Simulations*. 1996. URL: <http://www.cchem.berkeley.edu/cbe150b/docs/VLE/Guidelines.pdf>.

- [15] M.J. McKelvy; H. Béarat; A.V.G. Chizmeshya; R. Nunez; R.W. Carpenter. *UNDERSTANDING OLIVINE CO₂ MINERAL SEQUESTRATION MECHANISMS AT THE ATOMIC LEVEL: OPTIMIZING REACTION PROCESS DESIGN*. 2003. URL: <https://www.osti.gov/servlets/purl/822896>.
- [16] Valentin Gutknecht; Sandra Ósk Snæbjörnsdóttir; Bergur Sigfússon; Edda Sif Aradóttir; Louise Charles. *Creating a carbon dioxide removal solution by combining rapid mineralization of CO₂ with direct air capture*. 2018. URL: <https://www.sciencedirect.com/science/article/pii/S1876610218301498>.
- [17] Noah Chemicals. *Calcium Carbonate (CaCO₃) in The Concrete Industry and It's Carbon Footprint Reduction*. 2022. URL: <https://noahchemicals.com/blog/calcium-carbonate-caco3-in-the-concrete-industry-and-its-carbon-footprint-reduction/>.
- [18] Agro & Chemistry. *Asphalt with olivine eats tonnes of CO₂*. 2021. URL: <https://www.agro-chemistry.com/articles/asphalt-with-olivine-eats-tonnes-of-co2/>.
- [19] LibreText Chemistry. *Le Chatelier's Principle*. 2023. URL: [https://chem.libretexts.org/Bookshelves/Physical_and_Theoretical_Chemistry_Textbook_Maps/Supplemental_Modules_\(Physical_and_Theoretical_Chemistry\)/Equilibria/Le_Chateliers_Principle](https://chem.libretexts.org/Bookshelves/Physical_and_Theoretical_Chemistry_Textbook_Maps/Supplemental_Modules_(Physical_and_Theoretical_Chemistry)/Equilibria/Le_Chateliers_Principle).
- [20] T. Lopez-Montero; A. Maldonado-Alameda; J. Manosa; R. Miro; J.M. Chimenos. *Analysing the potential use of a low-grade magnesium carbonate by-product as a filler in hot asphalt mixtures*. 2022. URL: <https://www.tandfonline.com/doi/full/10.1080/10298436.2022.2083618>.
- [21] Teresa Lopez-Montero; Jofre Manosa; Rodrigo Miro; Josep Maria Chimenos. *Sustainable asphalt mixtures by partial replacement of fine aggregates with low-grade magnesium carbonate by-product*. 2022. URL: <https://www.sciencedirect.com/science/article/pii/S2214509522008373>.
- [22] Liquid Chromatography. *Centrifugal Filtration Equipment*. 2023. URL: <https://www.beyonddiscovery.org/liquid-chromatography/centrifugal-filtration-equipment.html>.
- [23] Climate-KIC. *Co-Action carbon capture project opens new field plots*. 2020. URL: <https://www.climate-kic.org/news/co-action-carbon-capture-project-opens-new-field-plots/#:~:text='Co%20DAction.-,' ,is%2020crushed%2020into%2020small%2020bits..>
- [24] Climeworks. *What is direct air capture?* 2023. URL: <https://climeworks.com/direct-air-capture>.
- [25] CNBC. *Carbon capture technology has been around for decades — here's why it hasn't taken off*. 2021. URL: <https://www.cnbc.com/2021/01/31/carbon-capture-technology.html>.
- [26] W.J.J. Huijgen; R.N.J. Comans. *Carbon Dioxide Sequestration by Mineral Carbonation: Literature Review Update 2003–2004*. 2005. URL: <https://www.osti.gov/etdeweb/biblio/20767421>.
- [27] Adrian Cowan. *ENALYSIS TIP 1.10 - RECIPROCATING COMPRESSOR LIMITATIONS*. 2020. URL: <https://www.detection.com/learningcenter/enalysis-tip-1.10-reciprocating-compressor-limitations>.
- [28] Kenneth C. Curry. *U.S. Geological Survey, Mineral Commodity Summaries*. 2020. URL: <https://pubs.usgs.gov/periodicals/mcs2020/mcs2020-wollastonite.pdf>.
- [29] Peter B. Kelemen; Juerg Matter; Elisabeth E. Streit; John F. Rudge; William B. Curry; and Jerzy Blusztajn. *Rates and Mechanisms of Mineral Carbonation in Peridotite: Natural Processes and Recipes for Enhanced, in situ CO₂ Capture and Storage*. 2011. URL: <https://www.annualreviews.org/doi/10.1146/annurev-earth-092010-152509>.
- [30] Mike Daniel. *Measurement of electrical energy consumption in a Bond ball mill*. 2011. URL: https://www.researchgate.net/publication/43460236_Measurement_of_electrical_energy_consumption_in_a_Bond_ball_mill.
- [31] Our World in Data. *CO₂ and Greenhouse Gas Emissions*. 2020. URL: <https://ourworldindata.org/co2-and-greenhouse-gas-emissions#:~:text=Human%20emissions%20of%20carbon%20dioxide,been%20true%20throughout%20Earth's%20history>. (visited on 02/06/2023).

- [32] Our World in Data. *Global Greenhouse Gas Emissions and Warming Scenarios*. 2020. URL: <https://ourworldindata.org/co2-and-greenhouse-gas-emissions> (visited on 02/07/2023).
- [33] Paul Fennell; Justin Driver; Christopher Bataille; Steven J. Davis. *Cement and steel — nine steps to net zero*. 2022. URL: <https://doi.org/10.1038/d41586-022-00758-4>.
- [34] Science Direct. *Fanning Equation*. 1994. URL: <https://www.sciencedirect.com/topics/engineering/fanning-equation>.
- [35] Science Direct. *Henry's Law*. 2017. URL: <https://www.sciencedirect.com.tudelft.idm.oclc.org/topics/chemistry/henrys-law>.
- [36] Science Direct. *Settling velocity*. 2005. URL: <https://www.sciencedirect.com/topics/physics-and-astronomy/settling-velocity>.
- [37] Fei Wang; David Dreisinger; Mark Jarvis; Tony Hitchins; Devy Dyson. *Quantifying kinetics of mineralization of carbon dioxide by olivine under moderate conditions*. 2019. URL: <https://www.sciencedirect.com/science/article/abs/pii/S1385894718324343>.
- [38] S. A. Didas E. S. Sanz-Perez C. R. Murdock and C. W. Jones. *Direct Capture of CO₂ from Ambient Air*. 2016. URL: <https://pubs.acs.org/doi/full/10.1021/acs.chemrev.6b00173> (visited on 08/25/2016).
- [39] P.C. Chiang E.E. Chang S.Y. Pan. *CO₂ capture by accelerated carbonation of alkaline wastes: a review on its principles and applications*. 2012. URL: [http://refhub.elsevier.com/S1385-8947\(15\)00740-8/h0460](http://refhub.elsevier.com/S1385-8947(15)00740-8/h0460).
- [40] Carbon Engineering. *Our Technology*. 2023. URL: <https://carbonengineering.com/our-technology/>.
- [41] evcValuation. *The Cost-to-Capacity Method and Scale Factors*. 2015. URL: <https://evcvaluation.com/the-cost-to-capacity-method-and-scale-factors/>.
- [42] K.S. Lackner F. Goff. *Carbon dioxide sequestering using ultramafic rocks*. 1998. URL: [http://refhub.elsevier.com/S1385-8947\(15\)00740-8/h0420](http://refhub.elsevier.com/S1385-8947(15)00740-8/h0420).
- [43] Johan Fagerlund. *Carbonation of Mg(OH)₂ in a pressurised fluidised bed for CO₂ sequestration*. 2012. URL: https://www.doria.fi/bitstream/handle/10024/74477/fagerlund_johan.pdf?sequence=2.
- [44] David Dreisinger Fei Wang. *Status of CO₂ mineralization and its utilization prospects*. 2022. URL: <https://www.oaepublish.com/minerals/articles/mmm.2022.02/> (visited on 02/06/2023).
- [45] World Economic Forum. *Analysis: Global CO₂ emissions from fossil fuels hits record high in 2022*. 2022. URL: <https://www.weforum.org/agenda/2022/11/global-co2-emissions-fossil-fuels-hit-record-2022/#:~:text=The%20atmospheric%20CO2%20concentration%20increased,relative%20to%20pre%2Dindustrial%20levels..> (visited on 02/06/2023).
- [46] Pump Fundamentals. *The Nature of Slurry*. 2023. URL: https://www.pumpfundamentals.com/slurry/nature_of_slurry.pdf.
- [47] Giving Green. *Climeworks*. 2021. URL: <https://www.givinggreen.earth/carbon-offsets-research/climeworks>.
- [48] Damien Daval; Isabelle Martinez; Jean-Michel Guigner; Roland Hellmann; Jérôme Corvisier; Nathaniel Findling; Christian Dominici; Bruno Goffé; François Guyot. *Mechanism of wollastonite carbonation deduced from micro- to nanometer length scale observations*. 2015. URL: <https://www.degruyter.com/document/doi/10.2138/am.2009.3294/html>.
- [49] Jan Harmsen; Andre B. de Haan; Pieter L.J. Swinkels. *Product and Process Design*. First Edition. The Netherlands: De Gruyter, 2018.
- [50] Warren L. McCabe; Julian C. Smith; Peter Harriott. *Unit Operations of Chemical Engineering*. 1993. URL: <https://ostad.nit.ac.ir/payaidea/ospic/file2634.pdf>.
- [51] Fei Wang; David Dreisinger; Mark Jarvis; Tony Hitchins. *Kinetics and mechanism of mineral carbonation of olivine for CO₂ sequestration*. 2019. URL: <https://www.sciencedirect.com/science/article/abs/pii/S0892687518305077>.

- [52] Fei Wang; David Dreisinger; Mark Jarvis; Tony Hitchins. *Kinetics and mechanism of mineral carbonation of olivine for CO₂ sequestration*. 2019. URL: <https://www.sciencedirect.com/science/article/abs/pii/S0892687518305077>.
- [53] Richard Huguenor. *Why A Centrifugal Air Compressor May be the Better Choice*. 2023. URL: <https://www.airbestpractices.com/industries/plastics/why-a-centrifugal-air-compressor-may-be-the-better-choice>.
- [54] Wouter J. J. Huijgen. *Carbon Dioxide Sequestration by Mineral Carbonation*. 2007. URL: <https://edepot.wur.nl/121870>.
- [55] Central States Industrial. *FOULING IN HEAT EXCHANGERS*. 2021. URL: <https://www.csidesigns.com/blog/articles/fouling-in-heat-exchangers>.
- [56] Central States Industrial. *A COMPLETE GUIDE TO PUMPING SLURRIES*. 2021. URL: <https://www.csidesigns.com/blog/articles/slurry-pump>.
- [57] Ipieca. *Heat exchangers*. 2022. URL: <https://www.ipieca.org/resources/energy-efficiency-solutions/heat-exchangers-2022>.
- [58] Ipieca. *Pinch analysis*. 2022. URL: <https://www.ipieca.org/resources/energy-efficiency-solutions/pinch-analysis-2022>.
- [59] S. Teir J. Sipila" and R. Zevenhoven. *Carbon Dioxide Sequestration by Mineral Carbonation: Literature Review Update 2005–2007*. 2008. URL: https://www.researchgate.net/publication/44448977_Carbon_Dioxide_Sequestration_by_Mineral_Carbonation_Literature_Review_Update_2005-2007.
- [60] Dea Hyun Moon; Sang Shin Park; Seong-Pil Kang; Wonhee Lee; Ki Tae Park; Dong Hyun Chun; Geun Bae Rhim; Sun-Mi Hwang; Min Hye Youn; Soon Kwan Jeong. *Determination of kinetic factors of CO₂ mineralization reaction for reducing CO₂ emissions in cement industry and verification using CFD modeling*. 2021. URL: <https://www.sciencedirect.com/science/article/abs/pii/S1385894721010081>.
- [61] Yeo Tze Yuen; Paul N. Sharratt; Bu Jie. *Carbon dioxide mineralization process design and evaluation: concepts, case studies, and considerations*. 2016. URL: <https://link.springer.com/article/10.1007/s11356-016-6512-9>.
- [62] Amin Azdarpour; Mohammad Asadullah; Erfan Mohammadian; Hossein Hamidi; Radzuan Junin; Mohammad Afkhami Karaei. *A review on carbon dioxide mineral carbonation through pH-swing process*. 2015. URL: <https://www.sciencedirect.com/science/article/abs/pii/S1385894715007408>.
- [63] Will Kenton. *Economies of Scale: What Are They and How Are They Used?* 2022. URL: <https://www.investopedia.com/terms/e/economiesofscale.asp>.
- [64] Georgette Kilgore. *Air Freight vs Sea Freight Carbon Footprint (The Real Numbers in 2023)*. 2023. URL: <https://8billontrees.com/carbon-offsets-credits/carbon-ecological-footprint-calculators/air-freight-vs-sea-freight-carbon-footprint>.
- [65] Georgette Kilgore. *Carbon Credit Price Chart: Live Updates (2023 Carbon Stock Chart)*. 2023. URL: <https://8billontrees.com/carbon-offsets-credits/carbon-credit-price-chart/>.
- [66] Georgette Kilgore. *Truck CO₂ Emissions Per Km Calculator: Find Semi Truck Carbon Footprint*. 2023. URL: <https://8billontrees.com/carbon-offsets-credits/carbon-ecological-footprint-calculators/truck-co2-emissions-per-km-calculator>.
- [67] Ron Zevenhoven; Jens Kohlmann. *CO₂ SEQUESTRATION BY MAGNESIUM SILICATE MINERAL CARBONATION IN FINLAND*. 2002. URL: https://www.researchgate.net/publication/237122745_CO2_sequestration_by_magnesium_silicate_mineral_carbonation_in_Finland.
- [68] Jennifer L. *Generating Carbon Credits from Mining Waste*. 2022. URL: <https://carboncredits.com/bhp-carbon-mineralization/>.

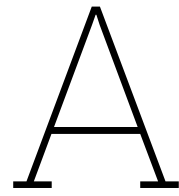
- [69] Berenika Kokoszka; Nina K. Jarrah; Cong Liu; Prof. Dr. David T. Moore; Prof. Dr. Kai Landskron. *Supercapacitive Swing Adsorption of Carbon Dioxide*. 2014. URL: <https://onlinelibrary.wiley.com/doi/full/10.1002/anie.201310308>.
- [70] Muhammad Bilal; Jiajie Li; Kai Landskron. *Activated Carbon Electrodes with Improved Sorption Capacity for Supercapacitive Swing Adsorption of Carbon Dioxide*. 2022. URL: https://www.researchgate.net/publication/363399861_Activated_Carbon_Electrodes_with_Improved_Sorption_Capacity_for_Supercapacitive_Swing_Adsorption_of_Carbon_Dioxide.
- [71] Heping Xie; Fuhuan Wang; Yufei Wang; Tao Liu; Yifan Wu; Bin Liang. *CO₂ mineralization of natural wollastonite into porous silica and CaCO₃ powders promoted via membrane electrolysis*. 2018. URL: <https://link.springer.com/article/10.1007/s12665-018-7330-9>.
- [72] LibreTextsChemistry. *Dalton's Law of Partial Pressures*. 2023. URL: [https://chem.libretexts.org/Bookshelves/Physical_and_Theoretical_Chemistry_Textbook_Maps/Supplemental_Modules_\(Physical_and_Theoretical_Chemistry\)/Physical_Properties_of_Matter/States_of_Matter/Properties_of_Gases/Gas_Laws/Dalton%27s_Law_\(Law_of_Partial_Pressures\)](https://chem.libretexts.org/Bookshelves/Physical_and_Theoretical_Chemistry_Textbook_Maps/Supplemental_Modules_(Physical_and_Theoretical_Chemistry)/Physical_Properties_of_Matter/States_of_Matter/Properties_of_Gases/Gas_Laws/Dalton%27s_Law_(Law_of_Partial_Pressures)).
- [73] Chemical Engineering Department LJIET. *Total Capital Investment Cost Index Six Tenth Rule*. 2022. URL: <https://youtu.be/I8vxrykV8I>.
- [74] Shiva S. Salek; Robbert Kleerebezem; Henk M. Jonkers; Geert-jan Witkamp; Mark C. M. van Loosdrecht. *Mineral CO₂ sequestration by environmental biotechnological processes*. 2013. URL: <https://pubmed.ncbi.nlm.nih.gov/23384505/>.
- [75] R. Symonds; D. Y. Lu; R. Hughes; E. Anthony; A. Macchi. *CO₂ Capture from Simulated Syngas via Cyclic Carbonation/Calcination for a Naturally Occurring Limestone: Pilot-Plant Testing*. 2009. URL: <https://www.semanticscholar.org/paper/C02-Capture-from-Simulated-Syngas-via-Cyclic-for-a-Symonds-Lu/7b2e9d10b900d0d6c8d894b3fc3289443a4fbabb>.
- [76] Neumann Machinery. *Grinding Mills: How they Work*. 2020. URL: <https://neumannmachinery.com/how-grinding-mills-work/>.
- [77] Mohammed D. Aminu; Seyed Ali Nabavi; Christopher A. Rochelle; Vasilije Manovic. *A review of developments in carbon dioxide storage*. 2017. URL: <https://www.sciencedirect.com/science/article/pii/S0306261917313016>.
- [78] Xiaolong Wang; M. Maroto-Valer. *Dissolution of serpentine using recyclable ammonium salts for CO₂ mineral carbonation*. 2011. URL: <https://www.semanticscholar.org/paper/Dissolution-of-serpentine-using-recyclable-ammonium-Wang-Maroto-Valer/a90d673da0c2dd0a763c00635b24994babe8ec8c>.
- [79] A. Sanna; M. Uibu; G. Caramanna; R. Kuusikb; M. M. Maroto-Valera. *A review of mineral carbonation technologies to sequester CO₂*. 2014. URL: <https://pubs.rsc.org/en/content/articlelanding/2014/cs/c4cs00035h>.
- [80] J.B.R. et. al. Matthews. *Climate Change 2021 The Physical Science Basis*. 2023. URL: <https://www.ipcc.ch/report/ar6/wg1/> (visited on 02/06/2023).
- [81] 911 Metallurgist. *Table of Bond Work Index by Minerals*. 2015. URL: <https://www.911metallurgist.com/blog/table-of-bond-work-index-by-minerals>.
- [82] Metso. *Metso in Filtration*. 2012. URL: mcilvainecompany.com/Decision_Tree/subscriber/Tree/DescriptionTextLinks/Metso_in_filtration_pdf_brochure.pdf.
- [83] Bert et. al. Metz. *Geo-Chemo-Mechanical Studies for Permanent CO₂ Storage in Geologic Reservoirs*. 2013. URL: <https://www.osti.gov/biblio/1131057>.
- [84] Bert et. al. Metz. *IPCC special report on carbon dioxide capture and storage*. 2005. URL: <https://www.osti.gov/biblio/20740954>.
- [85] The Engineering Mindset. *Spiral Heat Exchangers*. 2022. URL: <https://www.youtube.com/watch?v=kVuoa9ntPgA>.
- [86] Dakota Matrix Minerals. *wollastonite*. 1995. URL: <https://www.dakotamatrix.com/mineralpedia/9845/wollastonite>.

- [87] Green Minerals. *Concrete*. 2020. URL: <https://www.green-minerals.nl/concrete/>.
- [88] Subrahmaniam Hariharan Mischa Werner and Marco Mazzotti. *Flue gas CO₂ mineralization using thermally activated serpentine: from single- to double-step carbonation*. 2014. URL: <https://www.sciencedirect.com/science/article/pii/S1876610214024412> (visited on 02/06/2023).
- [89] Maria Carmela Dichicco; Salvatore Laurita; Michele Paternoster; Giovanna Rizzo; Rosa Sinisi; Giovanni Mongelli. *Serpentinite carbonation for CO₂ sequestration in the southern Apennines: preliminary study*. 2015. URL: <https://www.sciencedirect.com/science/article/pii/S1876610215016641>.
- [90] O'Connor W. K.; Dahlin D. C.; Rush G. E.; Gerdemann S. J.; Penner L. R.; Nilsen D. N. *Aqueous mineral carbonation: Mineral availability, pre-treatment, reaction parametrics and process studies*. 2005. URL: https://www.researchgate.net/publication/315844800_Aqueous_Mineral_Carbonation_Mineral_Availability_Pretreatment_Reaction_Parametrics_and_Process_Studies.
- [91] Adeline Nagle. *Harnessing Earth's natural cycles to reverse climate change*. 2023. URL: <https://news.miami.edu/stories/2023/03/harnessing-earths-natural-cycles-to-reverse-climate-change.html>.
- [92] Tom Nelthorpe. *Proximo Weekly: Direct air capture – direct to market?* 2021. URL: <https://www.proximoinfra.com/articles/8105/Proximo-Weekly-Direct-air-capture-direct-to-market>.
- [93] William Nicolle. *Four negative emission technologies that could get us to net zero*. 2020. URL: [https://policyexchange.org.uk/blogs/four-negative-emission-technologies-nets-that-could-get-us-to-net-zero/#:~:text='Negative%2020emissions'%2020technologies%20\(NETs,worst%2020effects%2020of%2020climate%20change..](https://policyexchange.org.uk/blogs/four-negative-emission-technologies-nets-that-could-get-us-to-net-zero/#:~:text='Negative%2020emissions'%2020technologies%20(NETs,worst%2020effects%2020of%2020climate%20change..)
- [94] Abass A. Olajire. *A review of mineral carbonation technology in sequestration of CO₂*. 2013. URL: <https://www.sciencedirect.com/science/article/pii/S0920410513000673>.
- [95] Aspen One. *Aspen Plus V8.6 teaching module on steam tables*. 2014. URL: https://aspentechsupport.blob.core.windows.net/cbt/Thermo002/presentation_html5.html.
- [96] L.S. Park A.H.A.; Fan. *CO₂ mineral sequestration: physically activated dissolution of serpentine and pH swing process*. 2004. URL: <https://www.sciencedirect.com/science/article/pii/S0009250904006773?via%3Dihub>.
- [97] Paddeu Daniela; Thomas Calvert; Ben Clark; Graham Peter Parkhurst. *New Technology and Automation in Freight Transport and Handling Systems New Technology and Automation in Freight Transport and Handling Systems*. 2019. URL: https://www.researchgate.net/publication/332423194_New_Technology_and_Automation_in_Freight_Transport_and_Handling_Systems_New_Technology_and_Automation_in_Freight_Transport_and_Handling_Systems.
- [98] S. J. Gerdemann; D. C. Dahlin; W. K. O'Connor; L. R. Penner. *CARBON DIOXIDE SEQUESTRATION BY AQUEOUS MINERAL CARBONATION OF MAGNESIUM SILICATE MINERALS*. 2003. URL: <https://www.sciencedirect.com/science/article/pii/B9780080442761501082>.
- [99] What is Piping. *Types of Heat Exchangers and Their Selection (PDF)*. 2022. URL: <https://whatispiping.com/types-of-heat-exchanger-selection/>.
- [100] plumtri. *Co-Action carbon capture project opens new field plots*. 2020. URL: <https://www.plumtri.org/node/1128>.
- [101] H. F. Da Costa; M. Fan; A. T. R. *Method to sequester CO₂ as mineral carbonate*. 2009. URL: <https://patentimages.storage.googleapis.com/96/f3/f1/e30c15d9e3dfcc/US20100221163A1.pdf>.
- [102] Big Rentz. *4 Types of Air Compressors: Which is Right for Your Project?* 2022. URL: <https://www.bigrertz.com/blog/air-compressor-types>.

- [103] Ding-Yu Peng; Donald B. Robinson. *A New Two-Constant Equation of State*. 1975. URL: <https://pubs.acs.org/doi/abs/10.1021/i160057a011>.
- [104] Sipilä Johan; Teir Sebastian; Zevenhoven Ron. *Carbon Dioxide Sequestration by Mineral Carbonation: Literature Review Update 2005–2007*. 2008. URL: https://www.researchgate.net/publication/44448977_Carbon_Dioxide_Sequstration_by_Mineral_Carbonation_Literature_Review_Update_2005-2007.
- [105] L. Jiang; R.Q. Wang; A. Gonzalez-Diaz; A. Smallbone; R.O. Lamidi; A.P. Roskilly. *Comparative analysis on temperature swing adsorption cycle for carbon capture by using internal heat/mass recovery*. 2020. URL: <https://www.sciencedirect.com/science/article/pii/S1359431119373181>.
- [106] Quin R. S. Miller; H. Todd Schaeff; John P. Kaszuba; Greeshma Gadikota; B. Peter McGrail; Kevin M. Rosso. *Quantitative Review of Olivine Carbonation Kinetics: Reactivity Trends, Mechanistic Insights, and Research Frontiers*. 2019. URL: https://www.researchgate.net/publication/334431626_Quantitative_Review_of_Olivine_Carbonation_Kinetics_Reactivity_Trends_Mechanistic_Insights_and_Research_Frontiers.
- [107] Stephen J Gerdemann; William K O'Connor; David C Dahlin; Larry R Penner; Hank Rush. *Ex situ aqueous mineral carbonation*. 2007. URL: <https://pubmed.ncbi.nlm.nih.gov/17438820/>.
- [108] Roelof D Schuiling. *Olivine: a supergreen fuel*. 2013. URL: <https://energsustainsoc.biomedcentral.com/articles/10.1186/2192-0567-3-18>.
- [109] National Academics of Sciences Engineering Medicine. *Negative Emissions Technologies and Reliable Sequestration*. 2019. URL: <https://nap.nationalacademies.org/catalog/25259/negative-emissions-technologies-and-reliable-sequestration-a-research-agenda>.
- [110] Daniel Nugent; Benjamin Sovacool. *Assessing the lifecycle greenhouse gas emissions from solar PV and wind energy: A critical meta-survey*. 2014. URL: https://www.researchgate.net/publication/259513614_Assessing_the_lifecycle_greenhouse_gas_emissions_from_solar_PV_and_wind_energy_A_critical_meta-survey.
- [111] Till Strunge; Phil Renforth; Mijndert Van der Spek. *Towards a business case for CO₂ mineralisation in the cement industry*. 2022. URL: <https://www.nature.com/articles/s43247-022-00390-0>.
- [112] Nancy W. Stauffer. *A new approach to carbon capture*. 2020. URL: <https://news.mit.edu/2020/new-approach-to-carbon-capture-0709>.
- [113] Gholam Ali Shafabakhsh; Mostafa Sadegnejad; Behzad Ahoor; Esmaiel Taheri. *Laboratory experiment on the effect of nano SiO₂ and TiO₂ on short and long-term aging behavior of bitumen*. 2020. URL: <https://www.sciencedirect.com/science/article/abs/pii/S0950061819330922>.
- [114] Giuseppe Tommasone. *Spiral Heat Exchangers: right solution for slurry, high viscosity fluids containing solids*. 2016. URL: <https://www.linkedin.com/pulse/spiral-heat-exchangers-right-solution-slurry-high-fluids-tommasone/>.
- [115] Chemical Engineering Transactions. *Heat Exchanger Network Synthesis Considering Different Minimum Approach Temperatures*. 2019. URL: <https://www.cetjournal.it/index.php/cet/article/view/CET1972048>.
- [116] Soonchul Kwon; Maohong Fan; Herbert F. M. Dacosta; Armistead G. Russell; Costas Tsouris. *Reaction Kinetics of CO₂ Carbonation with Mg-Rich Minerals*. 2011. URL: <https://pubmed.ncbi.nlm.nih.gov/21627148/>.
- [117] Jr. W. David Smith. *Needs and New Directions in Computing for the Chemical Process Industries*. 1999. URL: <https://www.ncbi.nlm.nih.gov/books/NBK44989/>.
- [118] W.SEIFRITZ. *CO₂ disposal by means of silicates*. 1990. URL: <https://www.nature.com/articles/345486b0>.
- [119] W.K. O'Connor; D.C. Dahlin; D.N. Nilsen; R.P. Walters; and P.C. Turner. *CARBON DIOXIDE SEQUESTRATION BY DIRECT AQUEOUS MINERAL CARBONATION*. 2001. URL: <https://www.osti.gov/servlets/purl/897125>.

- [120] Raghavendra Ragipani; Keerthana Sreenivasan; Robert P. Anex; Hang Zhai; Bu Wang. *Direct Air Capture and Sequestration of CO₂ by Accelerated Indirect Aqueous Mineral Carbonation under Ambient Conditions*. 2022. URL: <https://pubs.acs.org/doi/10.1021/acssuschemeng.1c07867>.
- [121] University of Waterloo. *Convection Heat Transfer*. 2023. URL: http://www.mh1t.uwaterloo.ca/courses/ece309_mechatronics/lectures/pdffiles/ach6_web.pdf.
- [122] Webqc. *Serpentine molar mass*. 2023. URL: <https://www.webqc.org/molecular-weight-of-Mg2Si2O5%20280H%20294.html>.
- [123] Wikipedia. *Chemical reactor*. 2022. URL: https://en.wikipedia.org/wiki/Chemical_reactor.
- [124] Wikipedia. *Continuous stirred-tank reactor*. 2023. URL: https://en.wikipedia.org/wiki/Continuous_stirred-tank_reactor.
- [125] Wikipedia. *Logarithmic mean temperature difference*. 2023. URL: https://en.wikipedia.org/wiki/Logarithmic_mean_temperature_difference.
- [126] Wikipedia. *Mohs scale*. 2023. URL: https://en.wikipedia.org/wiki/Mohs_scale.
- [127] Wikipedia. *Nusselt number*. 2023. URL: https://en.wikipedia.org/wiki/Nusselt_number.
- [128] Wikipedia. *Olivine*. 2023. URL: <https://en.wikipedia.org/wiki/Olivine>.
- [129] Wikipedia. *Prandtl number*. 2023. URL: https://en.wikipedia.org/wiki/Prandtl_number.
- [130] Wikipedia. *Serpentine*. 2023. URL: https://en.wikipedia.org/wiki/Serpentine_subgroup.
- [131] Wikipedia. *Wollastonite*. 2023. URL: <https://en.wikipedia.org/wiki/Wollastonite>.
- [132] Caleb M. Woodall; Isabella Piccione; Michela Benazzi; Jennifer Wilcox. *Capturing and Reusing CO₂ by Converting It To Rocks*. 2021. URL: <https://kids.frontiersin.org/articles/10.3389/frym.2020.592018>.
- [133] Peter Kelemen; Sally M. Benson; Hélène Pilorgé; Peter Psarras; Jennifer Wilcox. *An overview of the status and challenges of CO₂ storage in minerals and geological formations*. 2019. URL: <https://www.frontiersin.org/articles/10.3389/fclim.2019.00009/full>.
- [134] Wouter J. J. Huijgen; Gerrit Jan Ruijg; Rob N. J. Comans; Geert-Jan Witkamp. *Energy Consumption and Net CO₂ Sequestration of Aqueous Mineral Carbonation*. 2006. URL: <https://research.wur.nl/en/publications/energy-consumption-and-net-co2-sequestration-of-aqueous-mineral-c>.
- [135] Wouter J.J. Huijgen; Rob N.J. Comans; Geert-Jan Witkamp. *Cost evaluation of CO₂ sequestration by aqueous mineral carbonation*. 2007. URL: <https://www.sciencedirect.com/science/article/pii/S0196890407000520>.
- [136] Hamdallah Béarat; Michael J. McKelvy; Andrew V. G. Chizmeshya; Deirdre Gormley; Ryan Nunez; R. W. Carpenter; Kyle Squires; George H. Wolf. *Carbon Sequestration via Aqueous Olivine Mineral Carbonation: Role of Passivating Layer Formation*. 2006. URL: <https://pubs.acs.org/doi/10.1021/es0523340>.
- [137] Clarissa Wright. *What Happens to Carbon Stored Underground?* 2022. URL: <https://www.azocleantech.com/article.aspx?ArticleID=1582>.
- [138] Xchanger. *What is “Approach Temperature”?* 2023. URL: <https://xchanger.com/faq/>.
- [139] Wei Liu; Sheng Su; Kai Xu; Qindong Chen; Jun Xu; Zhijun Sun; Yi Wang; Song Hu; Xiaolong Wang; Yanting Xue; Jun Xiang. *CO₂ sequestration by direct gasesolid carbonation of fly ash with steam addition*. 2018. URL: <https://www.sciencedirect.com/science/article/pii/S0959652617332754>.
- [140] Pavan Kumar Naraharisetti; Tze Yuen Yeo; and Jie Bu. *Factors Influencing CO₂ and Energy Penalties of CO₂ Mineralization Processes*. 2017. URL: <https://chemistry-europe.onlinelibrary.wiley.com/doi/full/10.1002/cphc.201700565>.
- [141] Erin R. Bobicki; Qingxia Liu; Zhenghe Xu; Hongbo Zeng. *Carbon capture and storage using alkaline industrial wastes*. 2012. URL: <https://www.sciencedirect.com/science/article/pii/S0360128511000554>.

- [142] Hannu-Petteri Mattila; Inga Grigaliūnaitė; Ron Zevenhoven. *Chemical kinetics modeling and process parameter sensitivity for precipitated calcium carbonate production from steelmaking slags*. 2012. URL: <https://www.sciencedirect.com/science/article/pii/S1385894712004287>.



Appendix

Gas-Solid Olivine			Gas-Solid Wollastonite		
Consumption	Electrical/Thermal Energy (kWh/t-CO2)	Price (€/t-CO2)	Consumption	Electrical/Thermal Energy (kWh/t-CO2)	Price (€/t-CO2)
Compressor	465	622	Compressor	129	10
Water Pump	1.01	0.08	Water Pump	0.37	0.03
Grinding	188	15	Grinding	44	3
Total Electricity	654	52	Total Electricity	173	14
Water Heating	1010	81	Water Heating	244	20
Mineral Heating	297	24	Mineral Heating	147	12
Total Heat	1307	105	Total Heat	391	31
Feedstock	-	622	Feedstock	-	961
End Products	-	163	End Products	-	75
Final Price	-	941	Final Price	-	1081

Table A.1: Gas-solid comparison olivine vs. wollastonite

Direct Aqueous Carbonation without Additives			Direct Aqueous Carbonation with Additives		
Consumption	Electrical/Thermal Energy (kWh/t-CO2)	Price (€/t-CO2)	Consumption	Electrical/Thermal Energy (kWh/t-CO2)	Price (€/t-CO2)
Compressor	218	17	Compressor	158	13
Slurry Pump	12	1	Slurry Pump	8	1
Grinding	114	9	Grinding	83	7
Total Electricity	344	28	Total Electricity	249	20
Total Heat	444	36	Total Heat	322	26
Feedstock	-	183	Feedstock	-	133
End Products	-	60	End Products	-	48
Final Price	-	306	Final Price	-	227

Table A.2: Direct aqueous carbonation comparison without salts vs with salts

Carbon Credit Price (€)	Cash Flow (x1M)	Cash Flow (x1M)	Cash Flow (x1M)
	0.5 ktons/year	5 ktons/year	50 ktons/year
300	-0.076	-0.10	1.34
310	-0.073	-0.07	1.65
320	-0.070	-0.04	1.97
330	-0.067	-0.01	2.28
340	-0.064	0.03	2.60
350	-0.061	0.06	2.91
360	-0.057	0.09	3.23
370	-0.054	0.12	3.54
380	-0.051	0.15	3.86
390	-0.048	0.18	4.17
400	-0.045	0.21	4.49
410	-0.042	0.25	4.80
420	-0.039	0.28	5.12
430	-0.035	0.31	5.43
440	-0.032	0.34	5.75
450	-0.029	0.37	6.06
460	-0.026	0.40	6.38
470	-0.023	0.44	6.69
480	-0.020	0.47	7.01
490	-0.016	0.50	7.32
500	-0.013	0.53	7.64
510	-0.010	0.56	7.95
520	-0.007	0.59	8.27
530	-0.004	0.62	8.58
540	-0.001	0.66	8.90
550	0.002	0.69	9.21

Table A.3: Cash flow data for 3 different plant scales with varying carbon credit prices

Carbon Credit Price (€)	NPV (x1M)	NPV (x1M)	NPV (x1M)
	0.5 ktons/year	5 ktons/year	50 ktons/year
300	-4.80	-17.98	-62.75
350	-4.72	-17.20	-54.91
400	-4.64	-16.42	-47.07
450	-4.56	-15.63	-39.23
500	-4.48	-14.85	-31.38
550	-4.41	-14.06	-23.54
600	-4.33	-13.28	-15.70
650	-4.25	-12.49	-7.86
700	-4.17	-11.71	-0.02
750	-4.09	-10.93	7.82
800	-4.01	-10.14	15.67
850	-3.93	-9.36	23.51
900	-3.86	-8.57	31.35
950	-3.78	-7.79	39.19
1000	-3.70	-7.01	47.03

Table A.4: NPV data for 3 different plant scales with varying carbon credit prices

50 ktons/year	Olivine	Transportation	Carbon Credits	Electricity	IRR
80%	51	49	16	48	75
100%	47	47	47	47	47
120%	43	45	78	46	28

Table A.5: Sensitivity analysis data (NPV)

Name	Capacity (Q1)	Cost (C1)	System Capacity (Q2)	System Cost (C2)	X	FT	FP	FM	Final Equipment Cost
Crusher	8	3000	0.10815	227	0.6	1.06	1.15	1.3	359
Grinder	1.91	77853.42	0.10815	13902	0.6	1.06	1.15	1.3	22030
Compressor 1	0.393	2589.13	0.06798	772	0.69	1.06	1.15	1.3	1223
Compressor 2	0.393	2589.13	0.013596	254	0.69	1.06	1.15	1.3	403
Reactor	20	50000	0.57	7065	0.55	1.06	1.15	1.3	11196
Pump	5.76	999.65	0.078795	76	0.6	1.06	1.15	1.3	121
Heat Exchanger	40	10000	6.9	4615	0.44	1.06	1.15	1.3	7314
DAC	949	1235000	500	840793	0.6	-	-	-	840793
					Total				883439

Table A.6: Equipment sizing and cost data (0.5 ktons/year)

Name	Capacity (Q1)	Cost (C1)	System Capacity (Q2)	System Cost (C2)	X	FT	FP	FM	Final Equipment Cost
Crusher	8	3000	1.08101	903	0.6	1.06	1.15	1.3	1431
Grinder	1.91	77853.42	1.08101	55329	0.6	1.06	1.15	1.3	87680
Compressor 1	0.393	2589.13	0.679492	3778	0.69	1.06	1.15	1.3	5987
Compressor 2	0.393	2589.13	0.1358984	1244	0.69	1.06	1.15	1.3	1972
Reactor	20	50000	5.71	25093	0.55	1.06	1.15	1.3	39765
Pump	5.76	999.65	0.787593	303	0.6	1.06	1.15	1.3	480
Heat Exchanger	40	10000	22.5	7763	0.44	1.06	1.15	1.3	12303
DAC	949	1235000	5000	3347258	0.6	-	-	-	3347258
					Total				3496876

Table A.7: Equipment sizing and cost data (5 ktons/year)

Name	Capacity (Q1)	Cost (C1)	System Capacity (Q2)	System Cost (C2)	X	FT	FP	FM	Final Equipment Cost
Crusher	8	3000	10.81017	3594	0.6	1.06	1.15	1.3	5695
Grinder	1.91	77853.42	10.81017	220271	0.6	1.06	1.15	1.3	349063
Compressor 1	0.393	2589.13	6.794964	18503	0.69	1.06	1.15	1.3	29321
Compressor 2	0.393	2589.13	1.3589928	6095	0.69	1.06	1.15	1.3	9658
Reactor	20	50000	57.13	89059	0.55	1.06	1.15	1.3	141132
Pump	5.76	999.65	7.875981	1206	0.6	1.06	1.15	1.3	1911
Heat Exchanger	40	10000	71.4	12904	0.44	1.06	1.15	1.3	20449
DAC	949	1235000	50000	13325675	0.6	-	-	-	13325675
					Total				13882905

Table A.8: Equipment sizing and cost data (50 ktons/year)

Pressure (bar)	CO2 (mol/hr)	Compressor 2 (kWh/t-CO2)
1	51.0743802	272.2929872
3	51.0743802	202.7054347
5	51.0743802	172.0816548
7	51.0743802	152.2142116
9	51.0743802	137.3725116
11	51.0743802	125.5087656
13	50.0887138	39.54348736
15	48.4760819	20.81570753
17	46.8557995	15.1301831
19	45.2282276	12.06964337
21	43.593517	10.1316096
23	41.9517303	8.746939645
25	40.3028638	7.654740611
27	38.6471001	6.749061349
29	36.9843562	5.962890952
31	35.314621	5.265899091
33	33.6378724	4.654792273
35	31.9541216	4.098275511
37	30.2632507	3.605671463
39	28.5652623	3.159555994
41	26.8601107	2.752408835
43	25.147583	2.390930781
45	23.4279821	2.055273338
47	21.7010713	1.773162685
49	19.9667967	1.520530781
51	18.2251022	1.30360348
53	16.4759443	1.105493541
55	14.7192398	0.919143226
57	12.9549379	0.754196754
59	11.1829762	0.601060072
61	9.40329031	0.477451868
63	7.61581437	0.276659936
65	5.82047957	0.250409209
67	4.01730066	0.161559382
69	2.20604239	0.071026552
70	1.29747193	0.041363641
71	0.386641428	0.030111032

Table A.9: Flash drum optimization data

Residence Time (hour)	Amount of remaining CO ₂ (mols)	Residence Time (hour)	Amount of remaining CO ₂ (mols)
0	1545	3.1	724.672831
0.1	1486.59731	3.2	718.293861
0.2	1396.58366	3.3	712.215804
0.3	1321.08464	3.4	706.417856
0.4	1256.85709	3.5	700.881092
0.5	1201.55193	3.6	695.58825
0.6	1153.43056	3.7	690.523561
0.7	1111.17858	3.8	685.672582
0.8	1073.78385	3.9	681.022066
0.9	1040.4543	4	676.55984
1	1010.56121	4.1	672.258138
1.1	983.59915	4.2	668.141104
1.2	959.157185	4.3	664.181058
1.3	936.897765	4.4	660.369273
1.4	916.541049	4.5	656.697576
1.5	897.853075	4.6	653.158386
1.6	880.63673	4.7	649.744659
1.7	864.72477	4.8	646.449842
1.8	849.974365	4.9	643.267828
1.9	836.262808	5	640.192924
2	823.484083	5.1	637.219813
2.1	811.54613	5.2	634.343522
2.2	800.368613	5.3	631.559399
2.3	789.881116	5.4	628.863084
2.4	780.021658	5.5	626.250489
2.5	770.735464	5.6	623.717774
2.6	761.973949	5.7	621.261332
2.7	753.693867	5.8	618.877768
2.8	745.856598	5.9	616.563888
2.9	738.427546	6	614.31668
3	731.375625	-	-

Table A.10: CSTR CO₂ residence time data

Parameters	Wind Energy	Solar Energy	Natural Gas	Coal
CO ₂ Penalty Fraction (%)	2.1	3.1	26.7	53.6
Mineralization Energy Requirements (kWh/t-CO ₂)	250	250	250	250
Emission Rate (kg/kWh)	0.034	0.050	0.430	0.996
Energy Source Emissions (kg/t-CO ₂)	0.18	0.39	28.70	133.46
Feedstock - Cargo Ship (kg/t-CO ₂)	61.3	61.3	61.3	61.3
End Products - Trucks (kg/t-CO ₂)	24.3	24.3	24.3	24.3
Total Emissions (kg/t-CO₂)	85.78	85.99	114.30	219.06

Table A.11: CO₂ emissions with different energy sources data